uOttawa

L'Université canadienne
Canada's university

FACULTÉ DES ÉTUDES SUPÉRIEURES ET POSTOCTORALES

uOttawa

L'Université canadienne
Canada's university

FACULTY OF GRADUATE AND POSDOCTORAL STUDIES

Yuan Dong

AUTEUR DE LA THÈSE / AUTHOR OF THESIS

M.A.Sc. (Mechanical Engineering)

GRADE / DEGREE

Department of Mechanical Engineering

FACULTÉ, ÉCOLE, DÉPARTEMENT / FACULTY, SCHOOL, DEPARTMENT

Dynamic Analysis and Position Control of a Single Flexible-Link Flexible-Joint Robot Manipulator Using Time Delay

TITRE DE LA THÈSE / TITLE OF THESIS

Amor Jnifene

DIRECTEUR (DIRECTRICE) DE LA THÈSE / THESIS SUPERVISOR

CO-DIRECTEUR (CO-DIRECTRICE) DE LA THÈSE / THESIS CO-SUPERVISOR

EXAMINATEURS (EXAMINATRICES) DE LA THÈSE / THESIS EXAMINERS

W. Gueaieb

D. Redekop

Gary W. Slater

LE DOYEN DE LA FACULTÉ DES ÉTUDES SUPÉRIEURES ET POSTDOCTORALES /
DEAN OF THE FACULTY OF GRADUATE AND POSTDOCORAL STUDIES

DYNAMIC ANALYSIS AND POSITION CONTROL OF A SINGLE FLEXIBLE-LINK FLEXIBLE-JOINT ROBOT MANIPULATOR USING TIME DELAY

Yuan Dong

A thesis submitted to the Faculty of Graduate and Postdoctoral Studies in Partial fulfillment of the requirements for the degree of

MASTER OF APPLIED SCIENCE

In Mechanical Engineering

Ottawa-Carleton Institute for Mechanical and Aerospace Engineering
University of Ottawa
Ottawa, Canada

Your file Votre référence
ISBN: 0-494-14899-3
Our file Notre référence
ISBN: 0-494-14899-3

Abstract

In this thesis, a position control system for a single flexible-link flexible-joint (FLFJ) manipulator has been developed. It is presented in three parts: dynamic modeling and analysis, control system design, and experimental analysis of the designed control system. The assumed modes method and the Lagrange approach were combined to derive a dynamic model of the single FLFJ manipulator and then this model was linearized about zero deflection for both the flexible joint and the flexible link. The resulting linear dynamic model was used for the dynamic analysis and control system design. Equations of motion and their analytical solutions were derived for the single FLFJ manipulator at any rotation angle. The effects of the relative stiffness of the joint with respect to the link on the dynamic characteristics and open-loop responses of the single FLFJ manipulator were investigated based on the linear model. It was found that the higher order frequencies of the manipulator increased monotonically with the increments of the joint stiffness, while the lower order ones kept almost unchanged. This demonstrates that the higher order frequencies were more sensitive to the interaction between the flexible link and the flexible joint.

A time-Delayed Feedback Signal (DFS) controller was applied to the single FLFJ manipulator and the effect of the time delay on the stability of the system was examined. It was found that a suitable combination of control loop gain and time delay can improve the performance of the single FLFJ manipulator by eliminating the vibration of both the flexible link and the flexible joint. With the purpose of tracking a desired trajectory for the angular position of the single FLFJ manipulator, a proportional-plus-derivative (PD) controller was employed in conjunction with the DFS controller to make the manipulator track a desired trajectory and eliminate the vibration at the same time.

An experimental test-bed consisting of a FLFJ system was designed and built to examine the proposed control system by comparing the performance of the systems with and without the DFS controller. The vibration of the flexible link and the flexible joint was greatly reduced after adding the DFS controller.

Acknowledgements

I would like to give my sincere gratitude and appreciation to Dr. Amor Jnifene, the supervisor of this thesis, for his continuous instruction and guidance; Mr. John Perrins and Mr. Leo Denner, the department technicians, for their work and assistance in the experiment; The academic members of the mechanical engineering department for their advice and help; and my family, parents and husband, for their financial support, encouragement and love.

Table of Contents

List of Tables

List of Figures

Nomenclature

A : Cross-sectional area of the link

$[C]$: Damping matrix

$C(s)$: Laplace transform of the output from PD controller

C_n : Arbitrary constants

d : Diameter of the joint

E : Young's modulus of the link

$E(s)$: Laplace transform of the error between the reference input and the feedback signal

EI : Flexural rigidity of link

J_1: The moment of inertia of the motor shaft

J_2: The moment of inertia of the hub

j: $\sqrt{-1}$

H : Height of the hub

$H(s)$: Laplace transform of the transfer function of DFS controller

h : Height of the joint

I : Inertia of the area of the link

$G(s)$: Laplace transform of the transfer function of the open-loop system

G_{contr} : Laplace transform of the transfer function of PD controller

$G_{plant}(s)$: Laplace transform of the transfer function of the plant (including the open-loop system, the systems with DFS controller)

K : Control loop gain

K_d : Gain for the derivative controller

K_p : Gain for the proportional controller

Ks : Equivalent stiffness constant of the joint

$[K]$: Stiffness matrix

L : The torque applied to the FLFJ manipulator

l : Length of the link

$[M]$: Mass matrix

M_e : Elastic transformation matrix

M_r : Rigid transformation matrix

N : The number of degree of the system

n : The number of applied extra forces

$P(s), Q(s)$: Two polynomials with real coefficients in the characteristic equation

P_R, Q_R, P_I, Q_I : The real parts and imaginary parts of $P(s)$ and $Q(s)$

$q_i(t)$: The generalized coordinates of link

r/D: Radius/diameter of the hub

$R(s)$: Laplace transform of the reference input

r_S : Radius of the shaft in the experimental setup

${}^{l}r$: Position vector of any point on the link with respect to the moving frame 2

${}^{0}r$: Position vector of any point on the link under the global frame

T : The kinetic energy of the system

t : Width of the link in the cross section

$U(s)$: Laplace transform of the output of DFS controller

$\underline{U}$: The input weighting matrix

u : Control signal

V : The potential energy of the system

V_D : The dissipation function resulting from the internal structural damping of the link

W : Height of the link in the cross section

w : Bending deformation of link under the moving frame 2

X : State vector

X_0Y_0 : Fixed frame/inertial frame/global frame

X_mY_m : Moving frame1 that rotates together with motor shaft

X_lY_l : Moving frame2 that rotates together with link/hub

x : Distance of any point on the link from the outer radius of the hub

y : Bending deformation of link under the global frame

z : The number of terms retained in the approximation

α_n : Constant coefficient

δ : Joint torsional deformation

θ_1 : Rotating angle of the motor shaft

θ_2 : Rotating angle of the link/hub

$\lambda_n l$: The nth root of the system's characteristic equation

ρ : Mass density of link per length

ς : Damping ratio of the link

τ : Time delay

$\Phi_i(x)$: Mode shape function

ω : The root of the equation $F(\omega) = 0$ to get the critical time delays

ω_n : The nth natural frequency of the manipulator

Chapter 1: Introduction

1.1 Flexible-link flexible-joint manipulators

As the requirements for the operation speed of robot manipulators rise, the application of flexible manipulators has become increasingly significant since they can execute not only the same accurate tasks as traditional bulky rigid manipulators, but also can work at much higher speeds and use less energy. However, in order to obtain the required precision, an active vibration control system is needed for the flexible manipulator because its low stiffness causes excessive oscillation during operation.

The first step in designing a good control algorithm for a given dynamic system is to have an accurate model. Even though investigations into the modeling and control of flexible manipulators have been conducted for about thirty years and a number of efficient control techniques have been proposed and applied, few researchers have considered the flexibility of joints together with that of links. Therefore, the performance of their control systems is limited in application due to the fact that the joint flexibility can be predominant in the gear motor, bearing and long shaft which are used in most industrial and aerospace manipulators [1, 2].

In the present work, the joint flexibility was considered in the dynamic model, upon which the dynamic analysis and control system design were based.

1.2 Modeling methods

The dynamic equations for flexible manipulators are usually represented by a set of partial differential equations. They are usually parted into two terms, one being a function of space variables and the other being a function of time variables. Thus, the partial differential

equations can be solved analytically. The modal expansion model is another frequently used method to solve a dynamic system. Two approximation methods have commonly been used for the modal expansion model in the literature, the Assumed Modes Method (AMM) and the Finite Element Method (FEM). The resulting dynamic equations generally have the form of $M\ddot{X} + C\dot{X} + KX = Q$ where M , C and K are mass, damping and stiffness matrix, respectively; X and Q are variable and force vector, respectively. The difference between these two approximation methods is, taking a cantilever beam for example, that the variable vector in the assumed modes method is composed of generalized displacements, while the variable vector involved in the finite element method consists of nodal degrees of freedom. The assumed modes method is useful for systems whose geometry is simple enough and thus a good set of shape functions can be found, while the finite element method is suitable for systems with uneven geometry properties. Flexible joints have been simply modeled as a linear torsional spring in most literature where the joint flexibility was considered in the modeling [3, 4, 5].

In the dynamic modeling of this work, a combination of the assumed modes method and the Lagrange approach was employed to set up the model where the shape functions satisfied both geometric and physical boundary conditions, and could be differentiated as many times as the order of the system. The joint was modeled as a torsional spring.

1.3 Time delay control theory

Since the requirements of system performance and control speed are increasing, time delays, which are inherent and unavoidable in controllers, actuators and human interactions, have become more problematic in the operation of dynamic systems. The undesirable time delays may deteriorate system performance or even cause instability. Fortunately, it has been

found that appropriate time delays, however, could improve system performance and make unstable systems become stable [6, 7, 8, 9, 10]. Yang and Mote [11,12] used time delay approach to reduce excessive vibrations in elastic systems. Krodkiewski and Faragher [13] managed to apply a time delay equal to one period of the periodic motion of helicopter rotor blades in the control loop to improve the system's stability.

Stability switches of dynamic systems were studied by Z.H. Wang and H.Y. Hu [7], who produced a method to obtain critical time delays that stabilized or destabilized a system by moving poles across the imaginary axis on the complex plane. If the system is delay-dependent stable, a final time delay could be found to make the system stable, i.e. the system would become unstable forever after that time delay point.

The basic theory and methods in [7] were applied to the single flexible-link flexible-joint manipulator in the current study. The relation between the time delay in the control loop and the stability of the system was investigated for two controllers produced by two different feedback signals. It was found that system performance could be greatly improved by applying the time-delayed feedback signal (DFS) controller with appropriate time delay and control loop gain.

1.4 Vibration control of flexible-link flexible-joint manipulators

There was plenty of work done on the control of flexible manipulators with either only flexible links or flexible joints. However, few researchers have conducted research on the problem of the interaction between flexible links and flexible joints. Even though some results were reported [5], the control system is not suitable for real time application because full states availability has to be assumed. Researchers at Tohoku University used real time calculation and inverse kinematics in the control process to eliminate the vibration and

control the tip position of a 3D flexible manipulator. However, this control scheme is also difficult to execute due to the huge required computations. [14]

In this thesis, a control law based on two nested feedback loops was applied to the single flexible-link flexible-joint manipulator. The inner loop was used to control the excessive vibrations of both the link and the joint. Instead of using all the state variables, only the position angle of the motor shaft or the joint torsional deflection was used to control the vibration of the link and the joint. A time delay was introduced into the inner control loop as a vibration absorber. The outer loop, consisting of a modified PD controller, was applied to lead the angular position of the robot manipulator to track a desired trajectory.

1.5 Objective and outlines of the thesis

The objective of this thesis is to control the vibration and tip position of a single flexible-link flexible-joint manipulator. A time delay was included in the feedback control loop as a vibration absorber. A PD controller combined with the time delay was used to lead the manipulator to track a desired trajectory while damping out the excessive vibration.

The thesis is composed of seven chapters. In chapter one, the necessary introduction and background of the thesis is provided. In chapter two, a literature review on flexible structures is presented in three parts: dynamic modeling, dynamic behavior analysis and control. In chapter three, a nonlinear and a linearized dynamic model of the single flexible-link flexible-joint manipulator are developed using a combination of the assumed modes method and the Lagrange approach. In chapter four, an analysis of the system's characteristics and its dynamic behavior is introduced. In chapter five, a control system is designed to eliminate the vibration of the link and the joint at the same time while driving the rigid body of the flexible manipulator to a target position. The proposed control system is

then compared with the linear quadratic regulator (LQR) to display its superiority in terms of system performance. The robustness of the proposed control system with respect to external disturbances and system parameter uncertainties are also investigated. In chapter six, an experimental investigation is implemented to test the effectiveness of the proposed control system in a real model. Finally, in chapter seven, conclusions and recommendations for further work are made.

Chapter 2: Literature Review

2.1 Introduction

Research work on the dynamic modeling and control of flexible structures was first devoted about thirty years ago [15]. It is not only because this kind of flexible element has great application in aircrafts and industrial robots, but also there are many advantages of flexible structures, including lower weight and power consumption, higher payload-to-weight ratio and productivity as well as safer interaction with people and environment [1, 4, 5]. In this chapter, a literature survey about dynamic modeling of flexible manipulators and dynamic analysis and control of flexible-link flexible-joint manipulators is given.

2.2 Dynamic modeling of flexible manipulators

For distributed elastic systems, there are three methods commonly used to solve the dynamic system. The first one is solving partial differential equations to get mathematical solutions to the problem [16]. Even though this method can provide accurate expressions for the system, it is complex and difficult for physical understanding. The second method uses a lumped mass and spring model. The whole system is divided into finite parts and each part presents the local inertia and stiffness [17, 18]. The lumped mass and spring model is an easy and reduced order model for control system design, but its low precision affects the system analysis and control.

Therefore, a model which is not only simple but also can accurately represent the physical system is needed. This third method uses a modal expansion model, or called eigenfunction expansion model, which was a model frequently employed by researchers in the literature [1, 3, 4, 5, 15]. The solution to this kind of model is the summation of products

of shape function and time function. The shape functions can also be referred to as mode shapes, or eigenfunctions, which are the particular solutions to the problem; other general solutions could be expressed as the combination of these functions.

The Assumed Modes Method (AMM) and the Finite Element Method (FEM) are both spatial discretization methods applied to obtain the modal expansion model of a system. In AMM, the mode shapes are assumed for the entire structure based on boundary conditions, differentiability and other criteria [19]. In FEM, the system is first separated into finite elements which have their own shape functions and nodal variables [20]. Hence, the FEM is more suitable for systems having uneven cross-section and material properties. The AMM and FEM were generally combined with the Lagrange approach [1, 3, 4, 5, 21, 22] and Hamilton's principle [23, 24], which are both inspired by energy principles to derive the equations of motion for a system. Flexible joints are commonly modeled as a linear torsional spring. Its equivalent potential energy $V_J = \frac{1}{2} K_S \delta^2$ (where K_S denotes the equivalent stiffness of the flexible joint and δ signifies the joint torsional deformation) is added to the total potential energy of the system when applying the Lagrange approach or Hamilton's principle [1, 3, 4, 5, 23, 24].

2.3 Dynamic analysis of flexible-link flexible-joint manipulators

It has been proven by the researchers who studied the dynamic behavior of flexible link-joint manipulators that joint flexibility plays a significant role in the dynamic behavior of flexible manipulators by increasing the link oscillation. Al-Bedoor and Almusallam [3] compared the responses of a flexible-link flexible-joint system with those of a flexible-link rigid-joint system and found that the tip deflection became unstable due to the nonlinear

interaction between link flexibility and joint flexibility. Subudhi and Morris [5] also did a similar comparison and concluded that joint flexibility caused the link to display more oscillatory behavior than with rigid joints.

Other researchers have investigated the effects of joint stiffness on the roots of the system's characteristic equation and the natural frequencies as well as on the mode shapes. Li *et al.* [24] investigated the effect of joint stiffness on the roots of the flexible link and revealed that even a small joint flexibility had a great effect on the system frequencies. Xi *et al* in [25] produced an analytical solution for a flexible link-joint manipulator and illustrated its natural frequencies and mode shapes parameterized in terms of the relative moment of inertia and the relative stiffness of the link with respect to the joint. They used the change in the roots of the frequency equation after the relative inertia or the relative stiffness was set to different values to demonstrate the coupling effect of flexible link and flexible joint. A small rotating motion for the manipulator was assumed in the above two works. However, this assumption of a rotating angle is unacceptable in real systems [5].

2.4 Control of flexible-link flexible-joint manipulators

In the literature, various control techniques have been employed to eliminate the unexpected vibrations in order to improve the performance of flexible manipulators [22, 26, 27, 28, 29, 30, 31, 32]. Nevertheless, none of these studies considered joint flexibility in their dynamic models. Both the harmonic drive transmission and the shaft in the real system may introduce joint flexibility. Therefore, an effective controller is needed to eliminate the vibration of the flexible link and the flexible joint to achieve an accurate end-point position and a good tracking performance. Little work on the simultaneous control of the link and joint vibration was discovered in the literature.

Subudhi and Morris [5] applied a composite controller to the system which had been divided into two subsystems (slow and fast) by using a singular perturbation approach. Full state availability was assumed for the LQR controller in the fast subsystem control. However, sometimes acquiring all the state variables is hard or even impractical. Yue [33] used redundancy to eliminate the residual vibration in a flexible link-joint system. In his control technique, the generalized coordinates which describe the flexible deformation also need to be involved. In addition, researchers at the Space Machines Laboratory of Tohoku University calculated variable control gains in real time using an inertial matrix to suppress the vibration of a 3D flexible manipulator. To control its end-effector's trajectory, they solved the inverse kinematics of the 3D flexible manipulator using an iterative calculation method. [14] However, both real time calculation and solving the inverse kinematics require tremendous computing effort and thus have limited application. Karkoub and Tamma [34] designed two controllers for a two-link flexible manipulator using μ-synthesis technique. Theses two controllers were designed to use hub angles and relative tip displacements feedback and hub angles and relative tip acceleration feedback, respectively. Nevertheless, tip variables are not easy to measure and their differentials from sensors usually include lots of noise. Furthermore, this kind of feedback control system is non-collocated and therefore may results in non-minimum phase dynamics, causing the control system to be unstable.

Other results have been reported concerning the control problem with both link and joint flexibility [35, 36]. These researchers managed to control link vibration using the adjunctive joint compliance. However, they did not really treat the system like a flexible-link flexible-joint system and the controllers were either semi-active or passive. Pun and Semercigil [35] proposed a semi-active controller with a passive spring and an active spring

to change the effective stiffness of the controlled system between two cases (K and $K - \Delta K$) when the flexible link reached its peak displacement amplitudes, thus eliminating vibrations. Warkentin and Semercigil [36] used a passive spring damper system and a controller arm to control the oscillation of a flexible link. Their main objective was to find optimal values for the spring and the damper to produce a maximum reduction in settling time, as well as maximum acceleration and maximum deflection.

2.5 Summaries of the literature survey

From the literature review, it can be seen that joint flexibility has begun to catch the attention of researchers who are interested in the study of flexible manipulators. However, the research is still in the initial stages. A control system which is not only efficient but also easily implemented in the application is needed.

Chapter 3: Modeling of the Single Flexible-link Flexible-joint (FLFJ) Manipulator

3.1 Introduction

The dynamic modeling of a single FLFJ manipulator is presented in this chapter. In this study, the rational angle of the manipulator was not limited to be small. The setup model is suitable for the manipulator at any rational angle. A set of nonlinear equations of motion was obtained and then linearized around equilibrium positions to simplify the model based on which a new control system would be developed. Finally, the equations of motion were transferred to a set of state space model to obtain all the state variables of the system easily and resort to computers for the tedious computation involved in the analysis and control system design.

3.2 Description of the physical plant

A schematic representation of the single flexible-link flexible-joint manipulator is shown in Figure 1(a). It is typically composed of a lightweight cantilever beam and a flexible shaft which are both made of aluminum. The beam was designed to be a "slender" Euler-Bernoulli beam in order that vibrations were only in the horizontal plane and that the transverse shear and rotary inertia effects could be ignored. The link was driven at the clamped end through the flexible joint by a DC motor and the flexible joint was dynamically simplified as a linear torsional spring with the stiffness constant K_S. The moment of inertia of the motor shaft is denoted as J_1 and that of the hub which is connected with the link is J_2. Due to the flexibility of the joint, two angle variables θ_1 and θ_2 had to be used to define its

deformation. They represent the angles of the motor shaft and the link/hub under the inertial reference frame, respectively. The joint deformation was defined to be the difference between these two angles ($\theta_2 - \theta_1$), denoted as δ. Three coordinate frames, X_0Y_0 (fixed frame/inertial reference frame/global frame), X_mY_m (moving frame 1 that rotates with the motor shaft) and X_lY_l (moving frame 2 that rotates with the link/hub), were used to describe the deformation of the manipulator as shown in Figure 1(b).

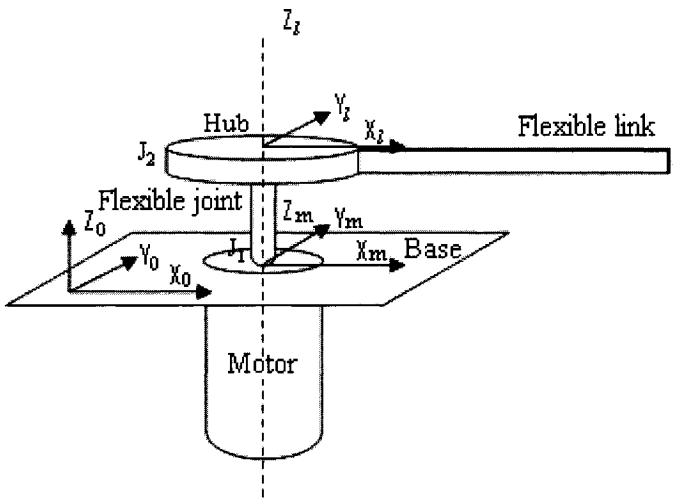

Figure 1 (a): Schematic representation of the single FLFJ manipulator

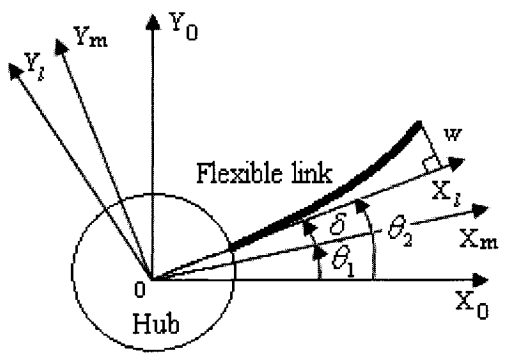

Figure 1 (b): Coordinate systems

The global position vector of a point on the link was obtained using the following formulation:

$$\underline{{}^{0}r} = M_r M_e \underline{{}^{l}r} \tag{3.2-1}$$

$$\underline{{}^{l}r} = \begin{bmatrix} x + r \\ w(x,t) \end{bmatrix}$$

where ${}^{l}r$ and ${}^{0}r$ are the position vectors of a point on the link measured with respect to the moving frame 2 and the inertial frame, respectively. The variable $w(x,t)$ represents the horizontal bending deformation of the link with respect to the moving frame 2 at time t and x is the distance of any point on the link away from the outer radius (r) of the hub.

The general elastic transformation matrix M_e from the link/hub coordinate system (the moving frame 2) to the motor shaft coordinate system (the moving frame 1) has the form of

$$M_e = \begin{bmatrix} \cos\delta(t) & -\sin\delta(t) \\ \sin\delta(t) & \cos\delta(t) \end{bmatrix}$$

In this study, it was assumed that the flexible joint had a very small torsional deformation and therefore the transformation matrix can be modified accordingly:

$$M_e = \begin{bmatrix} 1 & -\delta(t) \\ \delta(t) & 1 \end{bmatrix} \tag{3.2-2}$$

Another transformation matrix from the motor shaft coordinate system (the moving frame 1) to the global coordinate system (the inertial frame) is the rigid transformation matrix with the form:

$$M_r = \begin{bmatrix} \cos\theta_1(t) & -\sin\theta_1(t) \\ \sin\theta_1(t) & \cos\theta_1(t) \end{bmatrix} \tag{3.2-3}$$

where $\theta_1(t)$ is the position angle of the motor shaft under the inertial frame.

In addition to the assumptions made in the above description of the model, the following assumptions were also made in order to simplify the dynamic modeling of the single flexible-link flexible-joint manipulator:

a) The link was considered to have even geometrical and material properties;

b) The gravity effect of the system, the backlash in the motor gearbox and the joint viscous friction were ignored;

c) The centripetal acceleration was neglected based on the assumption of small angular velocity of the link [25];

d) The kinetic energy of the motor shaft was idealized to have only the rotation component, and its moment of inertia was calculated around the rotating axis symmetrically; and,

e) The deflection of the link was assumed to be small.

The physical parameters of the manipulator are given in Table 1.

Table 1: Parameters of the single FLFJ manipulator

Definition	Parameter	Value
Mass density of the link	ρ	0.169 Kg/m
Flexural rigidity of the link	EI	2.282 $N \cdot m^2$
Length of the link	l	0.5 m
Shaft inertia	J_1	1.45e-4 $Kg \cdot m^2$
Hub radius	r	0.092 m
Hub inertia	J_2	8.51e-3 $Kg \cdot m^2$
Torsional stiffness of the joint	K_S	166 $N \cdot m/rad$

3.3 Dynamic modeling

The assumed modes method and the Lagrange approach were combined together to obtain the dynamic model of the single flexible-link flexible-joint manipulator. To derive the mode shapes of the FLFJ robot manipulator, clamped-free modes were used to approximate the shape functions and the link was considered as an Euler-Bernoulli beam. The governing equation of the elastic cantilever beam can be expressed as:

$$EI\frac{\partial^4 w(x,t)}{\partial x^4}+\rho\frac{\partial^2 w(x,t)}{\partial t^2}=0 \tag{3.3-1}$$

The boundary conditions of this kind of configuration can be written as:

Geometric boundary conditions:

$$w(0,t)=0 \tag{3.3-2a}$$

$$\frac{\partial w(0,t)}{\partial x}=0\Rightarrow\frac{d\Phi_i(0)}{dx}=0 \tag{3.3-2b}$$

Physical boundary conditions:

$$EI\frac{\partial^3 w(l,t)}{\partial x^3}=0\Rightarrow\frac{d^3\Phi_i(l)}{dx^3}=0 \tag{3.3-2c}$$

$$EI\frac{\partial^2 w(l,t)}{\partial x^2}=0\Rightarrow\frac{d^2\Phi_i(l)}{dx^2}=0 \quad (l \text{ is the length of the link}) \tag{3.3-2d}$$

The deflection of the flexible link can be expressed as the superposition of mode-shapes and time-dependent generalized displacements:

$$w(x,t)=\sum_{i=1}^{z}\Phi_i(x)q_i(t) \tag{3.3-3}$$

where $q_i(t)$ denotes the i th generalized coordinate, $\Phi_i(x)$ denotes the i th mode shape function and z is the number of terms retained in the approximation.

To obtain an accurate dynamic model, the space-dependent shape functions were selected to satisfy both the geometric boundary conditions and the physical boundary conditions and to be a set of linearly independent functions differentiable as many times as the order of the system [19].

Based on all the criteria, the shape function can be defined as follows:

$$\Phi_i(x) = 1 - \cos\left(\frac{i\pi x}{l}\right) + \frac{1}{2}(-1)^{i+1}\left(\frac{i\pi x}{l}\right)^2, \; i = 1,2,3\cdots \tag{3.3-4}$$

The linear combination of the first two shape functions was applied to approximate the actual shape of the link. Therefore, the deflection of the link can be written as:

$$w(x,t) = \Phi_1(x)q_1(t) + \Phi_2(x)q_2(t) \tag{3.3-5}$$

where,

$$\Phi_1(x) = 1 - \cos\left(\frac{\pi x}{l}\right) + \frac{1}{2}\left(\frac{\pi x}{l}\right)^2 \tag{3.3-6}$$

$$\Phi_2(x) = 1 - \cos\left(\frac{2\pi x}{l}\right) - \frac{1}{2}\left(\frac{2\pi x}{l}\right)^2 \tag{3.3-7}$$

The kinetic energy of the system is derived as follows:

From Equation (3.2-1), the derivation of ${}^0\dot{r}$ is expressed as:

$$\underline{{}^0\dot{r}} = M_r M_e \, \underline{{}^l\dot{r}} + \dot{\theta}_1 \frac{dM_r}{d\theta_1} M_e \, \underline{{}^l r} + \dot{\delta} \frac{dM_e}{d\delta} M_r \, \underline{{}^l r} \tag{3.3-8}$$

Using the expressions of M_r and M_e obtained in Section 3.2, we get:

$$\underline{{}^0\dot{r}} = [C_1 \sin\theta_1 + C_2 \cos\theta_1] \cdot \underline{\hat{i}} + [-C_1 \cos\theta_1 + C_2 \sin\theta_1] \cdot \underline{\hat{j}} \tag{3.3-9}$$

where,

$$C_1 = -\dot{w}(x,t) - \dot{\theta}_1(x+r) + \dot{\theta}_1 \delta w(x,t) - \dot{\delta}(x+r)$$

$$C_2 = -\delta\dot{w}(x,t) - \dot{\theta}_1\delta(x+r) - \dot{\theta}_1 w(x,t) - \dot{\delta}w(x,t)$$

Therefore, the kinetic energy of the system is expressed as

$$T = \frac{1}{2}J_1\dot{\theta}_1^2 + \frac{1}{2}J_2\dot{\theta}_2^2 + \frac{1}{2}\int_0^l \rho\, {}^0\underline{\dot{r}} \cdot {}^0\underline{\dot{r}}\, dx \tag{3.3-10}$$

$$= \frac{1}{2}J_1\dot{\theta}_1^2 + \frac{1}{2}J_2\left(\dot{\theta}_1 + \dot{\delta}\right)^2 + \frac{1}{2}\rho\int_0^l \{[\left(\dot{\theta}_1 + \dot{\delta}\right)^2 + \delta^2\dot{\theta}_1^2][(x+r)^2 + w^2(x,t)]$$
$$+ \left(1+\delta^2\right)\dot{w}^2(x,t) + [2\left(1+\delta^2\right)\dot{\theta}_1 + 2\dot{\delta}](x+r)\dot{w}(x,t) + 2\delta\dot{\delta}w(x,t)\dot{w}(x,t)\}dx$$

where,

$$\dot{w} = \Phi_1\dot{q}_1 + \Phi_2\dot{q}_2$$

The potential energy of the system can be expressed as follows:

$$\mathrm{V} = \frac{1}{2}K_S\delta^2 + \frac{1}{2}\int_0^l EI\left(w''\right)^2 dx \tag{3.3-11}$$

$$w'' = \Phi_1''q_1 + \Phi_2''q_2$$

The first term in Equation (3.3-11) is the potential energy of the flexible joint and the second one is that of the flexible link. Using the Lagrange approach, the equations of motion for the single flexible-link flexible-joint manipulator were obtained. The only input actuation for the FLFJ manipulator was the torque $L(t)$ applied by a DC motor.

The virtual work can be written as:

$$\delta W = \delta\theta_1 \cdot L(t) \tag{3.3-12}$$

Substituting the kinetic energy and potential energy into the Lagrange's equation, a set of nonlinear equations of motion can be derived.

The Lagrange equation has the form of $\frac{d}{dt}\left(\frac{\partial T}{\partial \dot{q}_i}\right) - \frac{\partial T}{\partial q_i} + \frac{\partial V}{\partial q_i} = \underline{F}(t)$, where the variable vector $q_i = [\theta_1, \delta, q_1, q_2]^T$, and the general force vector $\underline{F}(t) = \begin{bmatrix} L(t) \\ 0 \\ 0 \\ 0 \end{bmatrix}$.

$$\begin{bmatrix} m_{\theta_1\theta_1} & m_{\theta_1\delta} & m_{\theta_1 q_1} & m_{\theta_1 q_2} \\ m_{\delta\theta_1} & m_{\delta\delta} & m_{\delta q_1} & m_{\delta q_2} \\ m_{q_1\theta_1} & m_{q_1\delta} & & \\ m_{q_2\theta_1} & m_{q_2\delta} & & [m_{qq}]_{4\times4} \end{bmatrix} \begin{Bmatrix} \ddot{\theta}_1 \\ \ddot{\delta} \\ \ddot{q}_1 \\ \ddot{q}_2 \end{Bmatrix} + 2\dot{\delta}\delta \begin{bmatrix} 0 & 0 & 0 & 0 \\ 0 & 0 & 0 & 0 \\ 0 & 0 & & \\ 0 & 0 & & [M]_{4\times4} \end{bmatrix} \begin{Bmatrix} \dot{\theta}_1 \\ \dot{\delta} \\ \dot{q}_1 \\ \dot{q}_2 \end{Bmatrix}$$

$$+ \begin{bmatrix} 0 & 0 & 0 & 0 \\ 0 & K_s & 0 & 0 \\ 0 & 0 & & \\ 0 & 0 & & [K_{qq}]_{4\times4} \end{bmatrix} \begin{Bmatrix} \theta_1 \\ \delta \\ q_1 \\ q_2 \end{Bmatrix} + \begin{Bmatrix} Q_{\theta_1} \\ Q_\delta \\ Q_{q_1} \\ Q_{q_2} \end{Bmatrix} = \begin{Bmatrix} L(t) \\ 0 \\ 0 \\ 0 \end{Bmatrix} \qquad (3.3\text{-}13)$$

The expression of every element in the matrices of Equation (3.3-13) is given in appendix A.

To simplify the development of a new complex control system in the following chapters, the model was linearized about zero deflection for both the joint torsional deformation and the link bending deformation to obtain linear equations of motion. The linearization process is given in appendix A. Therefore, only the linear coupling effects between the flexible joint and the flexible link was considered in this study.

The variable vector $\begin{Bmatrix} \theta_1 \\ \theta_2 \\ q_1 \\ q_2 \end{Bmatrix}$ was used in the linear model instead of $\begin{Bmatrix} \theta \\ \delta \\ q_1 \\ q_2 \end{Bmatrix}$,

where $\delta = \theta_2 - \theta_1$.

The linear model of the single flexible-link flexible-joint manipulator is expressed as:

$$M \cdot \underline{\ddot{X}} + K \cdot \underline{X} = \underline{F}\,; \underline{X} = \begin{bmatrix} \theta_1 \\ \theta_2 \\ q_1 \\ q_2 \end{bmatrix} \qquad (3.3\text{-}14)$$

Where:
$$M=\begin{bmatrix} J_1 & 0 & 0 & 0 \\ 0 & J_2+\rho\int_0^l (r+x)^2 dx & \rho\int_0^l (r+x)\Phi_1 dx & \rho\int_0^l (r+x)\Phi_2 dx \\ 0 & \rho\int_0^l (r+x)\Phi_1 dx & \rho\int_0^l \Phi_1^2 & 0 \\ 0 & \rho\int_0^l (r+x)\Phi_2 dx & 0 & \rho\int_0^l \Phi_2^2 dx \end{bmatrix}$$

$$K=\begin{bmatrix} K_S & -K_S & 0 & 0 \\ -K_S & K_S & 0 & 0 \\ 0 & 0 & EI\int_0^L \Phi_1''^2 dx & EI\int_0^L \Phi_1''\cdot\Phi_2'' dx \\ 0 & 0 & EI\int_0^L \Phi_1''\cdot\Phi_2'' dx & EI\int_0^L \Phi_2''^2 dx \end{bmatrix}$$

$$\underline{F}=\begin{bmatrix} L(t) \\ 0 \\ 0 \\ 0 \end{bmatrix}=\underline{U}\cdot L(t)=\begin{bmatrix} 1 \\ 0 \\ 0 \\ 0 \end{bmatrix}\cdot L(t)$$

where $\underline{U}$ is an input weighting matrix with the form of $[I_{n\times n} O_{n\times(N-n)}]^T$, N is the number of degree of the system and n is the number of applied forces.

Putting the expressions of shape functions and the parameter data of Table 1 into Equation (3.3-14), the matrices M and K can be written as:

$$M=\begin{bmatrix} 0.000145 & 0 & 0 & 0 \\ 0 & 0.020151 & 0.10237 & -0.23075 \\ 0 & 0.10237 & 0.9853 & 0 \\ 0 & -0.23075 & 0 & 5.7686 \end{bmatrix}$$

$$K=\begin{bmatrix} 166 & -166 & 0 & 0 \\ -166 & 166 & 0 & 0 \\ 0 & 0 & 2667.5 & -7113.2 \\ 0 & 0 & -7113.2 & 42679 \end{bmatrix}$$

The eigenvalues of the open-loop system are 0, 0, $\pm 37.6j$, $\pm 573.3j$, $\pm 1398.7j$.

To obtain all the outputs of a system including the variables and their differentials and resort to computers for the tedious computations necessary in the analysis, the state-space approach to system analysis is the most suitable [37].

Equations of motion were thus transferred to the state space model:

$$\dot{X} = AX + BU \tag{3.3-15a}$$

$$Y = CX + DU \tag{3.3-15b}$$

where X is the state vector, Y is the output vector and U is the input vector.

$$A = \begin{bmatrix} 0 & 0 & 0 & 0 & 1 & 0 & 0 & 0 \\ 0 & 0 & 0 & 0 & 0 & 1 & 0 & 0 \\ 0 & 0 & 0 & 0 & 0 & 0 & 1 & 0 \\ 0 & 0 & 0 & 0 & 0 & 0 & 0 & 1 \\ & & & & 0 & 0 & 0 & 0 \\ & M^{-1}(-K) & & & 0 & 0 & 0 & 0 \\ & & & & 0 & 0 & 0 & 0 \\ & & & & 0 & 0 & 0 & 0 \end{bmatrix}; \; B = \begin{bmatrix} 0 \\ 0 \\ 0 \\ 0 \\ \\ \\ M^{-1}\underline{U} \\ \end{bmatrix}; \; X = \begin{bmatrix} \theta_1 \\ \theta_2 \\ q_1 \\ q_2 \\ \dot{\theta}_1 \\ \dot{\theta}_2 \\ \dot{q}_1 \\ \dot{q}_2 \end{bmatrix}$$

The targets of the control for this system are the angular position of the manipulator (θ_1 and θ_2), the joint torsional deflection δ, and the tip bending deflection of the link with respect to the moving frame 2 and the moving frame 1. Thus, the C matrix can be structured as:

$$C = \begin{bmatrix} 1 & 0 & 0 & 0 & 0 & 0 & 0 & 0 \\ 0 & 1 & 0 & 0 & 0 & 0 & 0 & 0 \\ -1 & 1 & 0 & 0 & 0 & 0 & 0 & 0 \\ 0 & 0 & \Phi_1(l) & \Phi_2(l) & 0 & 0 & 0 & 0 \\ -(l+r) & (l+r) & \Phi_1(l) & \Phi_2(l) & 0 & 0 & 0 & 0 \end{bmatrix}$$

The simulation model of the FLFJ system is shown in Figure 2.

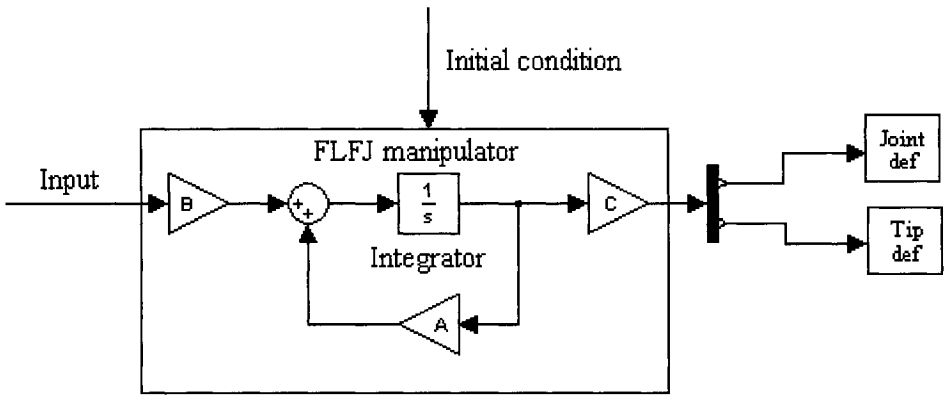

Figure 2: Simulation diagram of the open-loop system

The output responses of the open-loop system subjected to initial conditions $[0 \quad 0.05 \quad 0 \quad 0 \quad 0 \quad 0 \quad 0 \quad 0]$ are displayed in Figure 3. The figure shows that the responses of the joint torsional deflection and the tip bending deflection of the link are both oscillatory with no damping.

To make the model more accurate, the internal structural damping of the link was added to the dynamic model. Here, the damping was assumed to be viscoelastic and its dissipation function can be described as [4]:

$$V_D = \frac{1}{2}\int_0^l CI\left[\frac{\partial}{\partial t}\left(\frac{\partial^2 w(x,t)}{\partial x^2}\right)\right]^2 dx \qquad (3.3\text{-}16)$$

$$C = l^2 \varsigma \sqrt{AE/I}$$

where ς is the damping coefficient for the link and l is the length of the link.

$$V_D = \frac{1}{2}\int_0^l l^2 \varsigma \sqrt{AEI}\left(\frac{w''(x,t)}{\partial t}\right)^2 dx$$

Using the expressions of the shape functions $\Phi_1(x)$ and $\Phi_2(x)$, the dissipation function is derived as:

$$w(x,t) = \Phi_1(x)q_1(t) + \Phi_2(x)q_2(t)$$

$$w''(x,t) = \Phi_1''(x)q_1(t) + \Phi_2''(x)q_2(t)$$

$$\frac{\partial w''(x,t)}{\partial t} = \Phi_1''(x)\dot{q}_1(t) + \Phi_2''(x)\dot{q}_2(t)$$

$$V_D = (\frac{1}{2}l^2\varsigma\sqrt{AEI}\int_0^l \Phi_1''^{\,2}(x)dx)\dot{q}_1(t) + \left(l^2\varsigma\sqrt{AEI}\int_0^l \Phi_1''(x)\Phi_2''(x)dx\right)\dot{q}_1(t)\dot{q}_2(t)$$

$$+\left(\frac{1}{2}l^2\varsigma\sqrt{AEI}\int_0^l \Phi_2''^{\,2}(x)dx\right)\dot{q}_2(t)$$

The term V_D is included in the Lagrange equation and the equations of motion are derived as:

$$\frac{d}{dt}\left(\frac{\partial T}{\partial \dot{q}_i}\right) - \frac{\partial T}{\partial q_i} + \frac{\partial (V + V_D)}{\partial q_i} = F(t)$$

$$C = \begin{bmatrix} 0 & 0 & 0 & 0 \\ 0 & 0 & 0 & 0 \\ 0 & 0 & & \\ 0 & 0 & & C_{qq} \end{bmatrix}$$

where the expression of C_{qq} is given in Appendix A

Table 2: Additional parameters of the single FLFJ manipulator

Damping coefficient of the link	ς	0.005 [28]
Area of cross section of the link	A	0.625e-4 m^2

Using the data in Table 2, the matrix C is expressed as:

$$C = \begin{bmatrix} 0 & 0 & 0 & 0 \\ 0 & 0 & 0 & 0 \\ 0 & 0 & 0.01745 & -0.046533 \\ 0 & 0 & -0.046533 & 0.2792 \end{bmatrix}$$

The equations of motion for the FLFJ manipulator can be accordingly modified as:

$$M \cdot \underline{\ddot{X}} + C\underline{\dot{X}} + K \cdot \underline{X} = \underline{F} \tag{3.3-17}$$

$$M = \begin{bmatrix} J_1 & 0 & 0 & 0 \\ 0 & J_2 + \rho\int_0^L (r+x)^2 dx & \rho\int_0^L (r+x)\Phi_1 dx & \rho\int_0^L (r+x)\Phi_2 dx \\ 0 & \rho\int_0^L (r+x)\Phi_1 dx & \rho\int_0^L \Phi_1^2 & 0 \\ 0 & \rho\int_0^L (r+x)\Phi_2 dx & 0 & \rho\int_0^L \Phi_2^2 dx \end{bmatrix}$$

$$C = \begin{bmatrix} 0 & 0 & 0 & 0 \\ 0 & 0 & 0 & 0 \\ 0 & 0 & l^2\varsigma\sqrt{AEI}\int_0^l \Phi_1''^2 dx & l^2\varsigma\sqrt{AEI}\int_0^l \Phi_1''\Phi_2'' dx \\ 0 & 0 & l^2\varsigma\sqrt{AEI}\int_0^l \Phi_1''\Phi_2'' dx & l^2\varsigma\sqrt{AEI}\int_0^l \Phi_2''^2 dx \end{bmatrix}$$

$$K = \begin{bmatrix} K_S & -K_S & 0 & 0 \\ -K_S & K_S & 0 & 0 \\ 0 & 0 & EI\int_0^L \Phi_1''^2 dx & EI\int_0^L \Phi_1'' \cdot \Phi_2'' dx \\ 0 & 0 & EI\int_0^L \Phi_1'' \cdot \Phi_2'' dx & EI\int_0^L \Phi_2''^2 dx \end{bmatrix}$$

The eigenvalues of the current open-loop system thus become:

$$\lambda_{1,2} = 0,\ \lambda_{3,4} = \pm 37.6\, j$$

$$\lambda_{5,6} = -0.9 \pm 573.3\, j,\ \lambda_{7,8} = -0.9 \pm 1398.7\, j$$

The A matrix in the state space model also has to be modified as:

$$A = \begin{bmatrix} 0 & 0 & 0 & 0 & 1 & 0 & 0 & 0 \\ 0 & 0 & 0 & 0 & 0 & 1 & 0 & 0 \\ 0 & 0 & 0 & 0 & 0 & 0 & 1 & 0 \\ 0 & 0 & 0 & 0 & 0 & 0 & 0 & 1 \\ & & & & & & & \\ & M^{-1}(-K) & & & & & M^{-1}(-C) & \\ & & & & & & & \end{bmatrix}$$

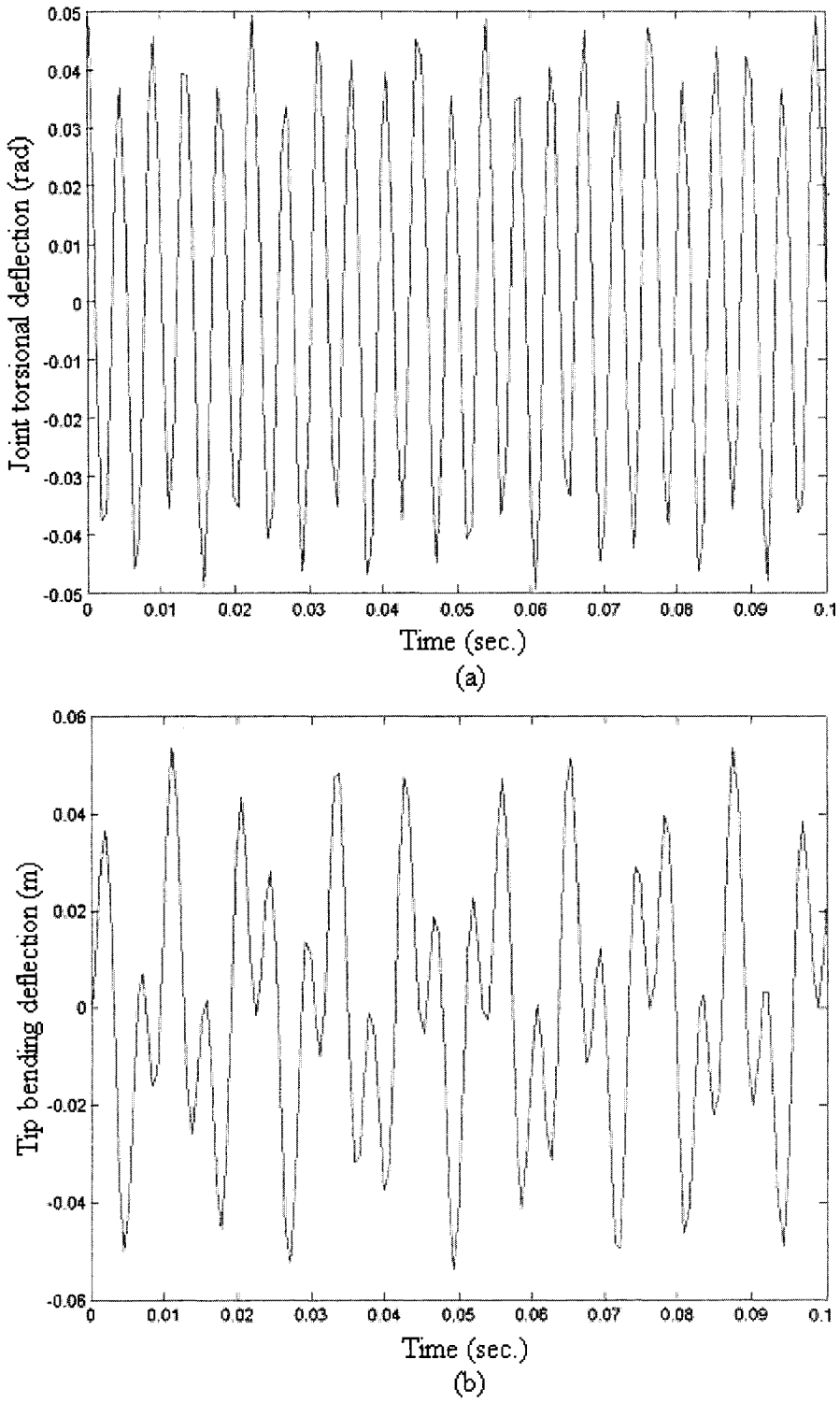

Figure 3: Open-loop responses of the system: (a) Joint torsional deflection (b) Tip bending deflection of the link measured with respect to the frame $X_l Y_l$

3.4 Summaries of modeling

One more coordinate system than for a flexible-link rigid-joint manipulator had to be used to describe the joint torsional deformation. The transformation matrices were used to obtain the global position vector of any point along the link with respect to the inertial frame. The clamped-free modes of the link were used to derive its shape functions. The linear combination of the first two shape functions was applied to represent the horizontal deflection of the link with respect to the local frame. A nonlinear model of the FLFJ system was obtained using the assumed modes method and the Lagrange approach. With the assumption of small elastic motions, the model was linearized around the zero deflection for both the link and the joint. The state space model of the system would be used for the following model analysis and control system design.

Chapter 4: Model Analysis

4.1 Introduction

In this chapter, the analytical solutions of the single FLFJ manipulator are developed. Additionally, the effects of the relative stiffness of the flexible joint with respect to the flexible link (expressed as $K_k = \frac{K_S}{EI/l}$) on the system characteristics and its open-loop responses are studied.

4.2 Analytical solutions of the single FLFJ manipulator

Using the expressions of the transformation matrices M_r and M_e derived in the Section 3.2, the position vector of a point on the link with respect to the global frame can be expressed as:

$$\underline{{}^0r} = \begin{bmatrix} {}^0x \\ y(x,t) \end{bmatrix} = \begin{bmatrix} \cos\theta_1 & -\sin\theta_1 \\ \sin\theta_1 & \cos\theta_1 \end{bmatrix} \begin{bmatrix} \cos\delta & -\sin\delta \\ \sin\delta & \cos\delta \end{bmatrix} \begin{bmatrix} x+r \\ w(x,t) \end{bmatrix}$$

where $\cos\delta \approx \delta$, $\sin\delta \approx \delta$, because the joint torsional deflection δ is assumed to be small in this study. Therefore, we have:

$$\underline{{}^0r} = \begin{bmatrix} {}^0x \\ y(x,t) \end{bmatrix} = \begin{bmatrix} \cos\theta_1 & -\sin\theta_1 \\ \sin\theta_1 & \cos\theta_1 \end{bmatrix} \begin{bmatrix} 0 & -\delta \\ \delta & 0 \end{bmatrix} \begin{bmatrix} x+r \\ w(x,t) \end{bmatrix}$$

The deflection of the link with respect to the global frame was obtained from the above equation (The derivation is given in Appendix A.):

$$y(x,t) = \sin\theta_2 (x+r) + \cos\theta_2 w(x,t) \tag{4.2-1}$$

where: $\theta_2 = \theta_1 + \delta$

Recall the boundary conditions of the cantilever beam:

Geometric boundary conditions:

1) $w(0,t)=0$

2) $\dfrac{\partial w(0,t)}{\partial x}=0 \Rightarrow \dfrac{d\Phi_i(0)}{dx}=0$

Physical boundary conditions:

3) $EI\dfrac{\partial^3 w(l,t)}{\partial x^3}=0 \Rightarrow \dfrac{d^3\Phi_i(l)}{dx^3}=0$

4) $EI\dfrac{\partial^2 w(l,t)}{\partial x^2}=0 \Rightarrow \dfrac{d^2\Phi_i(l)}{dx^2}=0$ (l is the length of the link)

Accordingly, the boundary conditions for the rotating beam are modified as follows:

Geometric boundary conditions:

$$y(0,t)=0 \tag{4.2-2a}$$

$$\frac{\partial y(0,t)}{\partial x}=\sin\theta_2+\cos\theta_2\frac{\partial w(0,t)}{\partial x}=\sin\theta_2 \tag{4.2-2b}$$

Physical boundary conditions:

$$EI\frac{\partial^3 y(l,t)}{\partial x^3}=0 \Rightarrow EI\cos\theta_2\frac{\partial w^3(l,t)}{\partial x^3}=0 \tag{4.2-2c}$$

$$EI\frac{\partial^2 y(l,t)}{\partial x^2}=0 \Rightarrow EI\cos\theta_2\frac{\partial w^2(l,t)}{\partial x^2}=0 \tag{4.2-2d}$$

The torque components applied to the system are represented on the flexible joint, as shown in Figure 4.

$$T_1=L-J_1\ddot{\theta}_1 \tag{4.2-3}$$

$$T_2=J_2\ddot{\theta}_2-EI\frac{\partial y^2(0,t)}{\partial x^2} \tag{4.2-4}$$

$$T_1=T_2$$

The dynamic equation of the joint is derived as:

$$T_1 = T_2 = K_S(\theta_1 - \theta_2)$$

$$L - J_1\ddot{\theta}_1 = J_2\ddot{\theta}_2 - EI\frac{\partial y^2(0,t)}{\partial x^2} = K_S(\theta_1 - \theta_2) = -K_S\delta \tag{4.2-5}$$

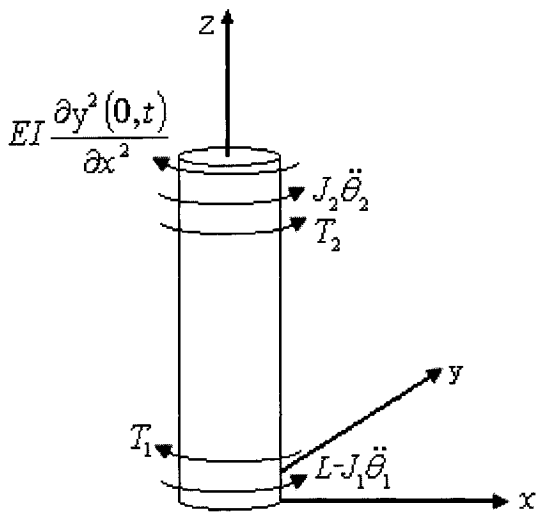

Figure 4: Free-body diagram of the flexible joint

The deflection of a point along the link with respect to the inertial frame is expressed as:

$$y(x,t) = \sum_{n=1}^{\infty} \overline{\Phi}_n(x)\cos(\omega_n t) \tag{4.2-6}$$

where $\overline{\Phi}(x)$ denotes the n th shape function and ω_n is the n th natural frequency of the manipulator.

$$\overline{\Phi}(x) = C_n[\sin\lambda_n x + \alpha_n \sinh\lambda_n x] \text{ [38]} \tag{4.2-7}$$

$$\alpha_n = \left(\frac{\sin\lambda_n l}{\sinh\lambda_n l}\right)$$

$$\omega_n = \lambda_n{}^2 l^2 \sqrt{\frac{EI}{\rho}} \tag{4.2-8}$$

To analyze the natural free vibration, all the external forces were set to be zero, i.e. $L = 0$. Derived from Equation (4.2-5),

$$\delta = -\frac{J_2}{K_S}\ddot{\theta}_2 + \frac{EI}{K_S}\left(\frac{\partial^2 y(0,t)}{\partial x^2}\right) \tag{4.2-9}$$

From the second geometric boundary condition of the rotating FLFJ manipulator, the following equations can be obtained:

$$\sin\theta_2 = \frac{\partial y(0,t)}{\partial x} \tag{4.2-10}$$

$$\theta_2(t) = \sin^{-1}\left(\sum_{n=1}^{\infty}\overline{\Phi}_n'(0)\cos(\omega_n t)\right), \left(|\theta_2| \le \frac{\pi}{2}\right) \tag{4.2-11}$$

The first derivative with respect to time of Equation (4.2-10) gives:

$$\dot{\theta}_2 \cos\theta_2 = \frac{\partial^2 y(0,t)}{\partial x \partial t} \tag{4.2-12}$$

The second derivative with respect to time of Equation (4.2-10) gives:

$$\ddot{\theta}_2 \cos\theta_2 - \dot{\theta}_2{}^2 \sin\theta_2 = \frac{\partial^3 y(0,t)}{\partial x \partial t^2} \tag{4.2-13}$$

Deriving from Equations (4.2-10),

$$\cos\theta_2 = \sqrt{1-\left(\frac{\partial y(0,t)}{\partial x}\right)^2}, \left(|\theta_2| \le \frac{\pi}{2}\right) \tag{4.2-14}$$

Putting Equation (4.2-14) into Equation (4.2-12),

$$\dot{\theta}_2(t) = \frac{\left(\frac{\partial^2 y(0,t)}{\partial x \partial t}\right)}{\sqrt{1-\left(\frac{\partial y(0,t)}{\partial x}\right)^2}} \tag{4.2-15}$$

Putting Equations (4.2-10, 4.2-14 and 4.2-15) into Equation (4.2-13),

$$\ddot{\theta}_2(t) = \frac{\left(\frac{\partial^3 y(0,t)}{\partial x \partial t^2}\right)\left[1-\left(\frac{\partial y(0,t)}{\partial x}\right)^2\right]+\left(\frac{\partial^2 y(0,t)}{\partial x \partial t}\right)^2\left(\frac{\partial y(0,t)}{\partial x}\right)}{\left[1-\left(\frac{\partial y(0,t)}{\partial x}\right)^2\right]^{\frac{3}{2}}} =$$

$$\frac{-\sum_{n=1}^{\infty}\omega_n{}^2\overline{\Phi}'_n(0)\left[1-\sum_{n=1}^{\infty}\left(\overline{\Phi}'_n(0)\cos(\omega_n t)\right)^2\right]\cos(\omega_n t)+[\sum_{n=1}^{\infty}\omega_n\overline{\Phi}'_n(0)\sin(\omega_n t)]^2\sum_{n=1}^{\infty}\overline{\Phi}'_n(0)\cos(\omega_n t)}{\left[1-\left(\sum_{n=1}^{\infty}\overline{\Phi}'_n(0)\cos(\omega_n t)\right)^2\right]^{\frac{3}{2}}}$$

(4.2-16)

Differentiating Equation (4.2-7) with respect to space variable x and putting x=0, we get:

$$\overline{\Phi}'_n(0) = C_n(1+\alpha_n)\lambda_n \tag{4.2-17}$$

$$\overline{\Phi}''_n(0) = 0 \tag{4.2-18}$$

Applying Equations (4.2-17 and 4.2-18) into Equations (4.2-9, 4.2-10, 4.2-11, 4.2-14 and 4.2-16), the following equations are derived as:

$$\delta(t) = -\frac{J_2}{K_S}\ddot{\theta}_2(t) + \frac{EI}{K_S}\left(\sum_{n=1}^{\infty}\Phi_n''(0)\cos(\omega_n t)\right) = -\frac{J_2}{K_S}\ddot{\theta}_2(t)$$

$$\ddot{\theta}_2(t) = \frac{-\sum_{n=1}^{\infty}\omega_n{}^2 C_n(1+\alpha_n)\lambda_n\left[1-\sum_{n=1}^{\infty}[C_n(1+\alpha_n)\lambda_n\cos(\omega_n t)]^2\right]\cos(\omega_n t) + [\sum_{n=1}^{\infty}\omega_n(C_n(1+\alpha_n)\lambda_n)\sin(\omega_n t)]^2\sum_{n=1}^{\infty}C_n(1+\alpha_n)\lambda_n\cos(\omega_n t)}{\left[1-\left(\sum_{n=1}^{\infty}C_n(1+\alpha_n)\lambda_n\cos(\omega_n t)\right)^2\right]^{\frac{3}{2}}}$$

$$\theta_2(t) = \sin^{-1}\left(\sum_{n=1}^{\infty}C_n(1+\alpha_n)\lambda_n\cos(\omega_n t)\right)$$

$$w(x,t) = \frac{y(x,t) - x\sin\theta_2}{\cos\theta_2} = \frac{\sum_{n=1}^{\infty}\overline{\Phi}_n(x)\cos(\omega_n t) - x\sum_{n=1}^{\infty}C_n(1+\alpha_n)\lambda_n\cos(\omega_n t)}{\left[1-\left(\sum_{n=1}^{\infty}C_n(1+\alpha_n)\lambda_n\cos(\omega_n t)\right)^2\right]^{\frac{1}{2}}}$$

$$\theta_1(t) = \theta_2 - \delta = \sin^{-1}\left(\sum_{n=1}^{\infty}C_n(1+\alpha_n)\lambda_n\cos(\omega_n t)\right) + \frac{J_2}{K_S}\ddot{\theta}_2(t)$$

4.3 Effect of the relative joint stiffness on the system characteristics

Li *et al.* [24] used an analytical method to investigate the tendency of modal roots of flexible links with incremental joint stiffness. All of the first four roots increased monotonically with the relative joint stiffness. In addition, it was concluded that even a small joint flexibility could have great effect on the system frequencies. In this study, the relation between the natural frequencies of the FLFJ manipulator and the relative joint stiffness was studied based on the model described in Chapter 3. The relative joint stiffness was defined as $K_K = \frac{K_S \cdot l}{EI}$. From Figure 5, it can be seen that the first frequency and the second frequency remain almost unchanged as the relative joint stiffness increases, while the third and the fourth ones have monotonically increasing trends.

The frequencies mentioned above were for the single FLFJ manipulator with linear interactions between the flexible joint and the flexible link and were named 'coupled frequencies'. The frequencies of the manipulator with only a flexible joint or a flexible link were called 'individual frequencies.' The interaction between the flexible joint and the flexible link in the FLFJ system was indicated by the difference between the coupled frequencies and the individual frequencies. The frequencies of a single Rigid-Link Flexible-Joint (RLFJ) manipulator with ten different joint stiffness values are given in Table 3(a). The first two modal frequencies of a single Flexible-Link Rigid-Joint (FLRJ) manipulator with a constant link flexural rigidity (EI) are also displayed in Table 3(a). The frequencies of a single FLFJ manipulator with ten combinations of joint stiffness and link flexural rigidity are shown in Table 3(b). In the FLFJ system, the joint stiffness values are those used in the RLFJ system and the link flexural rigidity is kept unchanged and equal to the value in the

FLRJ system. It was assumed that all the other system parameters are the same in these three systems. It can be seen from the comparison between Table 3(a) and Table 3(b) that the first modal frequency of the FLRJ manipulator was retained and kept unchanged in the FLFJ system, which was the second coupled frequency. However, both the torsional frequency of the RLFJ manipulator and the second modal frequency of the FLRJ manipulator were affected by the interactions between the flexible joint and the flexible link. The larger the joint stiffness was, the stronger was the effect. It can be also seen from Figure 5.

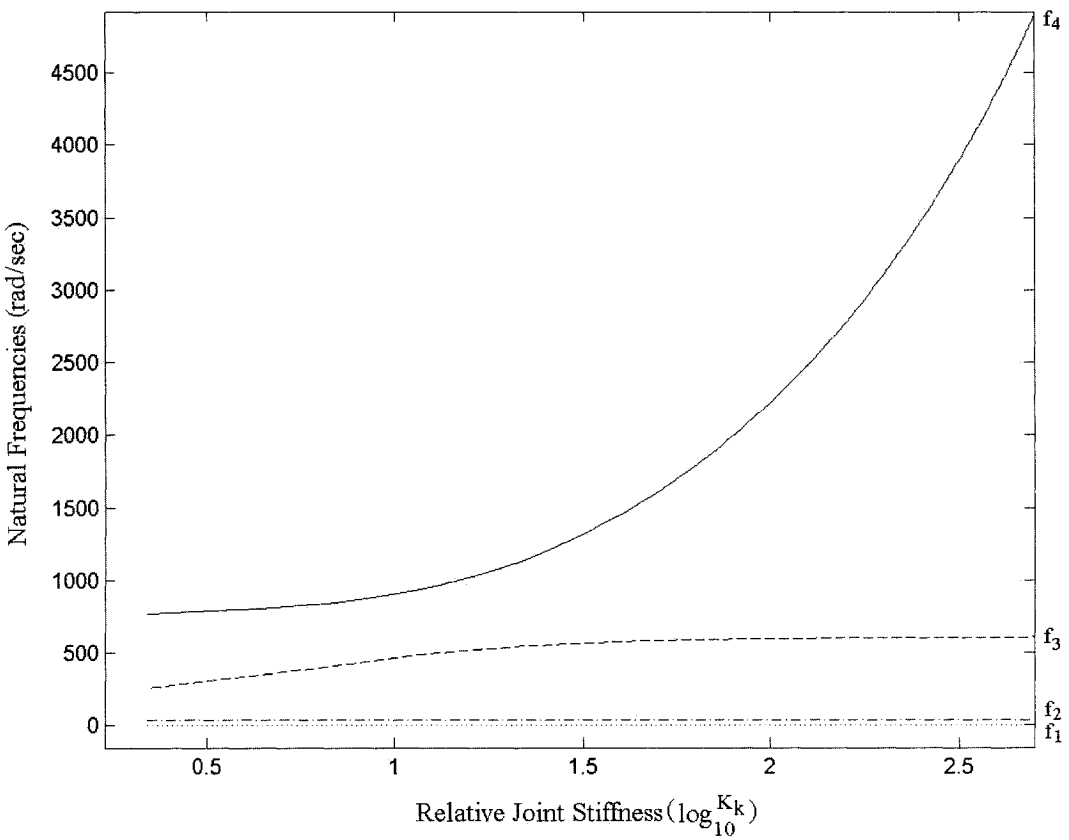

Figure 5: Effect of the relative joint stiffness on the first four frequencies of the single FLFJ manipulator

Table 3(a): Natural frequencies of a single RLFJ manipulator with ten different joint stiffness values and the first two frequencies of a single FLRJ manipulator

The individual frequencies (*rad* / sec)				
Rigid-link flexible-joint (RLFJ) manipulator			Flexible-link rigid-joint (FLRJ) manipulator (EI= 2.282 $N \cdot m^2$)	
Joint stiffness (*Nm* / *rad*)	Rigid body	Torsional	1st	2nd
10	0	263.83	37.577	610.19
20	0	373.12		
30	0	456.97		
40	0	527.67		
50	0	589.95		
60	0	646.26		
70	0	698.04		
80	0	746.24		
90	0	791.5		
100	0	834.32		

Table 3(b): Natural frequencies of a single FLFJ manipulator

The coupled frequencies (*rad* / sec)				
Joint stiffness (*Nm* / *rad*) Link flexural rigidity EI= 2.282 $N \cdot m^2$	1st	2nd	3rd	4th
10	0	37.577	254.86	772.5
20	0	37.577	346.48	803.6
30	0	37.577	406.14	839.63
40	0	37.577	447.68	879.55
50	0	37.577	477.45	922.05
60	0	37.577	499.28	965.9
70	0	37.577	515.65	1010.2
80	0	37.577	528.2	1054.3
90	0	37.577	538.04	1097.8
100	0	37.577	545.91	1140.5

4.4 Effect of the relative joint stiffness on the system open-loop responses

The analytical expressions for the two angular positions $\theta_1(t)$ and $\theta_2(t)$, the joint torsional deformation $\delta(t)$ and the tip deflection of the link with respect to the local frame $w(x,t)$ were given in Section 4.2. The simulated responses of the FLFJ manipulator based on the linear model derived in Chapter 3 were obtained using Matlab/Simulink. The system was excited by a sinusoidal torque with a period of 1 sec and a magnitude of 1 Nm. As expected, the deflections inside the system had a sinusoidal motion with the same period. The responses of the system with a joint flexibility of 166 Nm/rad are shown in Figure 6.

The stiffness of the flexible link was kept constant and the joint stiffness was changed from 10 to 1e4 (the reason why the value began with 10 was to make sure the joint deformation was kept small). Figure 7 shows that as the joint stiffness increased, changes occurred in both the maximum magnitudes for the joint torsional deflection and the tip bending deflection of the link with respect to the frame $X_m Y_m$. Increasing the joint stiffness from 10 to 1e4, the joint deformation converged to zero. When the joint stiffness reached 1e4, the joint became almost rigid. There was no joint deformation and the angular position of the motor shaft was equal to that of the hub/link. From Figure 7, it can be seen that there was little change in the maximum magnitude of the tip deflection of the link with respect to the frame $X_l Y_l$ with the variation of the joint stiffness when the manipulator was driven by a sinusoidal torque. The tip deflection of the link with respect to the frame $X_m Y_m$ can be obtained through the formula ${}^m y(l,t) = \delta(t)(l+r) + w(l,t)$, and it thus converged to the value measured with respect to the frame $X_l Y_l$ as the joint flexibility disappeared. In order to

eliminate vibrations, a control law intended to simultaneously eliminate the joint deflection and the tip deflection needs to be applied.

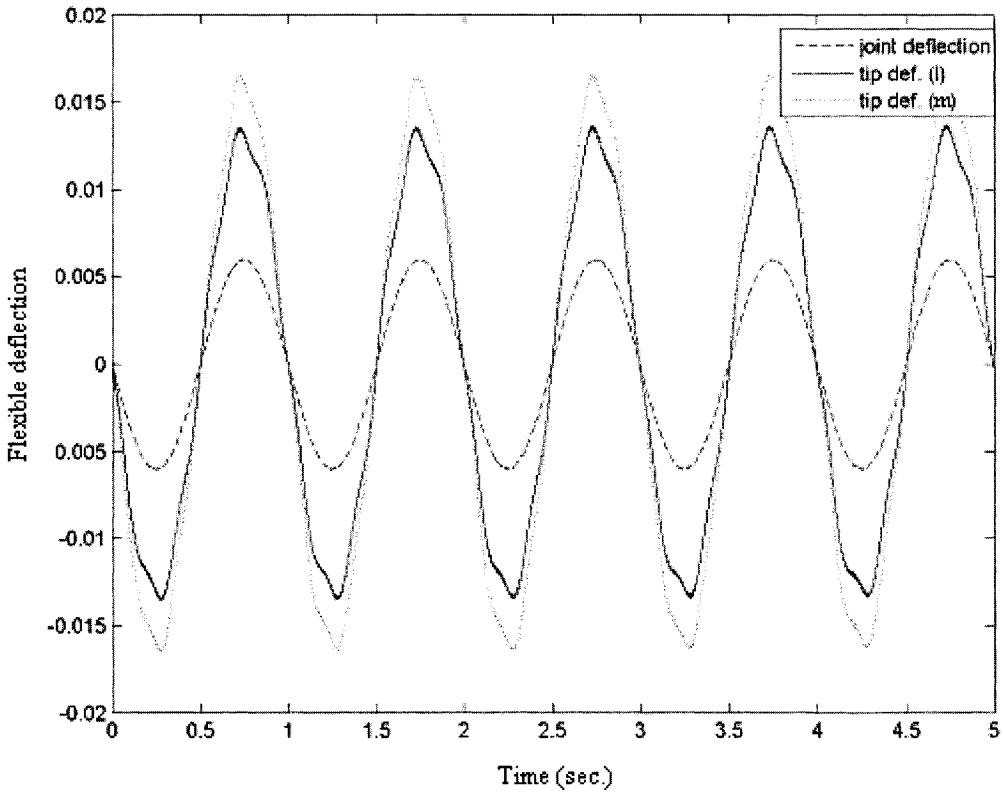

Figure 6: Open-loop responses of the system subjected to a sinusoidal input

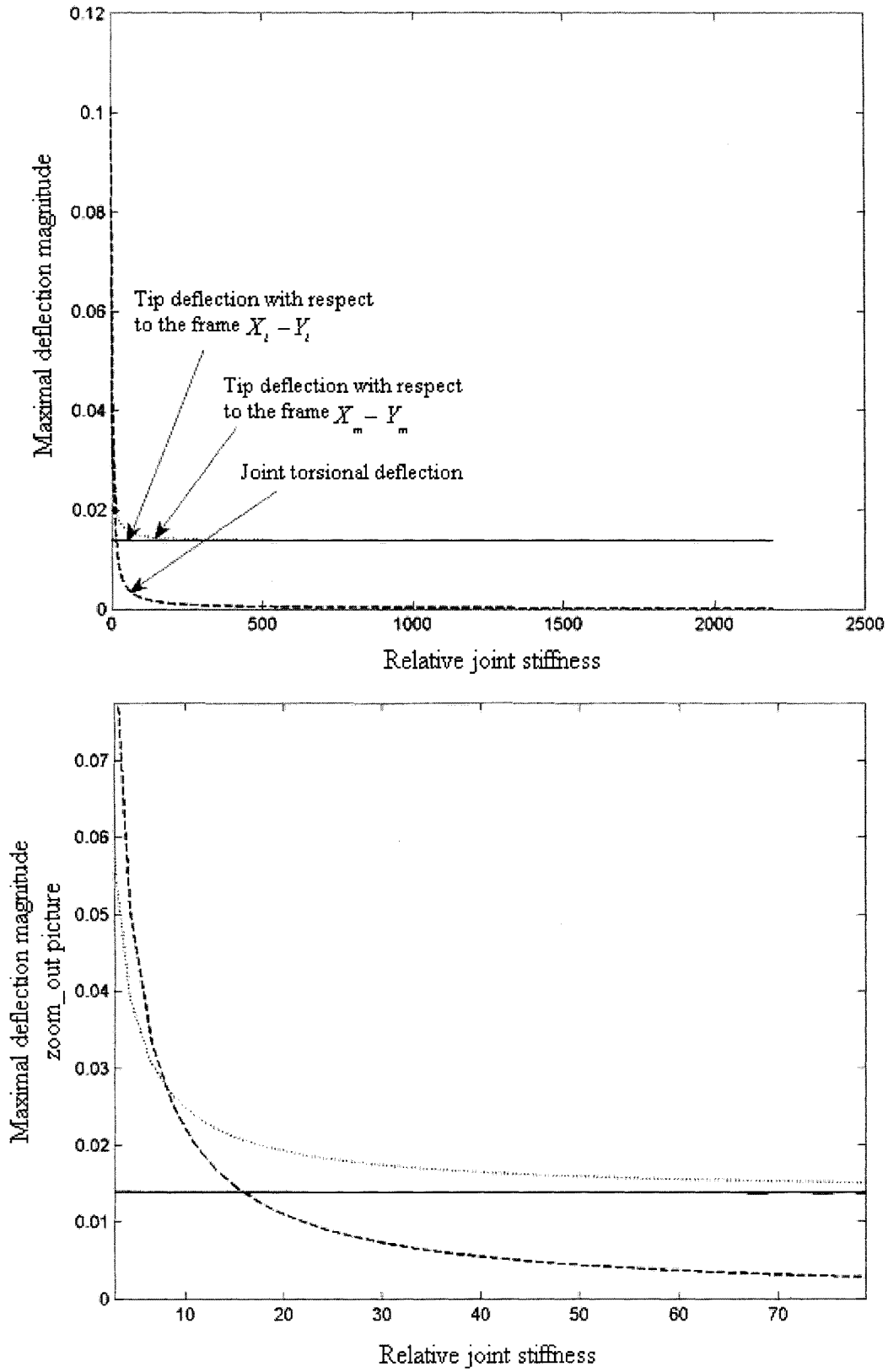

Figure 7: Effect of the relative joint stiffness on the open-loop responses

4.5 Conclusions

The analytical solutions of the single FLFJ manipulator were obtained for any rotational angle. It was found that the higher order frequencies of the system are more sensitive to the interaction between the link flexibility and the joint flexibility. In addition, it was also demonstrated using the methods in this study that the link deformation was increased by the flexible joint. The more flexible it is, the more serious the effect is.

Chapter 5: Control System Design and Simulation Results

5.1 Introduction

In this chapter, a control law based on two nested feedback loops is applied to control the unexpected vibration and angular position of the manipulator. In the inner loop, two time-delayed feedback signal controllers which only utilize the position angles of the manipulator are developed to eliminate the vibration. Critical time delays are obtained for both of the controllers, with which the system undergoes stability changes. In the outer loop, a modified PD controller is applied to make the position angle of the manipulator to track a step reference input. The proposed control system is then compared with LQR to show its superiority. The robustness of the control system is also investigated in two aspects, being subjected to an external disturbance and system parameter uncertainties. The analysis in this chapter is based on the computer simulation Matlab/Simulink.

5.2 Time-Delayed Feedback Signal (DFS) control

In this section, two control signals are applied to eliminate the unexpected vibration of the flexible link and the flexible joint. One control signal is $u = -K[\theta_1(t) - \theta_1(t-\tau)]$ and is named as 'position angle DFS controller'. The other one is $u = K[\delta(t) - \delta(t-\tau)]$ which is called 'joint deflection DFS controller'. They are equivalent to the proportional control action. The control signal is proportional to the difference between the current value of the system variable and its historical value. The block diagram of the delayed feedback signal control system is shown in Figure 8. The main objective of this controller is to control the vibration without having to obtain all the state variables of the system. It is especially

significant for the generalized displacements q_1 and q_2 of the flexible link because these variables are difficult or even impossible to measure.

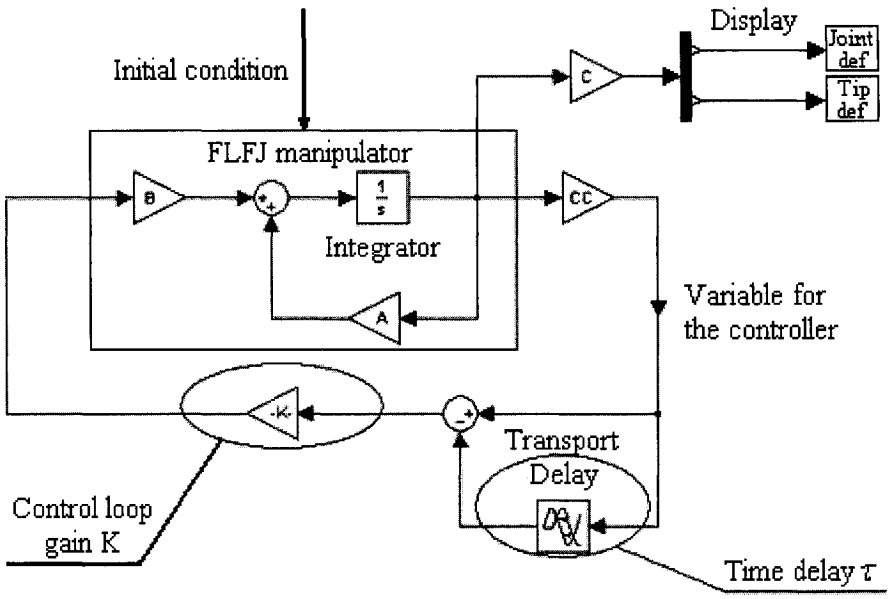

Figure 8: Simulation diagram of the system controlled by the DFS controller

5.2.1 Position angle DFS controller

The control signal takes the following form:

$$u = -K[\theta_1(t) - \theta_1(t-\tau)] \tag{5.2-1}$$

where, $\theta_1(t)$ is the current position angle of the motor shaft and $\theta_1(t-\tau)$ is its value τ seconds earlier. Within this controller, there are two parameters that need to be considered. One is the time delay τ and the other is the gain K. The method introduced in [7, 39] is applied here to the single FLFJ manipulator to obtain the critical time delays for each gain value. The reason why they are called critical time delays is that when τ is equal to one of theses values there are poles crossing the imaginary axis on the complex plane.

Based on the state space model $\dot{X} = AX + BU$ and the control feedback signal u (here $U = u$), the system is modified as:

$$\dot{X}(t) = (A - KBC)X(t) + KBCX(t-\tau) \tag{5.2-2}$$

where: $C = [1 \quad 0 \quad 0 \quad 0 \quad 0 \quad 0 \quad 0 \quad 0]$

Taking the Laplace transform for Equation (5.2-2), we get:

$$X(s)\cdot[sI - A + KBC(1 - \exp(-s\tau))] = 0 \tag{5.2-3}$$

The characteristic equation of the system is:

$$\left|sI - A + KBC(1 - \exp(-s\tau))\right| = 0 \tag{5.2-4}$$

Equation (5.2-4) can be written in the following compact form:

$$P(s) + Q(s)\exp(-s\tau) = 0$$

where $\tau \geq 0$ is the time delay, $P(s)$ and $Q(s)$ are two polynomials with real coefficients. In order to analyze the marginal stability, $s = j\omega$ was set in the characteristic equation.

$$P(j\omega) + Q(j\omega)\exp(-j\omega\tau) = 0 \tag{5.2-5}$$

$$P(j\omega) = P_R(\omega) + jP_I(\omega) \tag{5.2-6a}$$

$$Q(j\omega) = Q_R(\omega) + jQ_I(\omega) \tag{5.2-6b}$$

In order to have roots on the imaginary axis,

$$\left|P(j\omega) + Q(j\omega)\exp(-j\omega\tau)\right| = 0 \tag{5.2-7}$$

Substituting $\cos(\omega\tau) - j\sin(\omega\tau)$ for $\exp(-j\omega\tau)$ and putting Equation (5.2-6) into Equation (5.2-7),

$$\left|P_R(\omega) + jP_I(\omega) + (Q_R(\omega) + jQ_I(\omega))(\cos(\omega\tau) - j\sin(\omega\tau))\right| = 0$$

For a vector $(a + jb)$, if $|a + jb|$ is equal to zero, its real part a and imaginary part b must be both zero. Therefore:

$$P_R(\omega) + Q_R(\omega)\cos(\omega\tau) + Q_I(\omega)\sin(\omega\tau) = 0 \tag{5.2-8a}$$

$$P_I(\omega) - Q_R(\omega)\sin(\omega\tau) + Q_I(\omega)\cos(\omega) = 0 \tag{5.2-8b}$$

Derived from Equation (5.2-8), we get:

$$F(\omega) = P_R{}^2 + P_I{}^2 - \left(Q_R{}^2 + Q_I{}^2\right) = 0$$

The critical time delays could be found, if and only if $F(\omega) = 0$ has at least one simple positive root [7]. If it has no simple positive roots, the system is delay-independent stable if the system free of delay is stable or delay-independent unstable if the system is unstable when the time delay disappears. The authors of [7, 39] provided the formula to obtain the critical time delays from the roots of $F(\omega) = 0$.

$$\tau_p = \frac{\theta}{\omega} + \frac{2p\pi}{\omega},\ p = 0,1,2\cdots \tag{5.2-9}$$

$$\begin{cases} \sin\theta = \dfrac{-P_R Q_I + P_I Q_R}{Q_R{}^2 + Q_I{}^2} \\ \cos\theta = \dfrac{-P_R Q_R - P_I Q_I}{Q_R{}^2 + Q_I{}^2} \end{cases}, \qquad \theta \in [0, 2\pi) \tag{5.2-10}$$

Using the data in Table 1 and Table 2, the four polynomials $P_R(\omega), P_I(\omega), Q_R(\omega)$ and $Q_I(\omega)$ are written as:

$$\begin{aligned} P_R(\omega) &= \left(\omega^8 - 2.2872e6\omega^6 + 6.4666e11\omega^4 - 9.0855e14\omega^2\right) \\ &+ \left(-6.8966e3\omega^6 + 7.8782e9\omega^4 - 4.6089e13\omega^2 + 4.4765e16\right)K \end{aligned}$$

$$P_I(\omega) = \left(-3.657\omega^7 + 4.2355e6\omega^5 - 1.1887e10\omega^3\right) + \left(2.522e4\omega^5 - 3.3705e8\omega^3 + 5.8568e11\omega\right)K$$

$$Q_R(\omega) = -\left(-6.8966e3\omega^6 + 7.8782e9\omega^4 - 4.6089e13\omega^2 + 4.4765e16\right)K$$

$$Q_I(\omega) = -\left(2.522e4\omega^5 - 3.3705e8\omega^3 + 5.8568e11\omega\right)K$$

The root ω was calculated for different gain values. If the gain value was selected from 20 to 300 with a step of 40, 7 positive roots could be found for each gain (see Table 4).

Table 5 and Table 6 shows the critical time delays calculated and described for four gain values (20, 100, 180 and 300). When the gain value was chosen as 20, the critical time delays were obtained for every root ω based on the formulas 5.2-9 and 5.2-10. The first 20 time delays ($p = 0,1,...,20$) for each root were considered. They were put in an increasing order no matter which root ω and which coefficient p were used to obtain them. If the critical time delay corresponded to an odd order root (ω_1, ω_3, ..., ω_{2i-1} ...), a pair of poles of the system moved from left region to right region on the complex plane; the corresponding time delay was called a unstable critical time delay. If the critical time delay was produced by an even order root (ω_2, ω_4, ..., ω_{2i} ...), it was called a stable critical time delay because a pair of poles of the system crossed the imaginary axis from the right to left area on the complex plane. The number of the pairs of the poles on the right region for each critical time delay is also displayed in Table 5. If the number is greater than zero, the system with the corresponding time delay is unstable; the system becomes stable again after the number is changed back to zero. The last critical time delay with which the system can be stable was achieved when the number would not come back to zero any more. In Table 5, the last critical time delay point is shown in the shadowed box. In other words, the system would be unstable forever after this critical point. The same procedure was applied to the other three gains (100, 180, and 300). For these three gain values, the first critical time delay is the last time delay at which the system remains stable. All the time delays after it would destabilize the system. The critical time delays for $K = 100$, 180 and 300 are given in Table 6.

A new term named "boundary time point" was proposed here, because there was not only one unstable critical time delay between two stable critical time delay points for each gain setting. For example, in Table 5, there are five unstable critical time delays between the

two stable critical time delays of 0.004465 sec and 0.013448 sec. The system would be unstable when the time delay was set at them. Therefore, the "boundary time point" clearly defines the time delay point at which the stability of the system changes. Table 5 and Table 6 were compacted into Table 7 to display only the boundary time points. If the boundary time point was an unstable critical time delay, the system was still stable at this point (a state called 'critical stable') and became unstable immediately after it. If the boundary time point was a stable critical time delay, the system became stable beginning at this boundary point. The tip deflection of the link with respect to the moving frame 2 and the joint torsional deflection were examined for different combinations of gain and time delay values when the system was subjected to initial conditions $[0 \quad 0.05 \quad 0 \quad 0 \quad 0 \quad 0 \quad 0 \quad 0]$. For example, taking $K = 20$ and $\tau = 0.001 < 0.002183$ sec, the system response was asymptotically stable, meaning that there were no poles on the right region of the complex plane. When the time delay reached the first critical time delay (the first boundary time point), the system became critical stable. Right after that, the system became unstable when $\tau = 0.003$ sec. At this time, there was one pair of poles on the right region. The system was stable again when τ was set at the second critical time delay (the second boundary time point) which was the stable critical time delay. Therefore, the system was certainly stable when the time delay was set at any time value between this boundary time point and the next one. The stable response of the system at $\tau = 0.0046$ sec is shown in Figure9 for the tip deflection of the link and in Figure 13 for the joint torsional deflection. The last critical time delay to stabilize the system was $\tau = 0.022431$ sec, while the next critical time delay $\tau = 0.02338$ sec would destabilize the system forever. Three time delay values were examined for gains $K = 100,\ 180$ and 300, because they only had one boundary time point. When $\tau = 0.001$ sec, which was smaller

than the boundary time point, the system was stable. The response became critical stable when time delay was set at the boundary time point and unstable instantly after it. The unstable responses of the system at $\tau = 0.5$ sec were also investigated. The stability switches of the systems with gains $K = 100$, 180 and 300 can be seen in Figures 10-12 and Figures 14-16. It was found that an appropriate combination of control loop gain K and time delay value τ (i.e. $K = 180$ and $\tau = 0.001$ sec) could eliminate the unexpected vibration of the flexible link and joint greatly.

Table 4: Positive real roots for different gain values in the system under the position angle DFS controller

k=20	k=60	k=100	k=140	k=180	k=220	k=260	k=300
1451.6	1572.2	1703.5	1836.9	1967.6	2094	2215.4	2331.9
1399	1398.9	1398.9	1398.9	1398.9	1398.9	1398.9	1398.9
672.95	799.33	871.77	916.15	945.17	965.26	979.86	990.88
573.37	573.37	573.37	573.37	573.37	573.37	573.37	573.37
43.376	53.815	58.188	60.52	61.969	62.956	63.671	64.214
37.579	37.579	37.579	37.579	37.579	37.579	37.579	37.579
31.579	34.271	34.626	34.762	34.833	34.877	34.907	34.928

Table 5: Critical time delays (sec.) for $K = 20$ in the system under the position angle DFS controller

k=20					
τ	0.002183	**0.004465**	0.004706	0.006511	0.008957
#	1	**0**	1	2	1
τ	0.010839	0.010931	**0.013448**	0.014043	0.015168
#	2	1	**0**	1	2
τ	0.017939	0.019496	0.021889	**0.022431**	0.02338
#	1	2	1	**0**	1
τ	0.023824	0.026922	0.028153	0.031413	0.032481
#	2	1	2	1	2

Note: The symbol τ denotes the critical time delay while the symbol # represents the number of the pairs of poles on the right region of the complex plane corresponding to each time delay. The value in the shadowed box is the final time delay at which the system could still be stable, meaning that the system would be unstable forever after this critical point.

Table 6: Critical time delays (sec.) for $K = 100,\ 180,\ 300$ in the system under the position angle DFS controller

k=100					
τ	0.001845	0.003629	0.004486	0.005534	0.008978
#	1	2	1	2	1
k=180					
τ	0.001597	0.003357	0.004489	0.00479	0.007983
#	1	2	1	2	3
k=300					
τ	0.001347	0.003219	0.004042	0.00449	0.006736
#	1	2	3	2	3

Table 7: Boundary time points (sec.) for the system under the control of the position angle DFS controller

k=20	k=100	k=180	k=300
0.002183	0.001845	0.001597	0.001347
0.004465			
0.004706			
0.013448			
0.014043			
0.022431			
0.02338			

Note: The odd time point marks the end of a stable state and the beginning of an unstable state, while the even one marks the end of an unstable state and the beginning of a stable state. All of the boundary points were obtained from the critical time delays in Table 5 and Table 6.

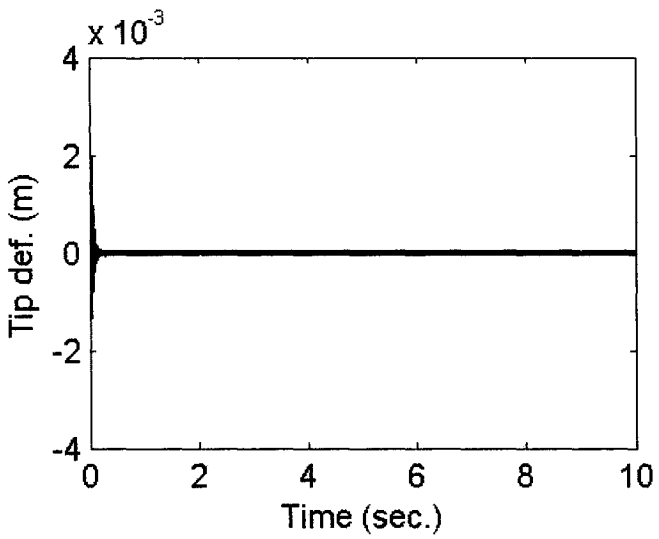

(a) K=20, τ=0.001

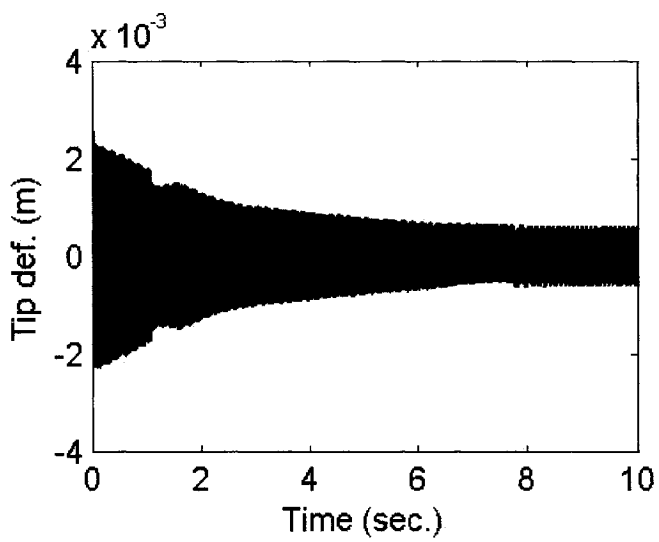

(b) K=20, τ =0.002183

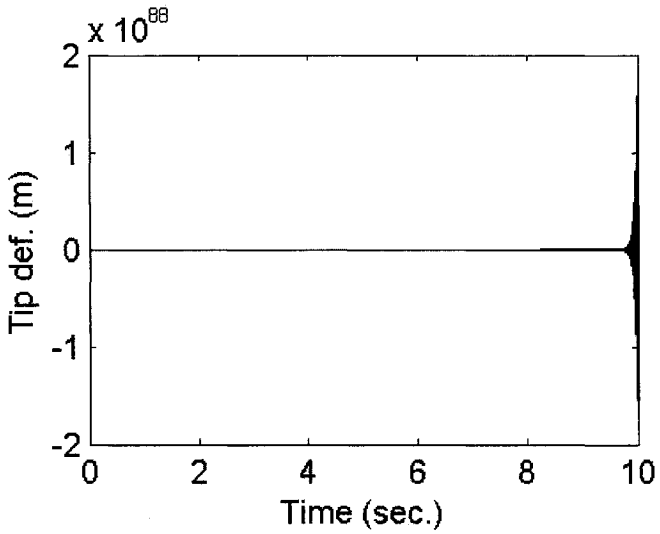

(c) K=20, τ =0.003

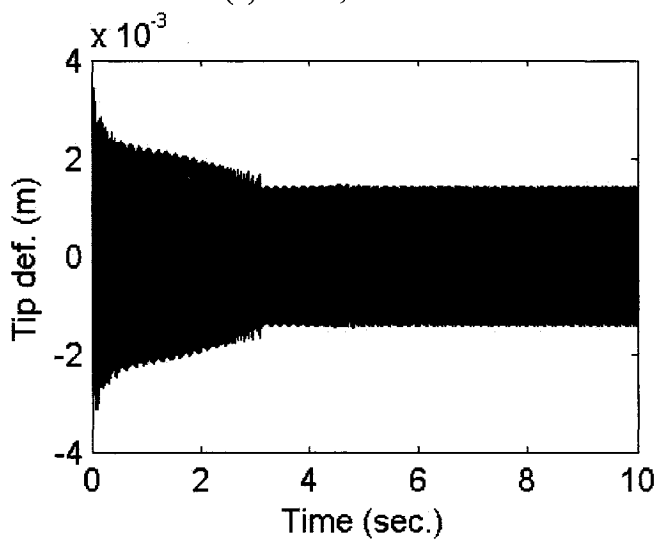

(d) K=20, τ =0.004465

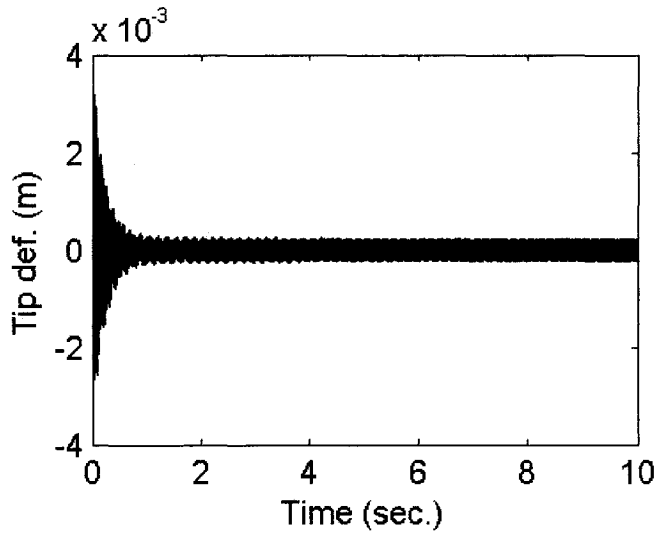

(e) K=20, τ =0.0046

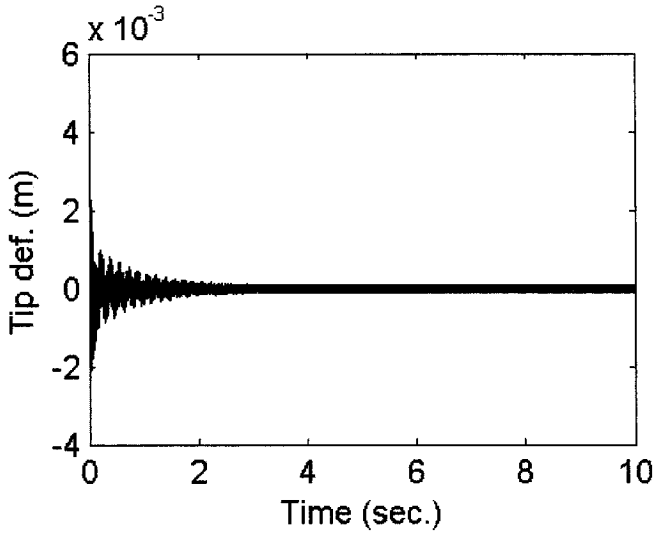

(f) K=20, τ =0.02338

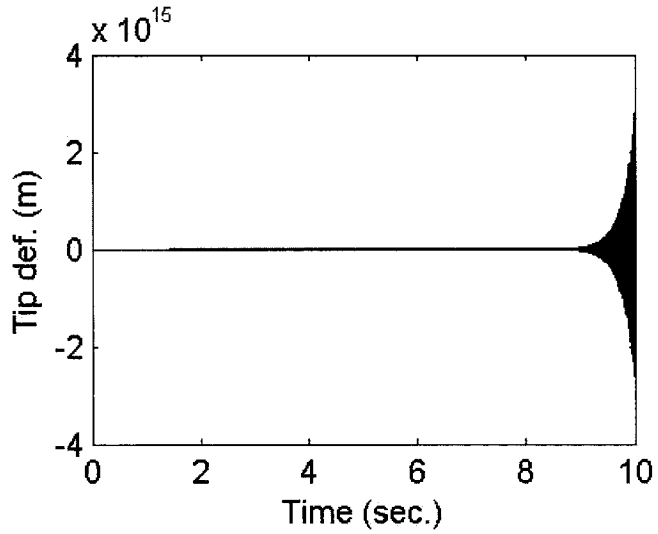

(g) K=20, τ =0.5

Figure 9: Tip deflection of the link under the position angle DFS controller (K=20)

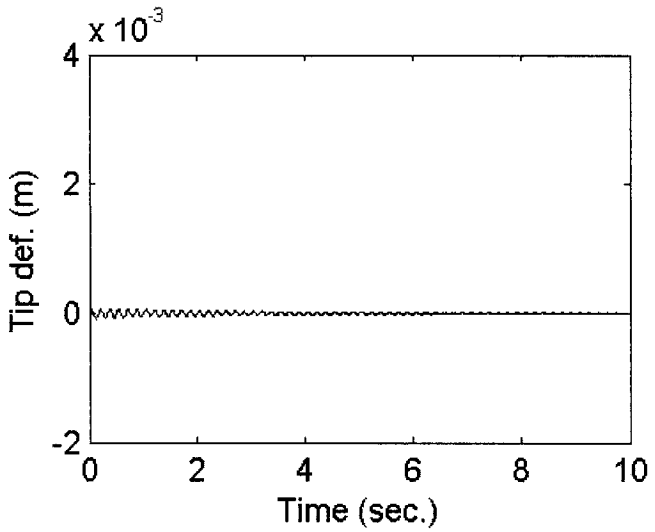

(a) K=100, τ =0.001

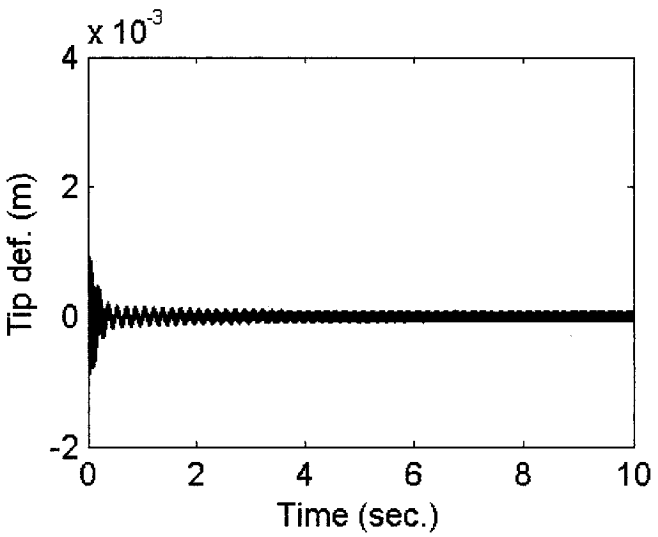

(b) K=100, τ =0.001845

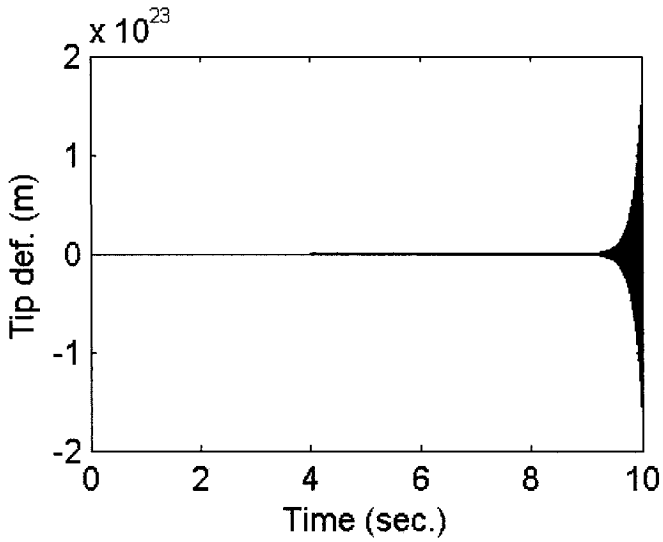

(c) K=100, τ =0.5

Figure 10: Tip deflection of the link under the position angle DFS controller (K=100)

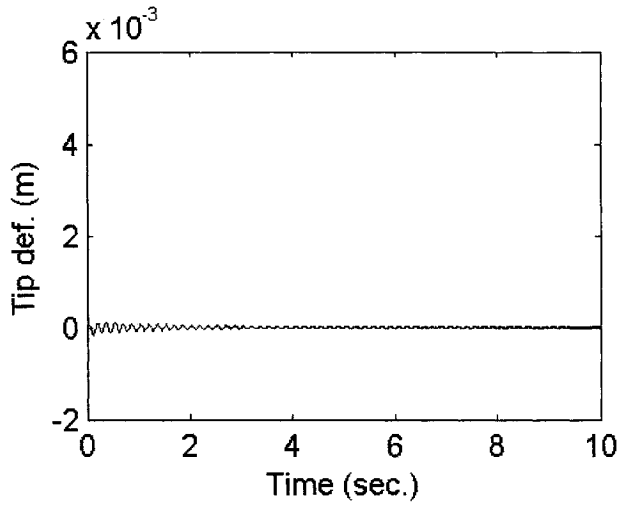

(a) K=180, τ =0.001

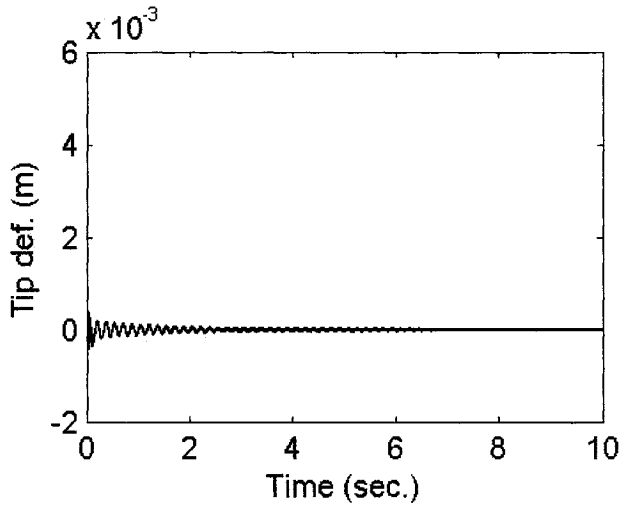

(b) K=180, τ =0.001597

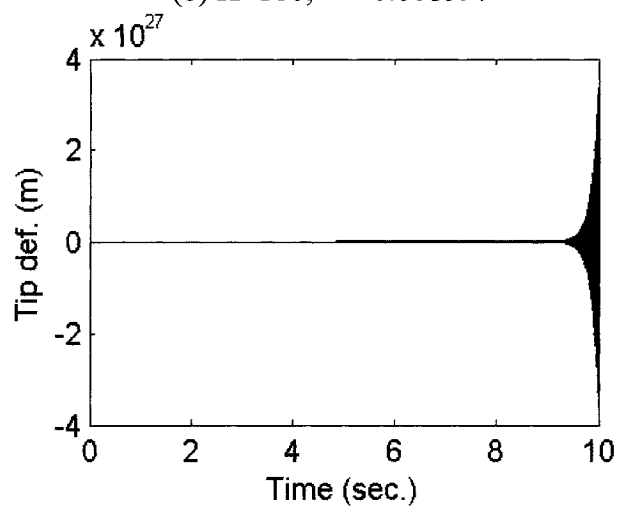

(c) K=180, τ =0.5

Figure 11: Tip deflection of the link under the position angle DFS controller (K=180)

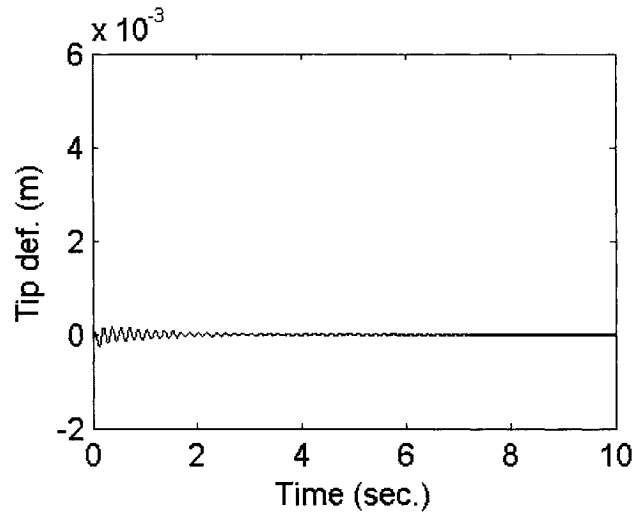

(a) K=300, τ =0.001

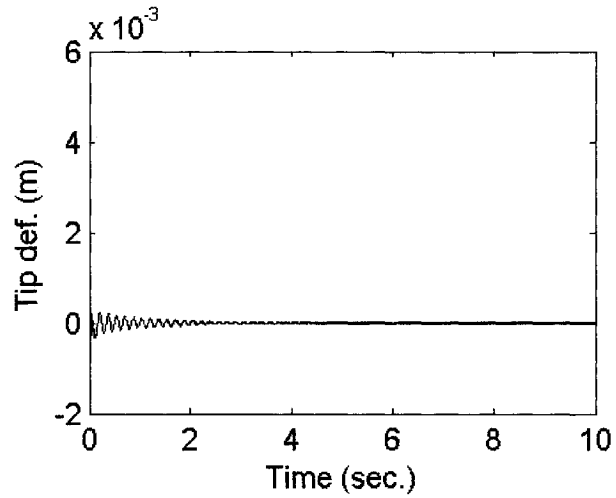

(b) K=300, τ =0.001347

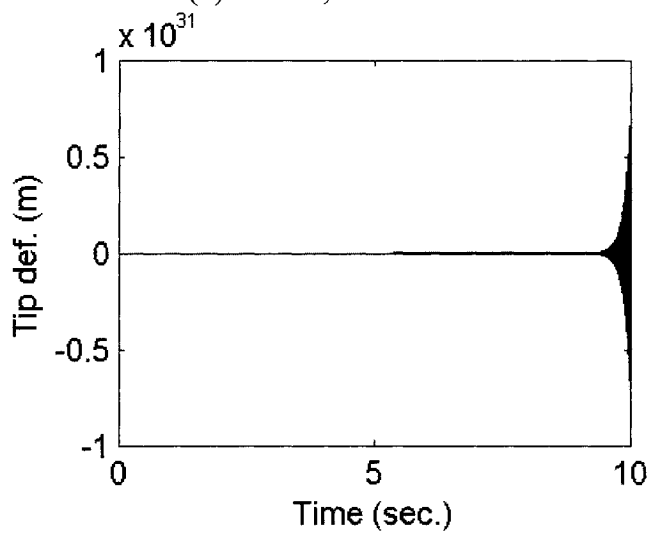

(c) K=300, τ =0.05

Figure 12: Tip deflection of the link under the position angle DFS controller (K=300)

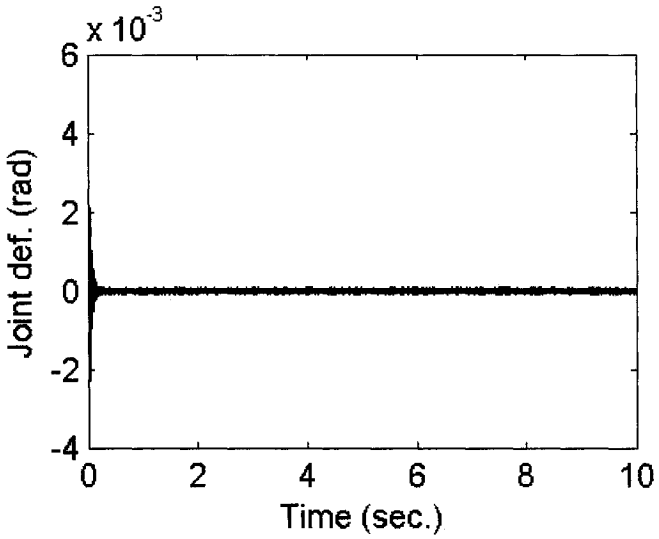

(a) K=20, τ =0.001

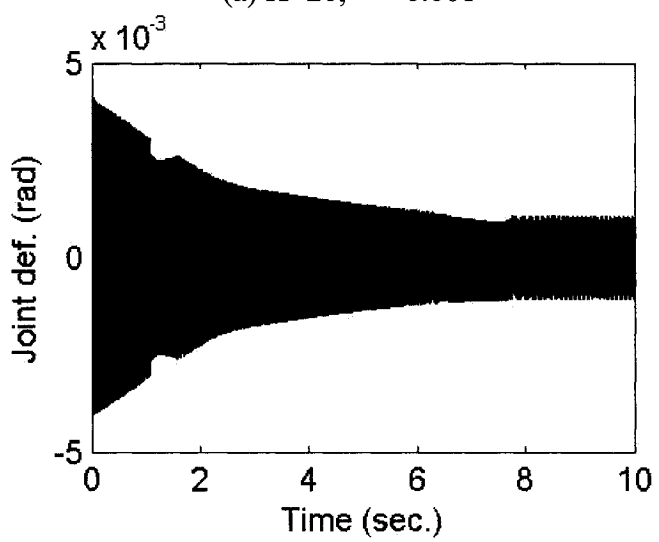

(b) K=20, τ =0.002183

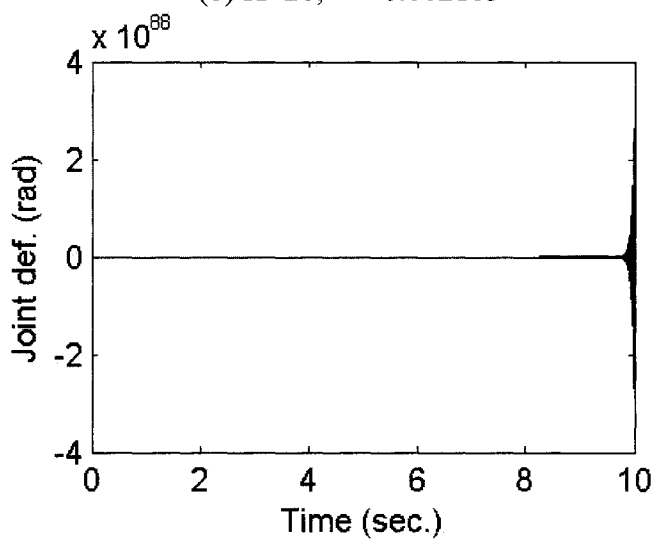

(c) K=20, τ =0.003

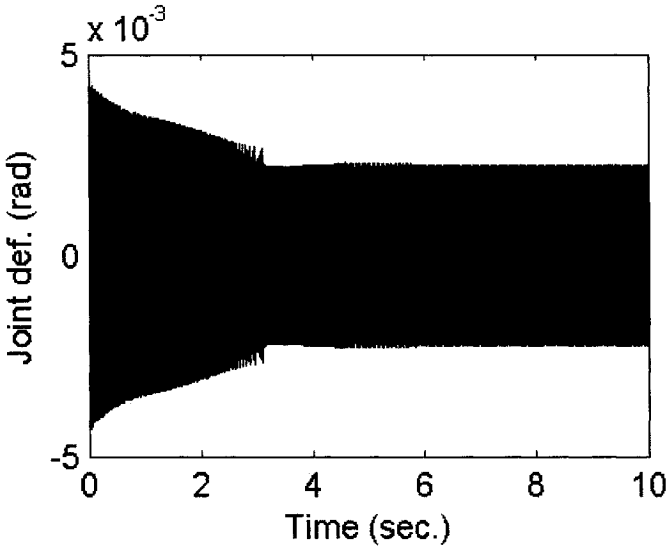

(d) K=20, τ =0.004465

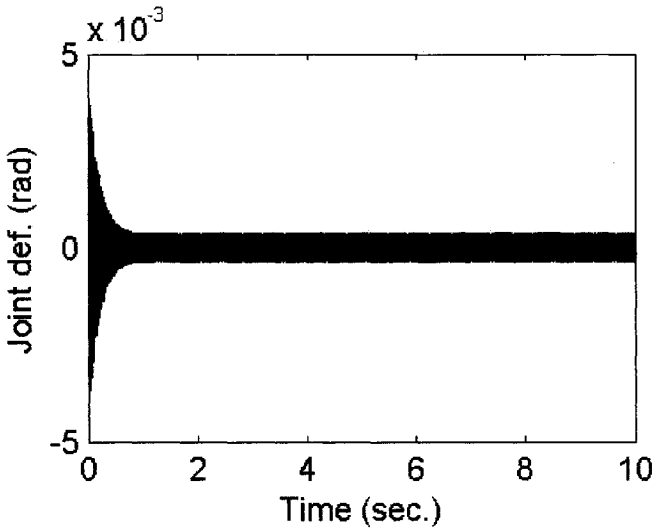

(e) K=20, τ =0.0046

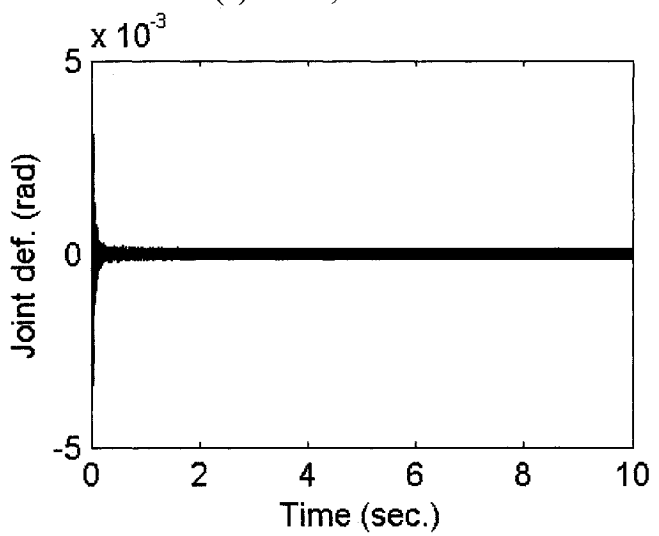

(f) K=20, τ =0.02338

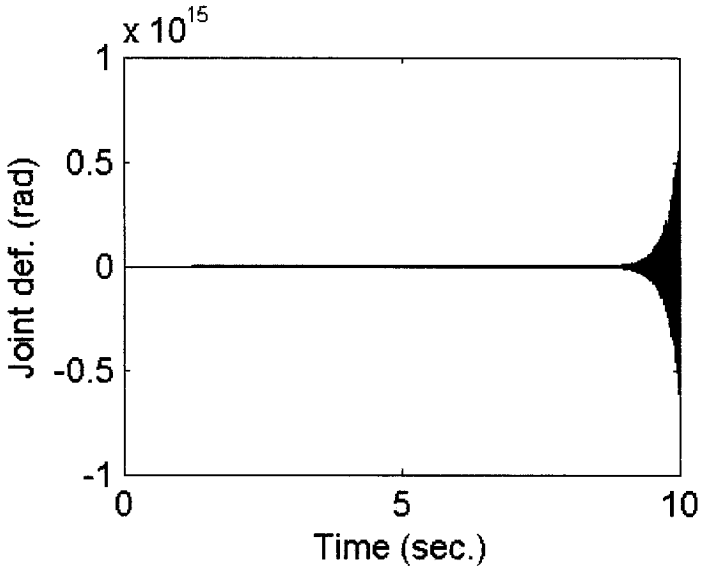

(g) K=20, τ =0.5

Figure 13: Joint torsional deflection under the position angle DFS controller (K=20)

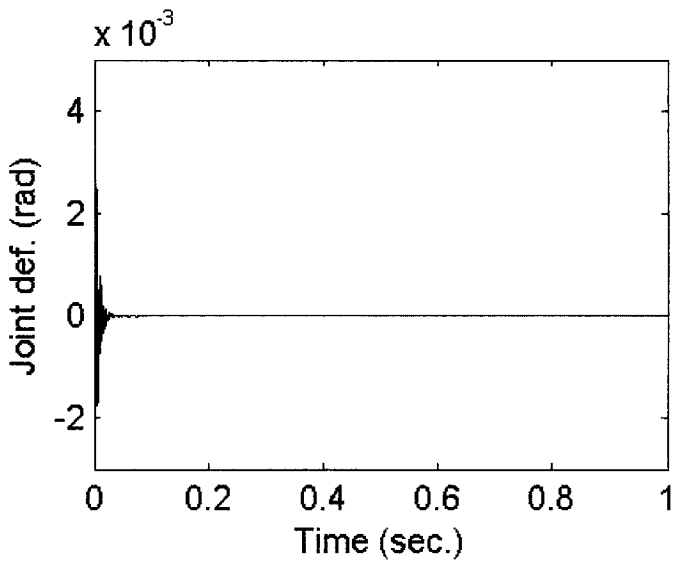

(a) K=100, τ =0.001

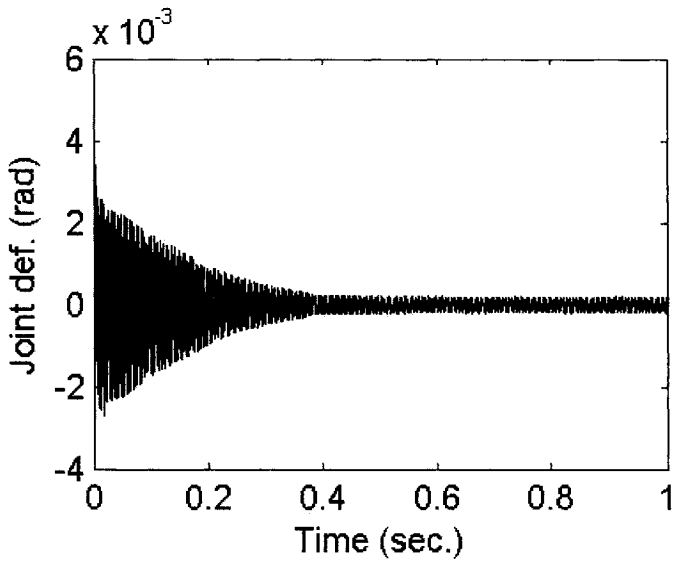

(b) K=100, τ =0.001845

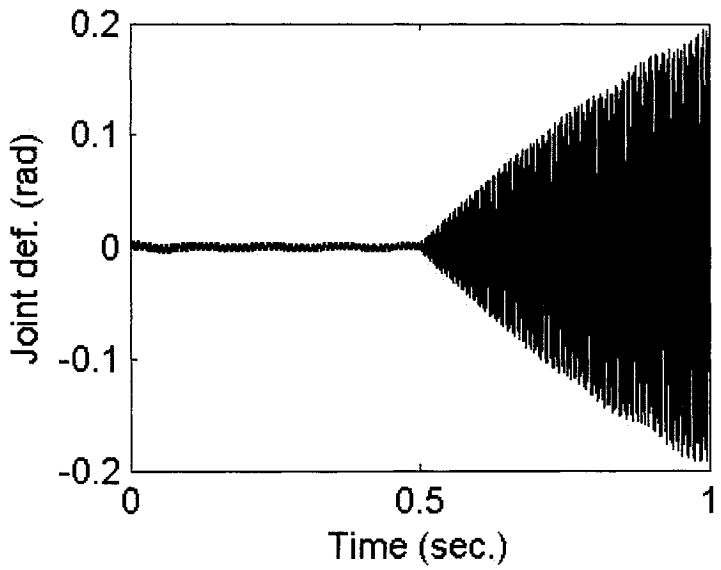

(c) K=100, τ =0.5

Figure 14: Joint torsional deflection under the position angle DFS controller (K=100)

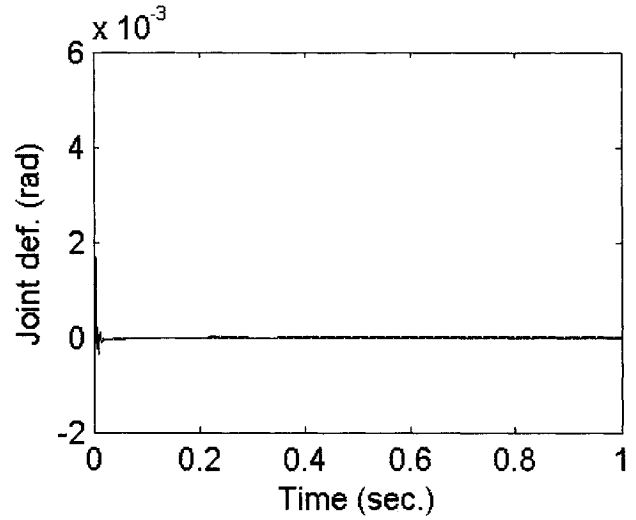

(a) K=180, τ =0.001

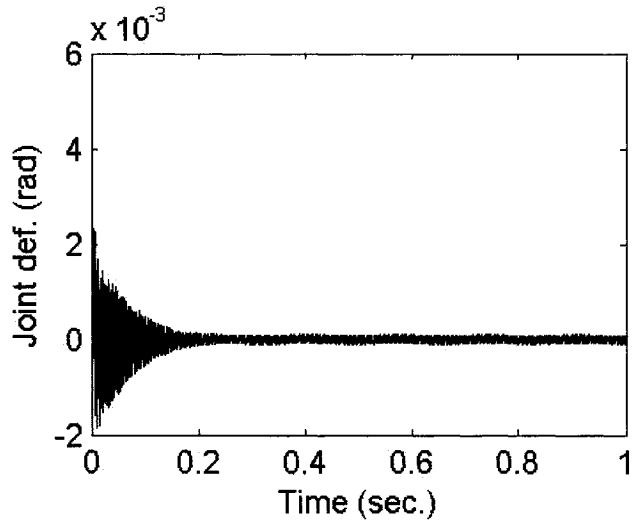

(b) K=180, τ =0.001597

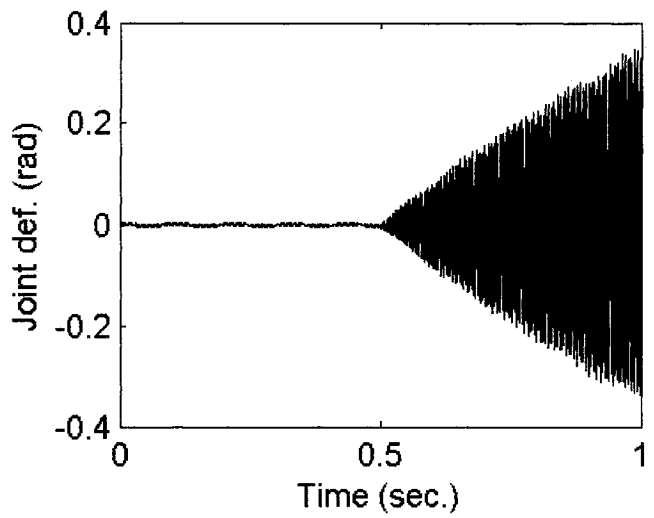

(c) K=180, τ =0.5

Figure 15: Joint torsional deflection under the position angle DFS controller (K=180)

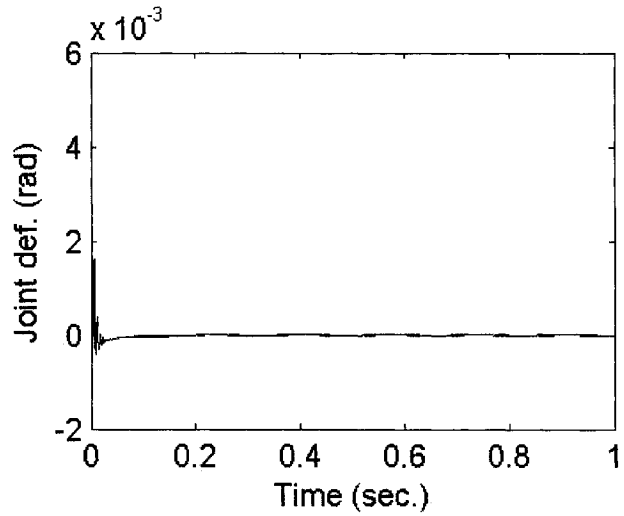

(a) K=300, τ =0.001

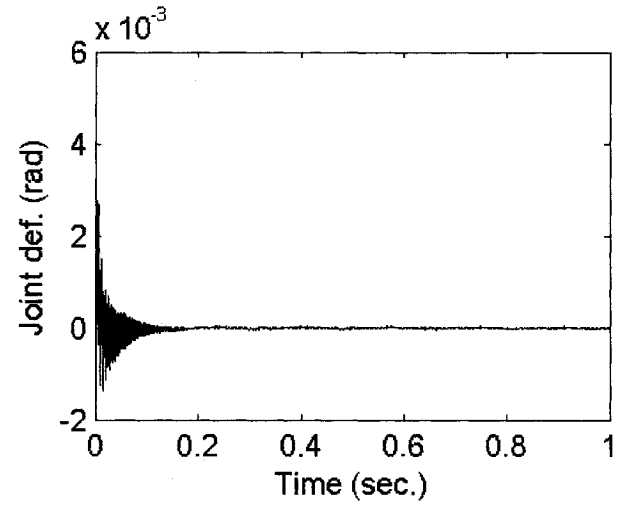

(b) K=300, τ =0.001347

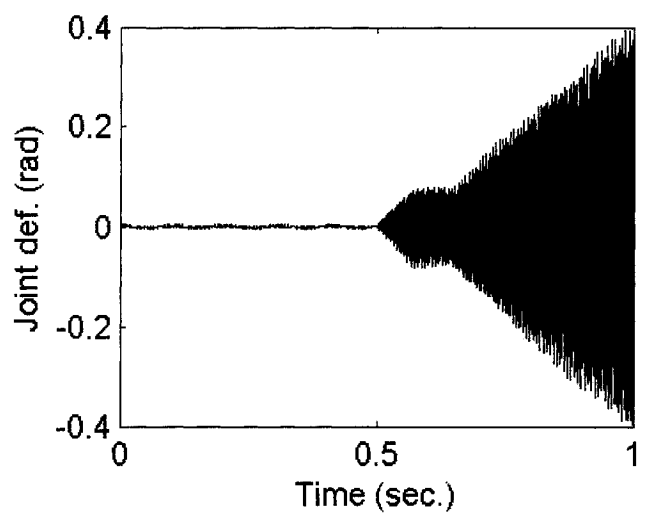

(c) K=300, τ =0.5

Figure 16: Joint torsional deflection under the position angle DFS controller (K=300)

5.2.2 Joint deflection DFS controller

This control signal is expressed as $u = K[\delta(t) - \delta(t-\tau)]$, and the state space model is modified as:

$$\dot{X}(t) = (A + KBC)X(t) - KBCX(t-\tau)$$

$$C = [-1 \quad 1 \quad 0 \quad 0 \quad 0 \quad 0 \quad 0 \quad 0]$$

Taking the Laplace transformation for the state space model, we get:

$$X(s)\cdot[sI - A - KBC(1 - \exp(-s\tau))] = 0$$

The characteristic equation of the system is:

$$|sI - A - KBC(1 - \exp(-s\tau))| = 0$$

This equation could be also derived to the compact form:

$$P(s) + Q(s)\exp(-s\tau) = 0$$

$$P(j\omega) = P_R(\omega) + jP_I(\omega),\ Q(j\omega) = Q_R(\omega) + jQ_I(\omega)$$

The four polynomials $P_R(\omega), P_I(\omega), Q_R(\omega)$ and $Q_I(\omega)$ can be expressed as:

$$P_R(\omega) = (\omega^8 - 2.2864e6\omega^6 + 6.4626e11\omega^4 - 9.0798e14\omega^2) + (-6.8966e3\omega^6 + 3.8529e9\omega^4 - 5.4307e12\omega^2)K$$

$$P_I(\omega) = (-3.6547\omega^7 + 4.2328e6\omega^5 - 11.88\omega^3) + (2.5205e4\omega^5 - 7.1052e7\omega^3)K$$

$$Q_R(\omega) = -(-6.8966e3\omega^6 + 3.8529e9\omega^4 - 5.4307e12\omega^2)K$$

$$Q_I(\omega) = -(2.5205e4\omega^5 - 7.1052e7\omega^3)K$$

The roots of $F(\omega) = P_R^2 + P_I^2 - (Q_R^2 + Q_I^2) = 0$ were calculated for different gain values. If only the integer value was considered for the gain, for $K > 46$, six positive real roots could be found including a pair of repeated roots, two positive real roots for $K < 2$ and

four positive real roots for $2 < K < 46$. Because the moving direction of the poles can not be determined with repeated roots [7, 39], the gain values $K > 46$ were not considered. In this study, nine gain values were considered from 5 to 45 with a step of 5, and four real positive roots were obtained for each of them. The roots and the corresponding critical time delays obtained using the method mentioned in the last section are displayed in Tables 8-13. The stability switches of the system were examined for four gain values $K = 10$, 20, 30 and 40. When $K = 10$, nineteen (19) boundary time points were obtained including ten (10) unstable critical time delays (removing poles from the left to right region on the complex plane) and nine (9) stable critical time delays. Similar results were also obtained for K = 20, 30 and 40.

The initial conditions were given as $[0 \quad 0.05 \quad 0 \quad 0 \quad 0 \quad 0 \quad 0 \quad 0]$. The stability changes of the tip deflection of the link for the gain values of 10, 20, 30 and 40 and the corresponding time delays are shown in Figure 17-20, while those of the joint torsional deflection are given in Figure 21-24.

Table 8: Positive real roots for different gain values in the system under the joint deflection DFS controller

k=5	k=10	k=15	k=20	k=25	k=30	k=35	k=40	k=45
573.44	573.39	573.37	573.36	573.35	573.35	573.35	573.35	573.34
581.3	588.79	595.65	601.98	607.84	613.27	618.32	623.02	627.42
1398.7	1398.7	1398.7	1398.7	1398.7	1398.7	1398.7	1398.7	1398.7
1419.8	1440.9	1461.8	1482.7	1503.4	1524	1544.5	1564.8	1584.9

Table 9: Critical time delays (sec.) for $K = 10$ in the system under the joint deflection DFS controller

	K=10							
τ	0.002208	**0.004462**	0.005576	0.006568	0.008954	**0.010764**	0.010929	**0.013446**
#	1	**0**	1	2	1	**0**	1	**0**
τ	0.01529	0.016247	0.017939	0.01965	0.021722	**0.022431**	0.024011	0.026919
#	1	2	1	2	1	**0**	1	2
τ	0.026923	0.028372	0.031415	**0.03268**	0.032732	**0.035907**	0.037093	0.03759
#	1	2	1	**0**	1	**0**	1	2
τ	0.0404	0.041454	0.043639	**0.044892**	0.045814	0.048262	0.049384	0.050175
#	1	2	1	**0**	1	2	1	2
τ	0.053876	0.054536	0.054597	**0.058368**	0.058896	0.058933	0.06286	0.063257
#	1	2	1	**0**	1	2	1	2
τ	0.065555	**0.067353**	0.067618	0.069604	0.071845	0.071978	0.076337	0.076339
#	1	**0**	1	2	1	2	1	2
τ	0.076513	0.080276	0.0807	0.080829	0.08506	0.085321	0.087471	0.089421
#	1	2	3	2	3	2	1	2

Table 10: Critical time delays (sec.) for $K = 20$ in the system under the joint deflection DFS controller

	K=20							
τ	0.002131	**0.004477**	0.005365	0.006369	0.008969	0.010607	0.010862	**0.013462**
#	1	**0**	1	2	1	2	1	**0**
τ	0.014844	0.015802	0.017954	0.019082	0.02182	**0.022446**	0.023319	0.02624
#	1	2	1	2	1	**0**	1	2
τ	0.026938	0.027557	0.03143	0.031795	0.032779	**0.035923**	0.036032	0.036677
#	1	2	1	2	1	**0**	1	2
τ	0.04027	0.040415	0.043738	0.044508	0.044907	0.047115	0.048745	0.049399
#	3	2	1	2	1	2	3	2
τ	0.052983	0.053892	0.054696	0.057221	0.057553	0.058384	0.061458	0.062876
#	3	2	1	2	3	2	3	2

Table 11: Critical time delays (sec.) for $K = 30$ in the system under the joint deflection DFS controller

	K=30							
τ	0.002069	**0.004482**	0.00524	0.006192	0.008974	0.010314	0.010894	**0.013467**
#	1	**0**	1	2	1	2	1	**0**
τ	0.014437	0.015485	0.017959	0.01856	0.021853	**0.022451**	0.022683	0.02573
#	1	2	1	2	1	**0**	1	2
τ	0.026806	0.026943	0.030928	0.031436	0.032812	0.035051	0.035928	0.035976
#	3	2	3	2	1	2	1	2
τ	0.039174	0.04042	0.043297	0.04377	0.044912	0.046221	0.047419	0.049405
#	3	2	3	2	1	2	3	2

Table 12: Critical time delays (sec.) for $K = 40$ in the system under the joint deflection DFS controller

	K=40							
τ	0.002013	**0.004485**	0.005146	0.006028	0.008977	0.010044	0.01091	**0.013469**
#	1	**0**	1	2	1	2	1	**0**
τ	0.014059	0.015231	0.017961	0.018074	0.021869	0.02209	0.022454	0.025316
#	1	2	1	2	1	2	1	2
τ	0.026105	0.026946	0.030121	0.031438	0.032828	0.034136	0.035401	0.03593
#	3	2	3	2	1	2	3	2
τ	0.038151	0.040423	0.042167	0.043787	0.044915	0.045486	0.046182	0.049407
#	3	2	3	2	1	2	3	2

Table 13: Boundary time points (sec.) for the system under the control of the joint deflection DFS controller

K=10	K=20	K=30	K=40
0.002208	0.002131	0.002069	0.002013
0.004462	0.004477	0.004482	0.004485
0.005576	0.005365	0.00524	0.005146
0.010764	0.013462	0.013467	0.013469
0.010929	0.014844	0.014437	0.014059
0.013446	0.022446	0.022451	
0.01529	0.023319	0.022683	
0.022431	0.035923		
0.024011	0.036032		
0.03268			
0.032732			
0.035907			
0.037093			
0.044892			
0.045814			
0.058368			
0.058896			
0.067353			
0.067618			

Note: The odd time point marks the end of a stable state and the beginning of an unstable state, while the even one marks the end of an unstable state and the beginning of a stable state. All of the boundary points were obtained from the critical time delays in Tables 9-12.

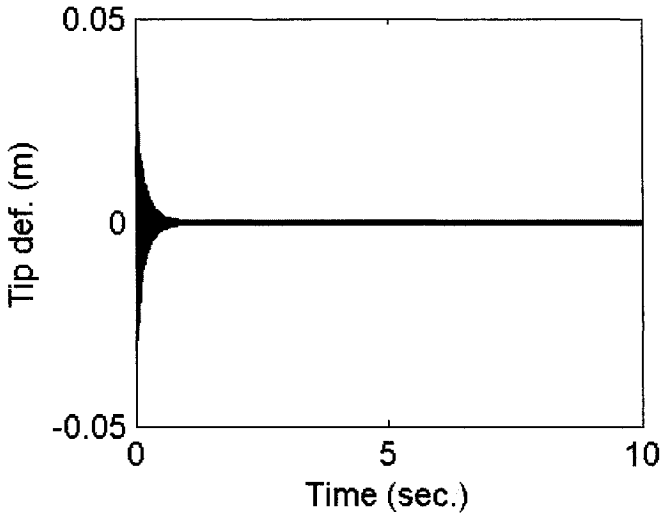

(a) K=10, τ =0.001

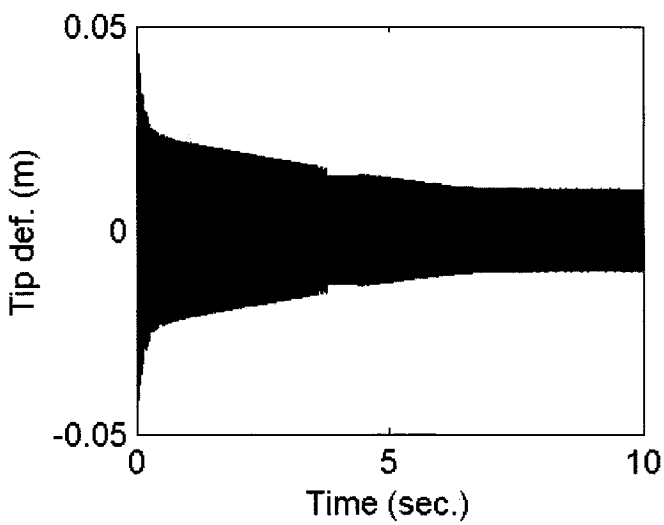

(b) K=10, τ =0.002208

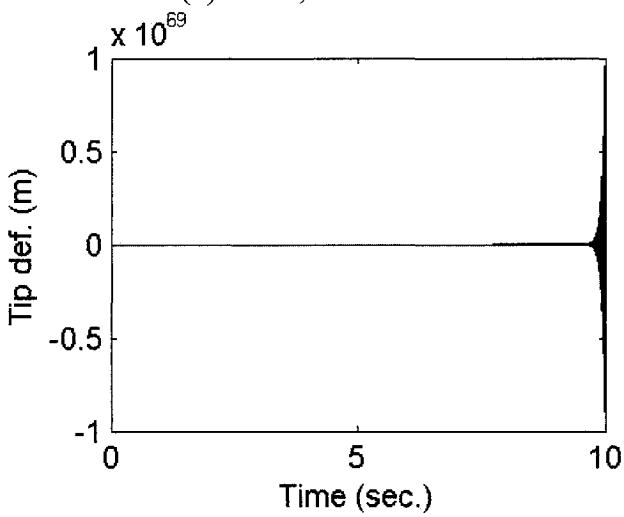

(c) K=10, τ =0.003

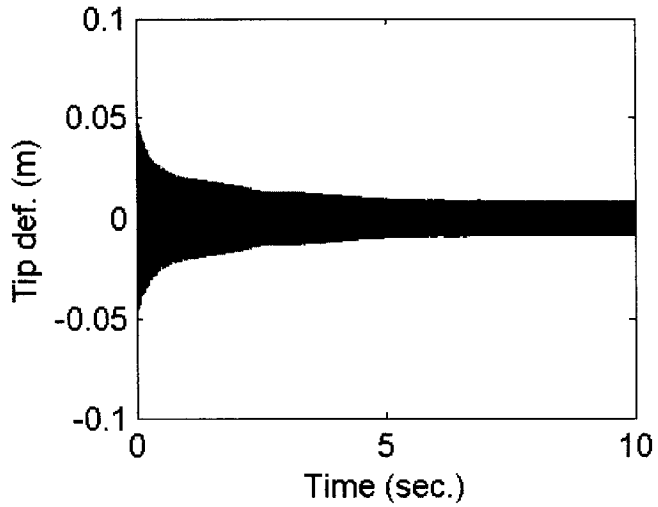

(d) K=10, τ =0.004462

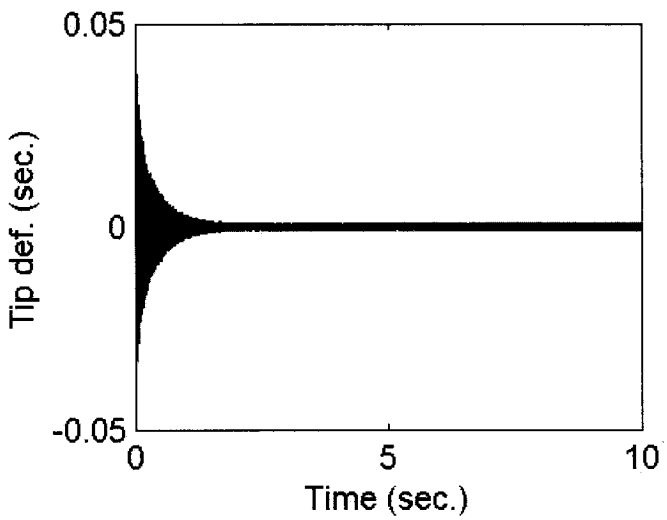

(e) K=10, τ =0.005

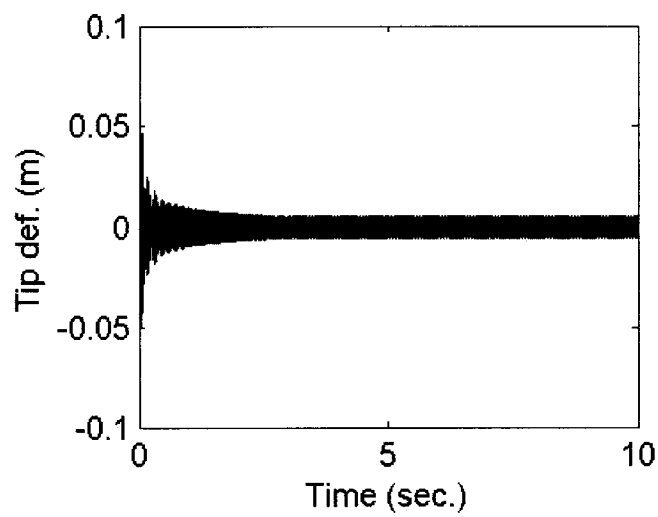

(f) K=10, τ =0.067618

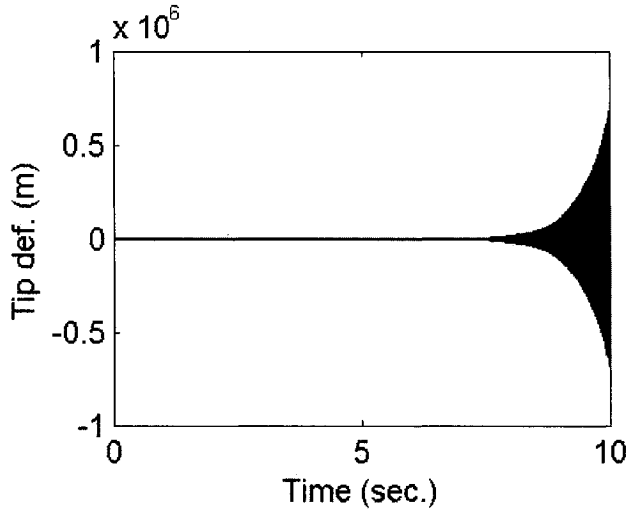

(g) K=10, τ =1

Figure 17: Tip deflection of the link under the joint deflection DFS controller (K=10)

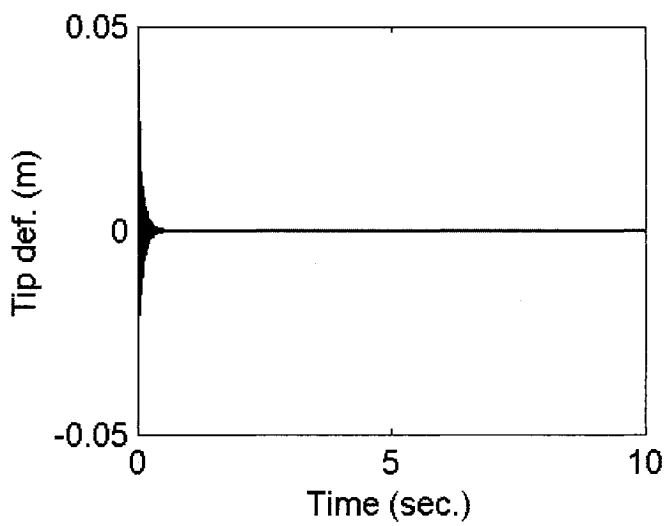

(a) K=20, τ =0.001

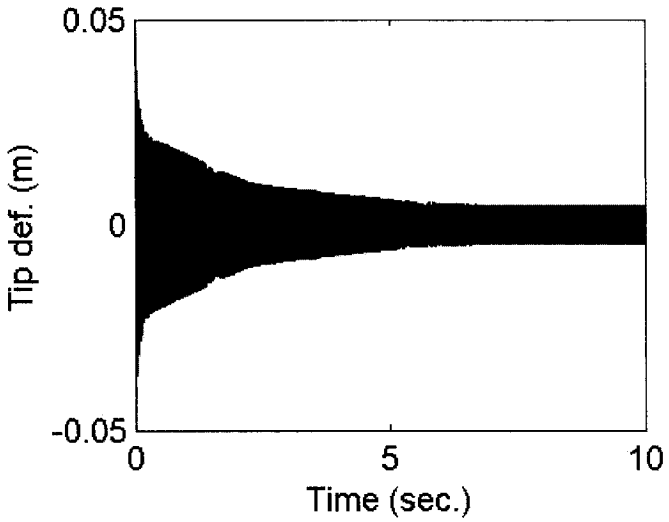

(b) K=20, τ =0.002131

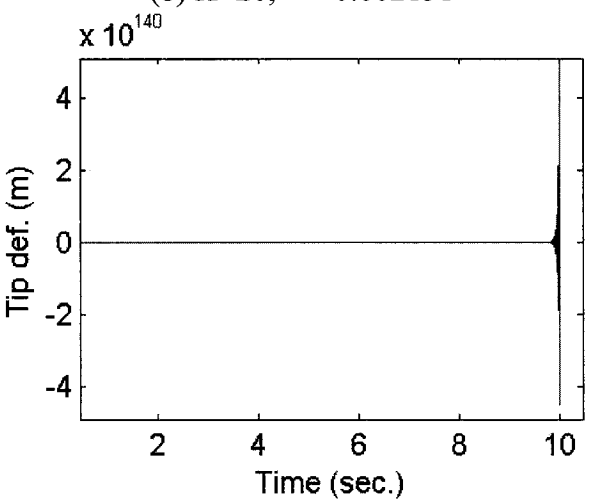

(c) K=20, τ =0.003

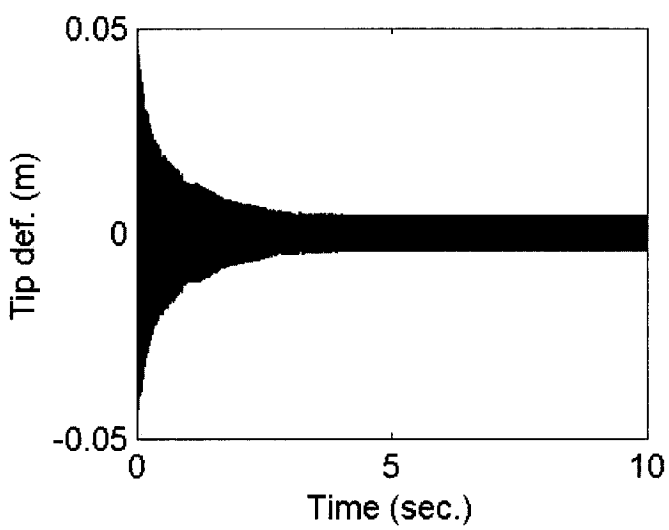

(d) K=20, τ =0.004477

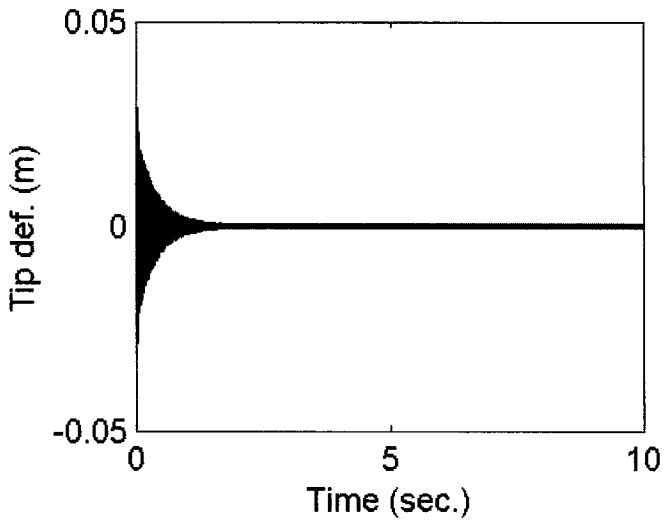

(e) K=20, τ =0.005

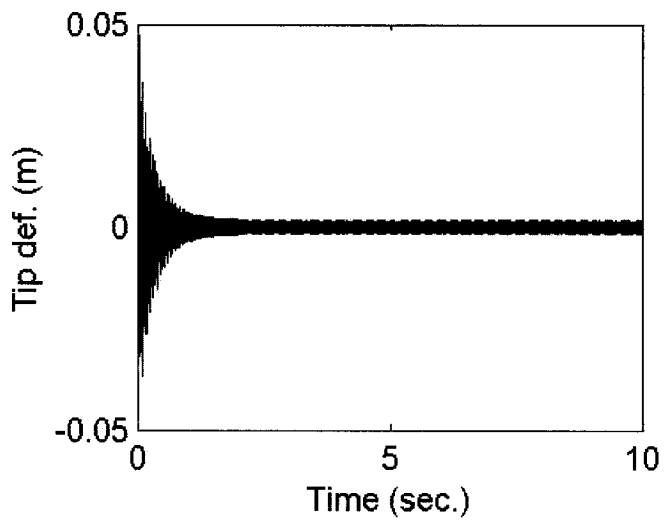

(f) K=20, τ =0.036032

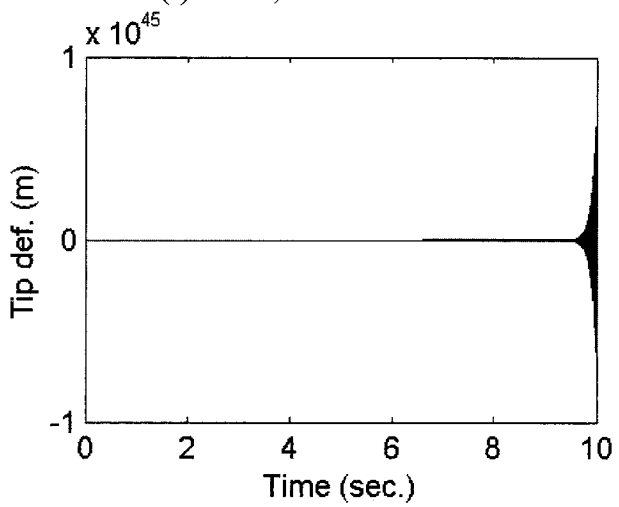

(g) K=20, τ =0.1

Figure 18: Tip deflection of the link under the joint deflection DFS controller (K=20)

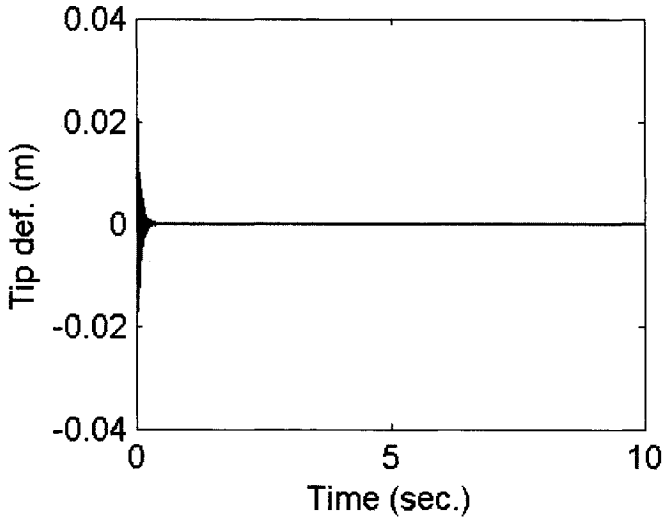

(a) K=30, τ =0.001

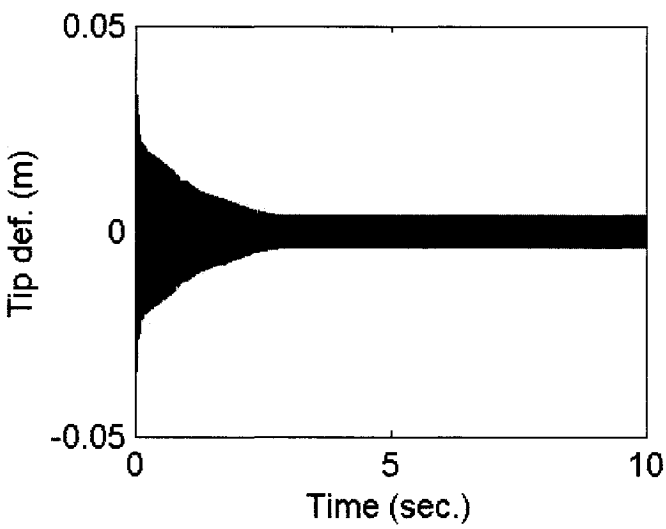

(b) K=30, τ =0.002069

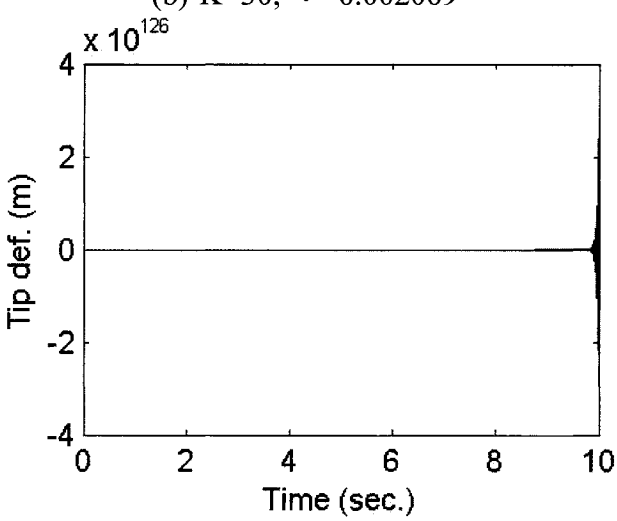

(c) K=30, τ =0.004

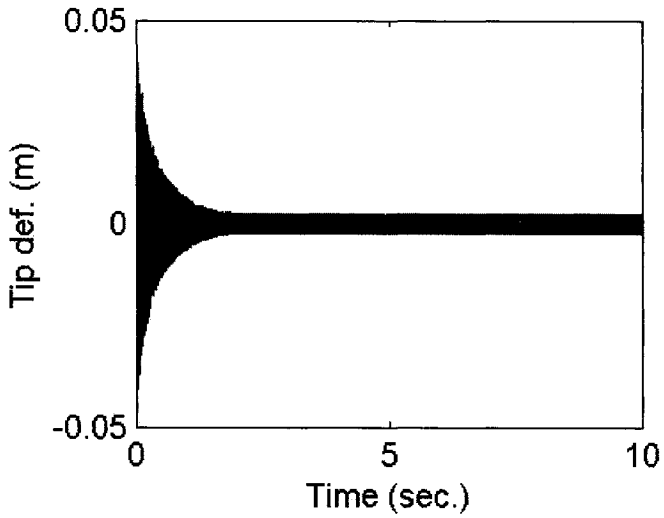

(d) K=30, τ =0.004482

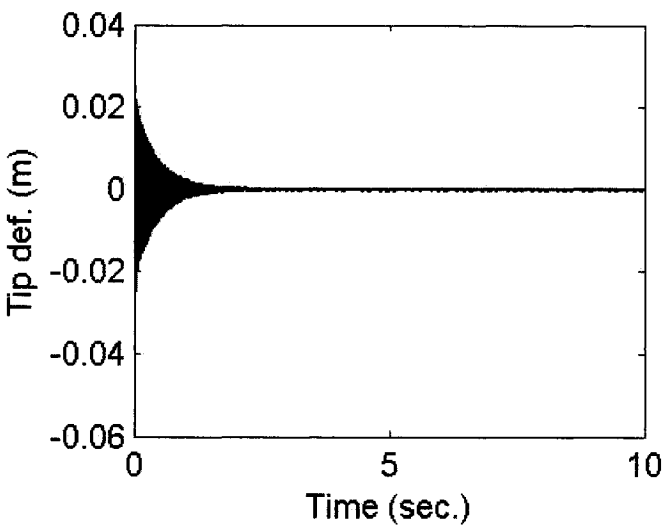

(e) K=30, τ =0.005

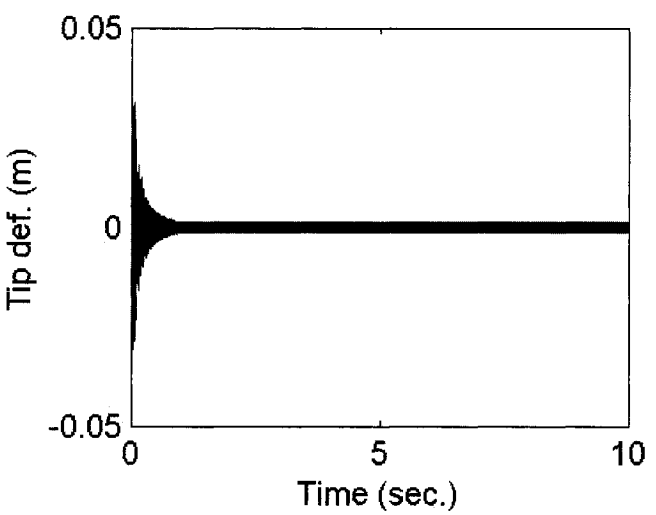

(f) K=30, τ =0.022683

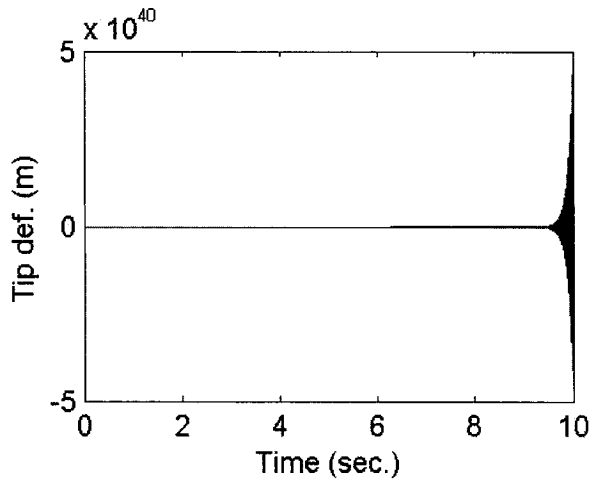

(g) K=30, τ =0.1

Figure 19: Tip deflection of the link under the joint deflection DFS controller (K=30)

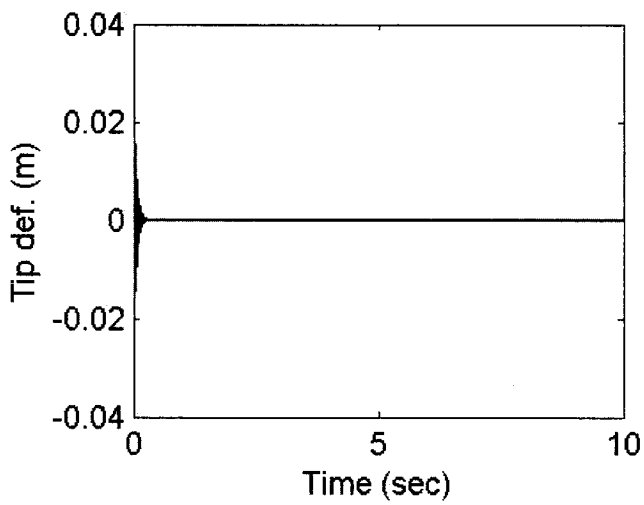

(a) K=40, τ =0.001

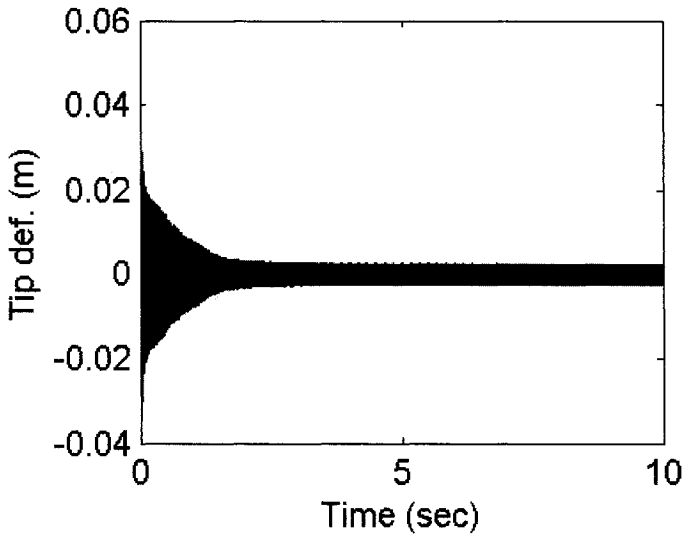

(b) K=40, τ =0.002013

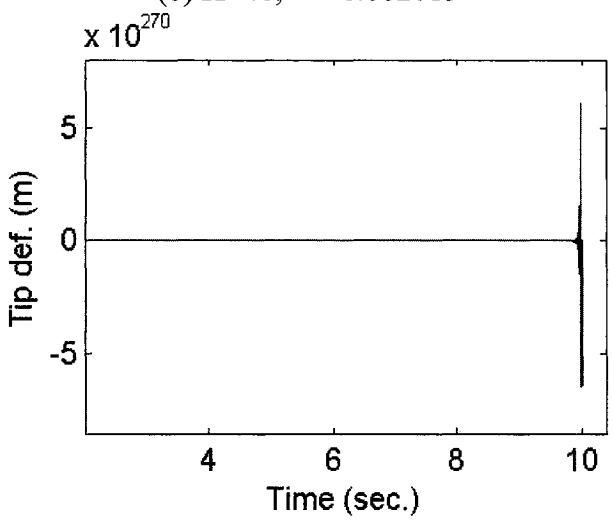

(c) K=40, τ =0.003

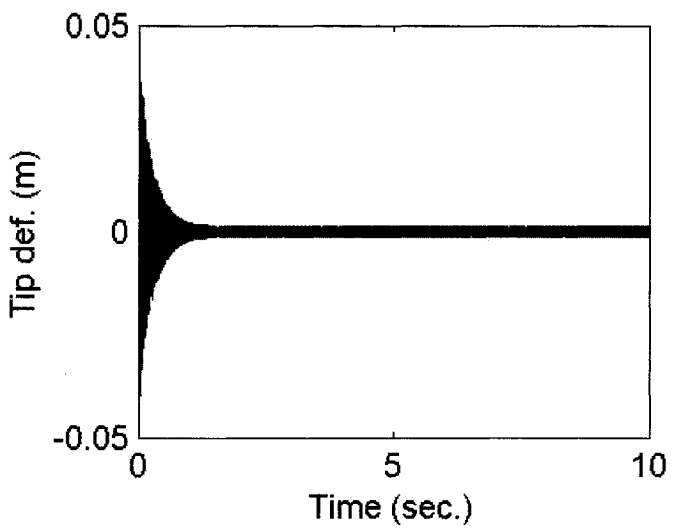

(d) K=40, τ =0.004485

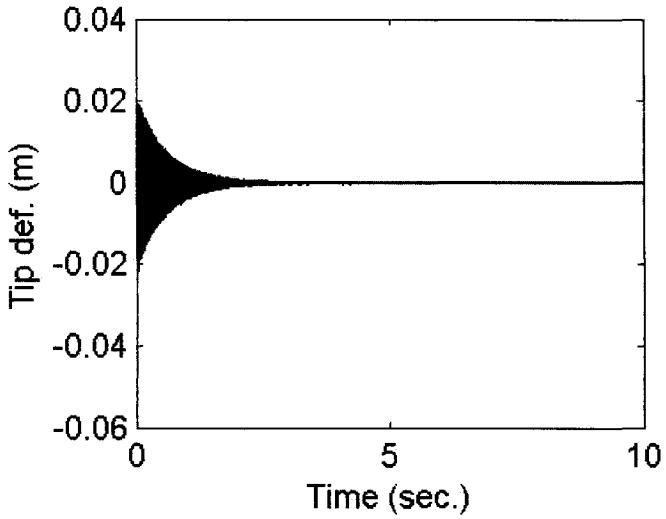

(e) K=40, τ =0.005

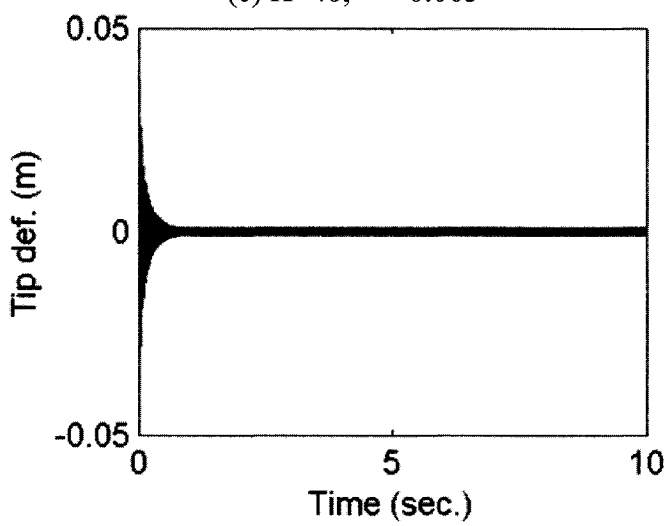

(f) K=40, τ =0.014059

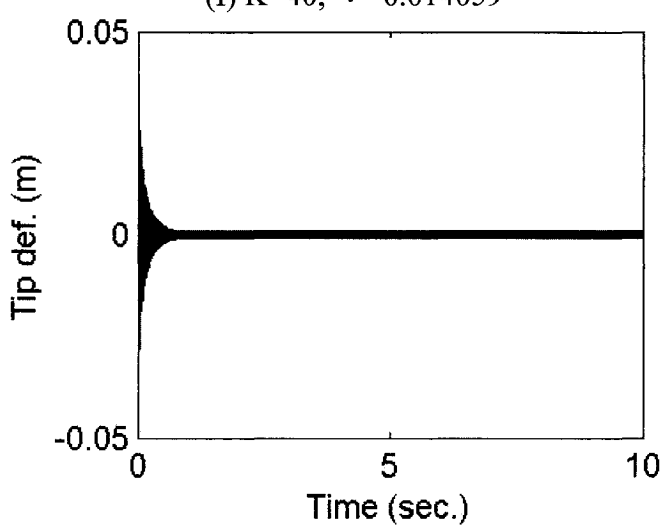

(g) K=40, τ =1

Figure 20: Tip deflection of the link under the joint deflection DFS controller (K=40)

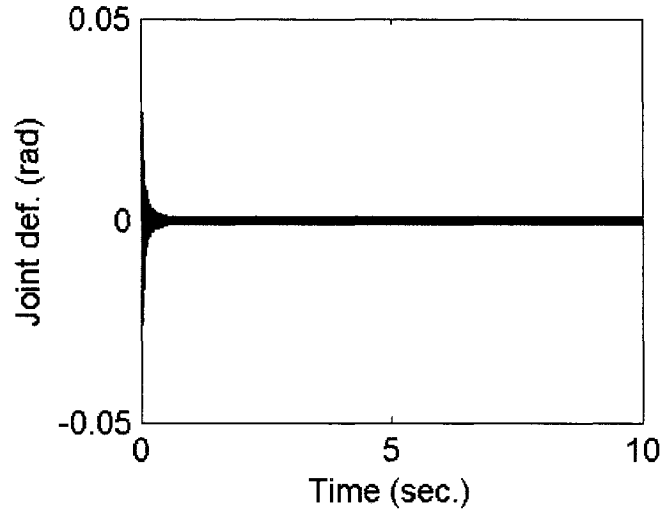

(a) K=10, τ =0.001

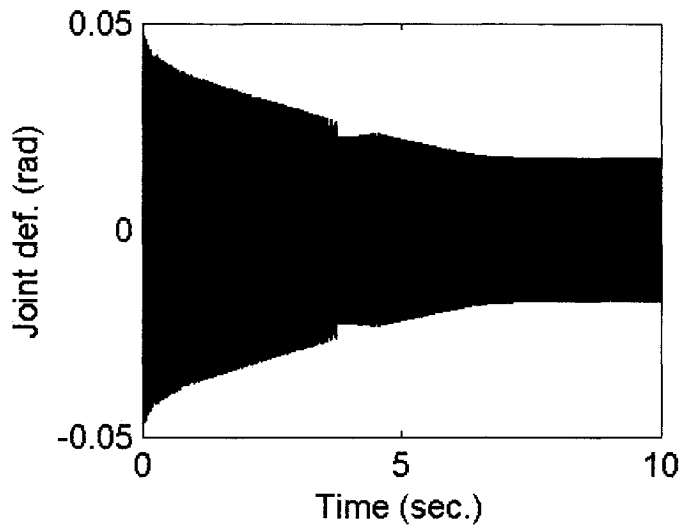

(b) K=10, τ =0.002208

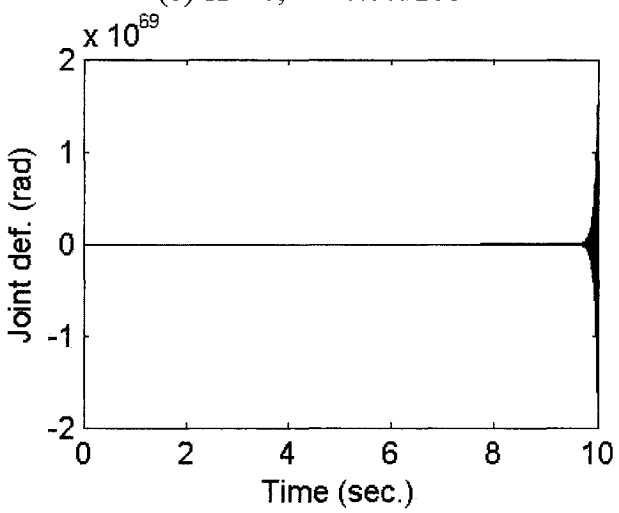

(c) K=10, τ =0.003

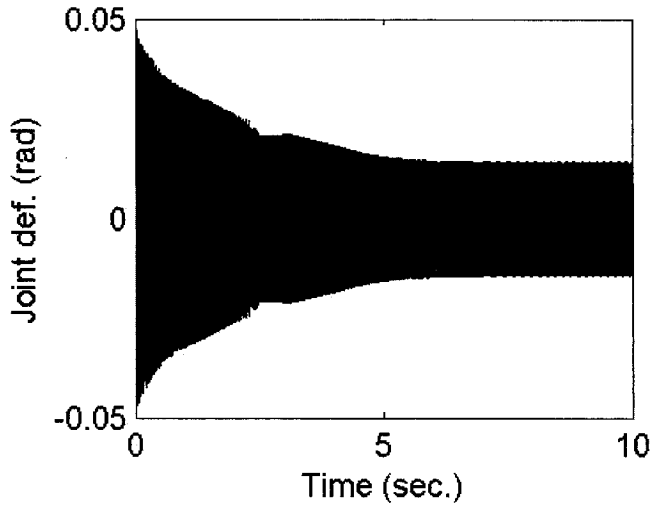

(d) K=10, τ =0.004462

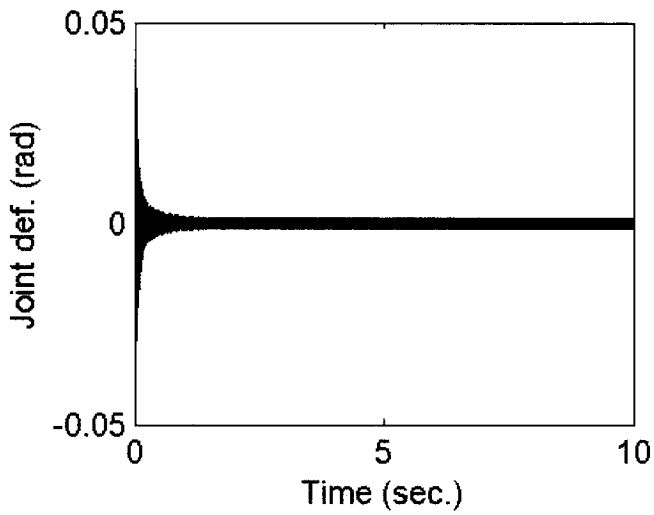

(e) K=10, τ =0.005

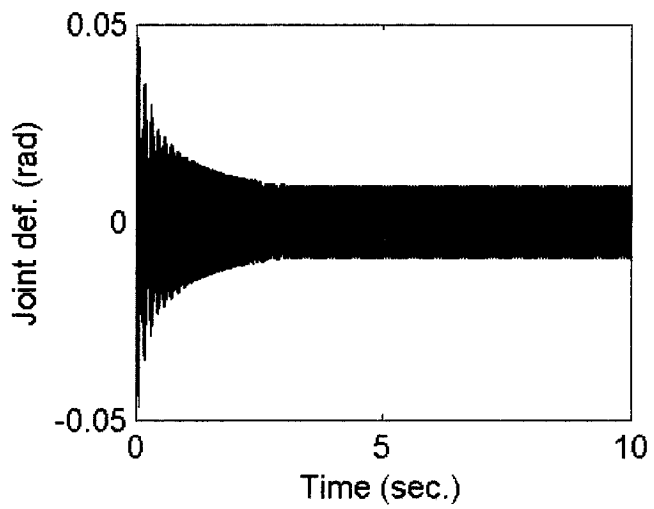

(f) K=10, τ =0.067618

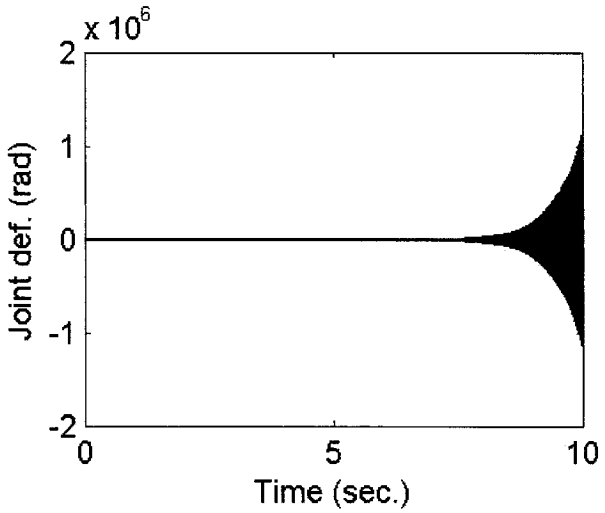

(g) K=10, τ =1

Figure 21: Joint torsional deflection under the joint deflection DFS controller (K=10)

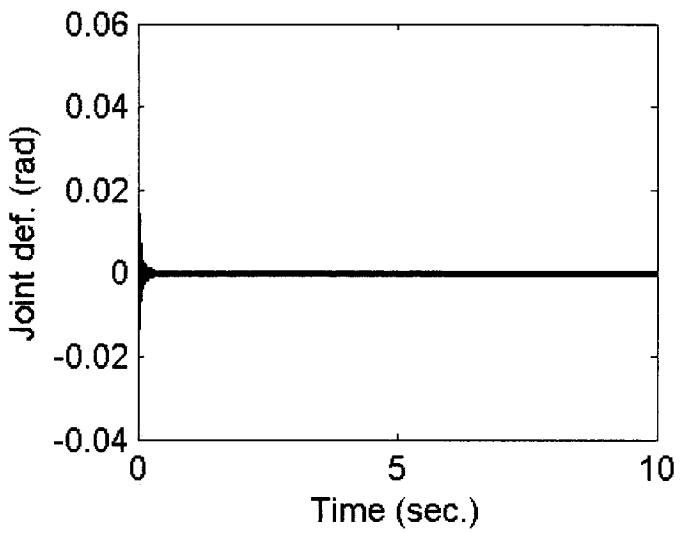

(a) K=20, τ =0.001

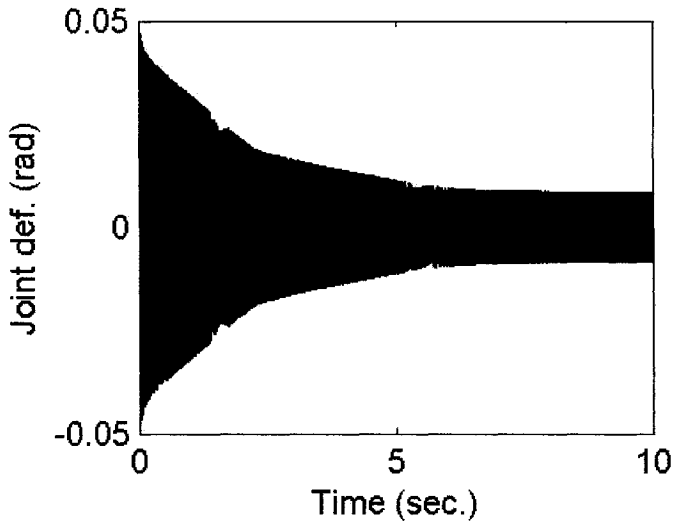

(b) K=20, τ =0.002131

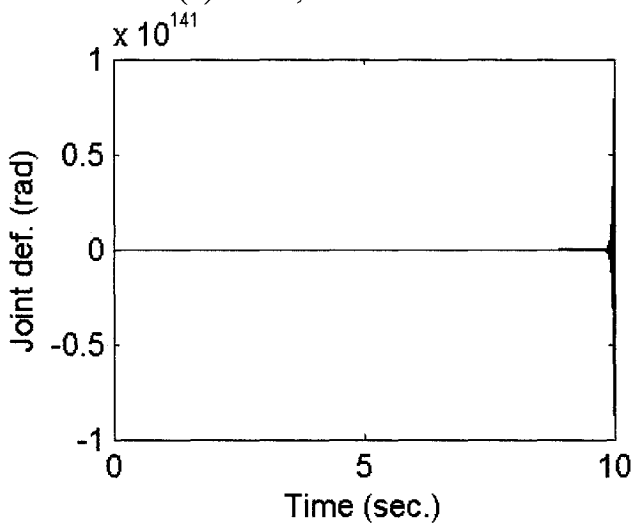

(c) K=20, τ =0.003

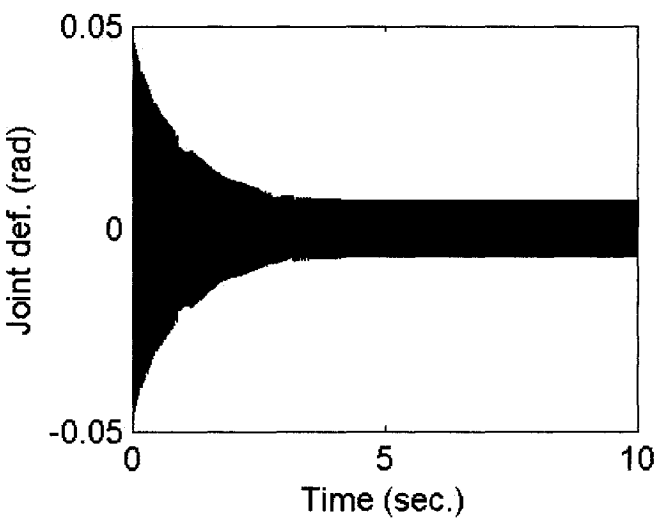

(d) K=20, τ =0.004477

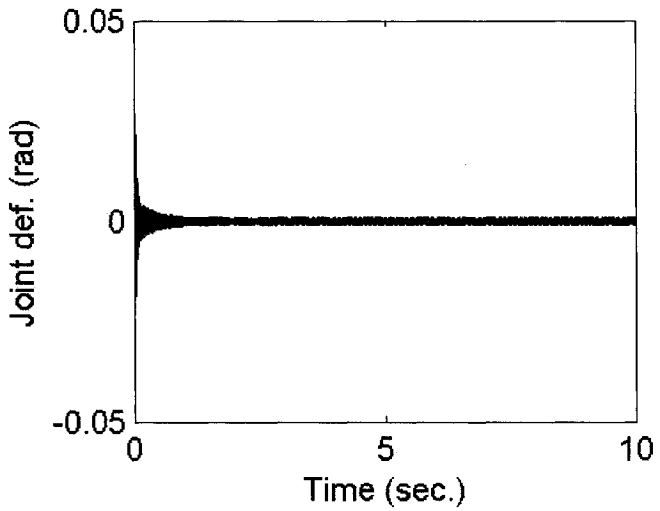

(e) K=20, τ =0.005

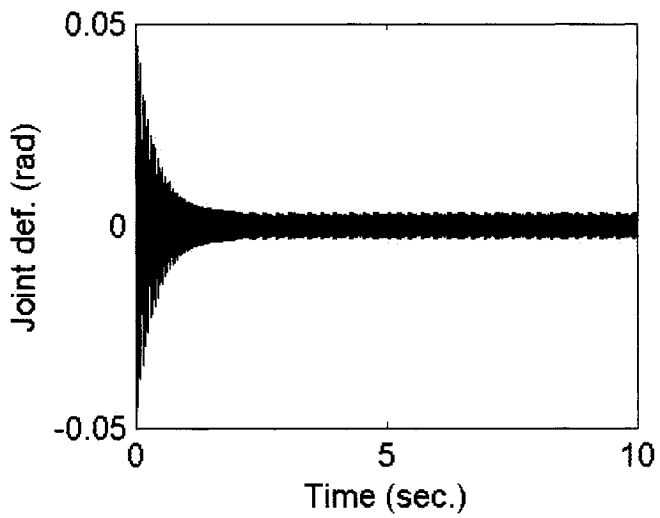

(f) K=20, τ =0.036032

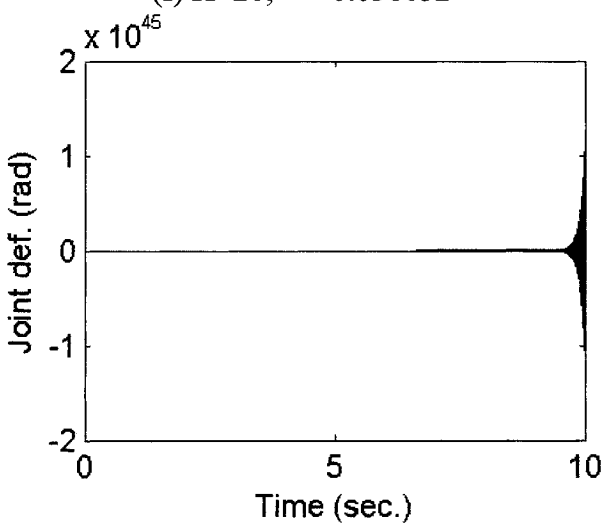

(g) K=20, τ =0.1

Figure 22: Joint torsional deflection under the joint deflection DFS controller (K=20)

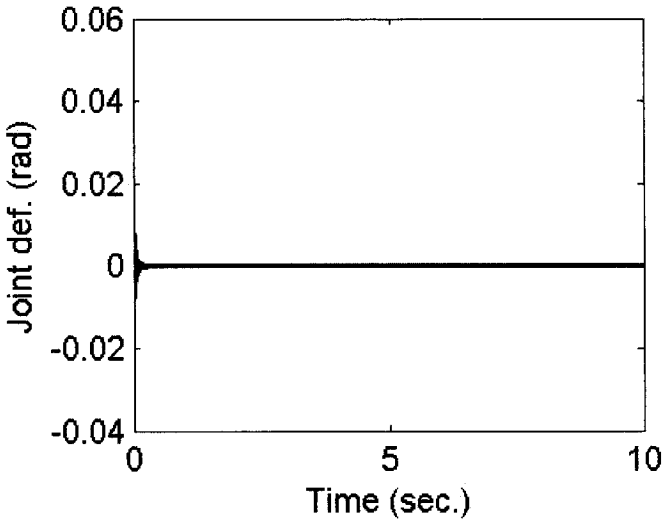

(a) K=30, τ =0.001

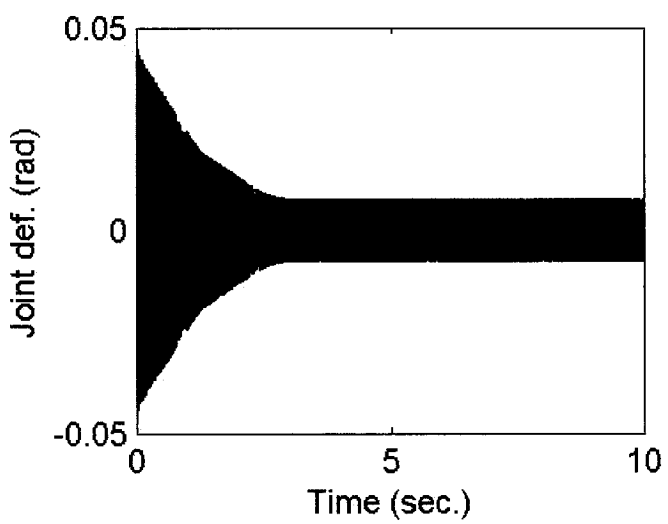

(b) K=30, τ =0.002069

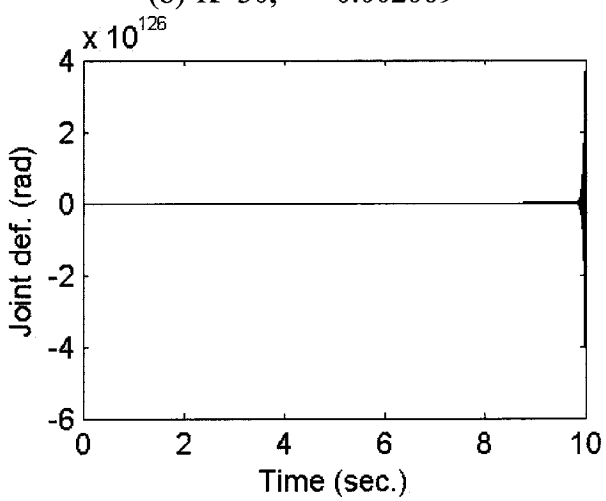

(c) K=30, τ =0.004

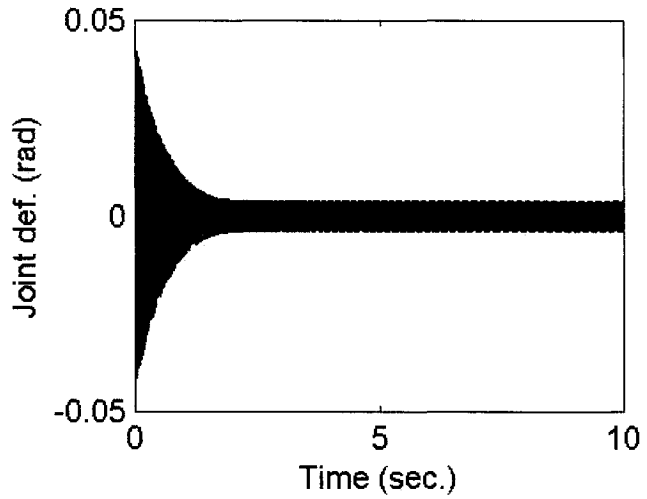

(d) K=30, τ =0.004482

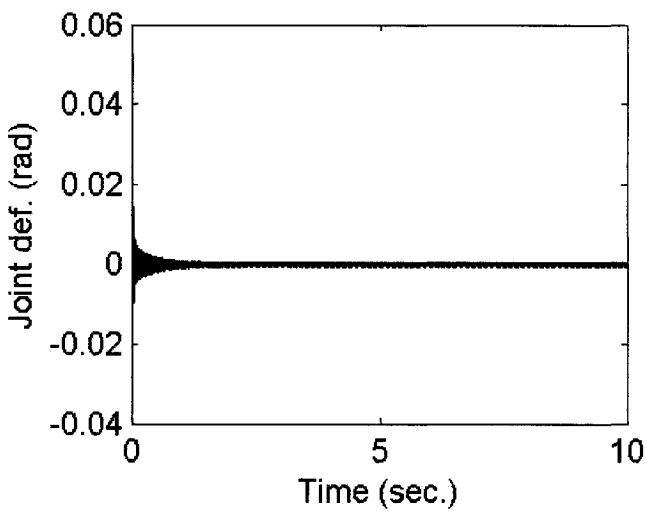

(e) K=30, τ =0.005

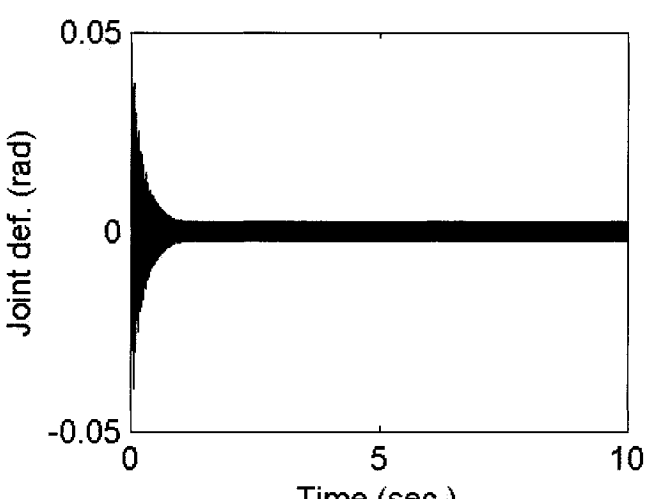

(f) K=30, τ =0.022683

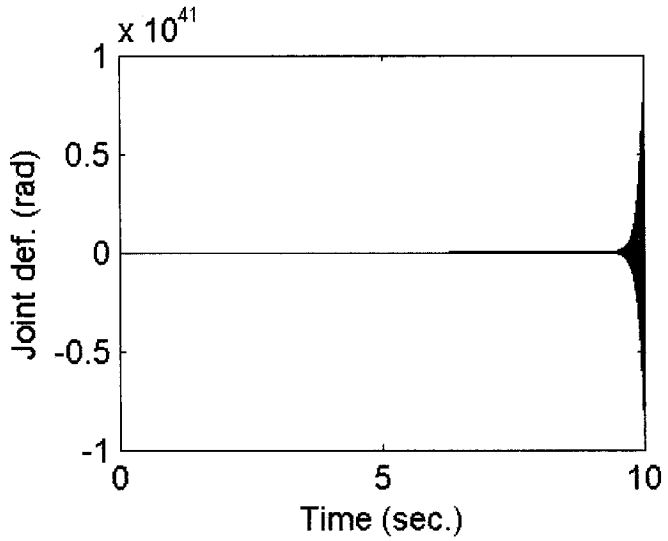

(g) K=30, τ =0.1

Figure 23: Joint torsional deflection under the joint deflection DFS controller (K=30)

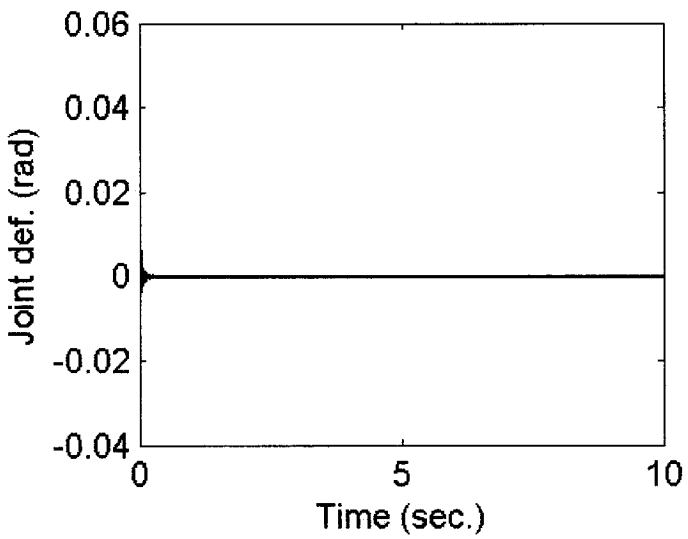

(a) K=40, τ =0.001

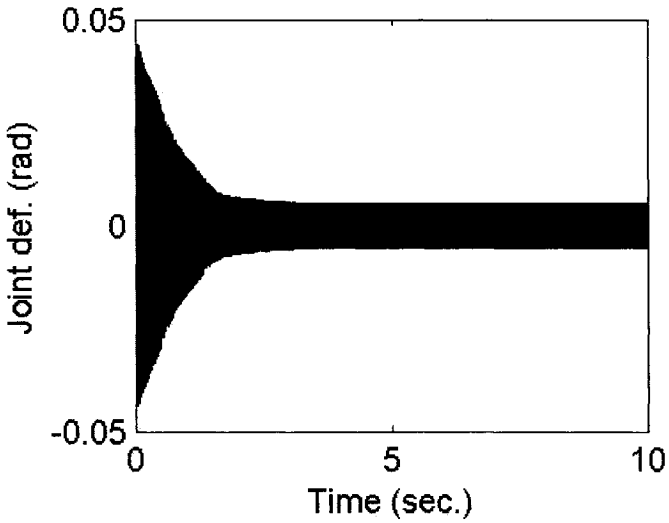

(b) K=40, τ =0.002013

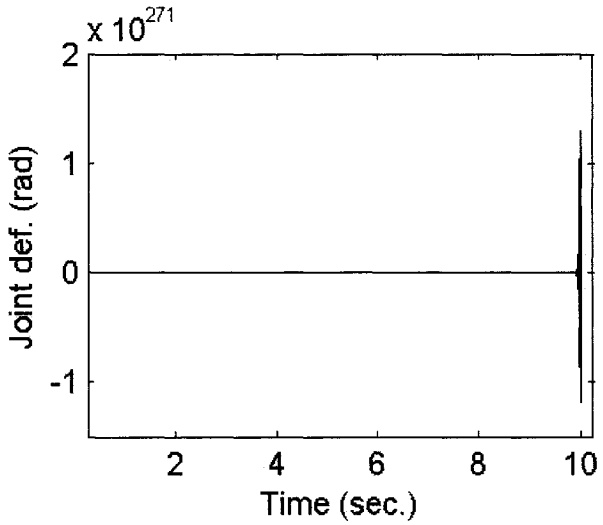

(c) K=40, τ =0.003

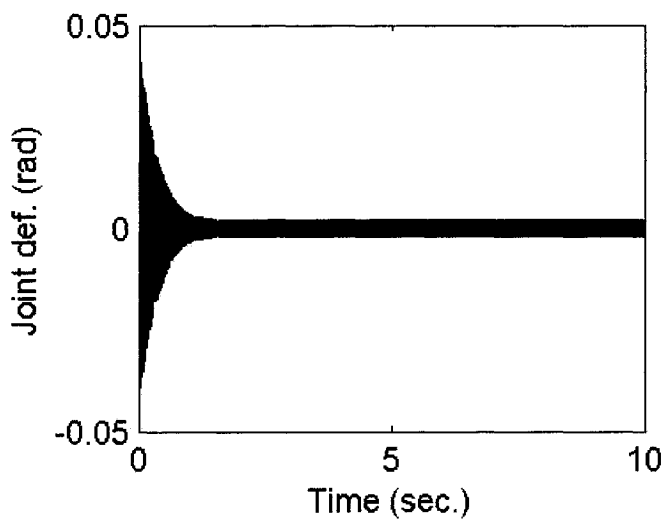

(d) K=40, τ =0.004485

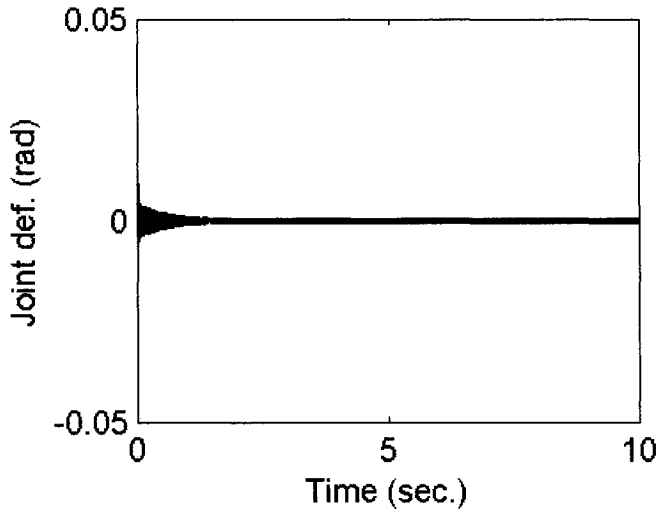

(e) K=40, τ =0.005

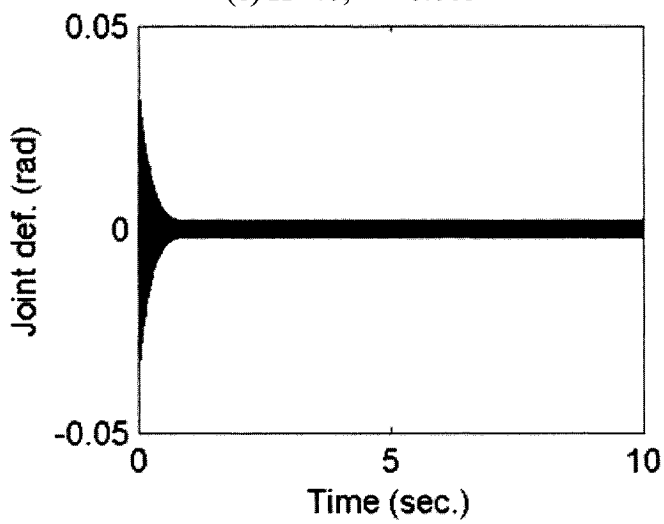

(f) K=40, τ =0.014059

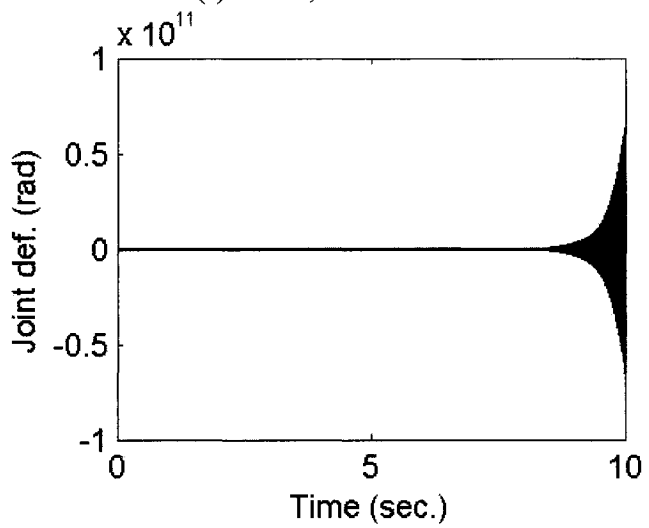

(g) K=40, τ =1

Figure 24: Joint torsional deflection under the joint deflection DFS controller (K=40)

5.3 Position trajectory tracking

In practice, the angular position of the manipulator is usually designed to track a pre-defined trajectory. In this work, the angular position of the FJFL manipulator θ_1 was set to track a unit step input. The control of the angular position of the link/hub ($\theta_2 = \theta_1 + \delta$) was fulfilled by eliminating the joint torsional vibration which was done together with the control of the link bending vibration by using the DFS controller proposed in Section 5.2.

In order to track a reference input, another controller needs to be added into the system. To obtain a compromise between acceptable transient-response behavior and steady-state behavior, a proportional-plus-derivative (PD) controller is usually applied [37]. PD controller has been applied for the position and vibration control of a two-link rigid-flexible manipulator [40]. In the present study, the PD controller was combined with the DFS controller to make the manipulator reach the desired position with much less vibration. The block diagram of the closed-loop system of trajectory tracking and vibration damping is given in Figure 25. The optimal gain values K_p and K_d for the PD controller were obtained using Matlab & Simulink Response Optimization with output constraints. Figure 26 shows the processing block diagram of PD gains' optimal tuning.

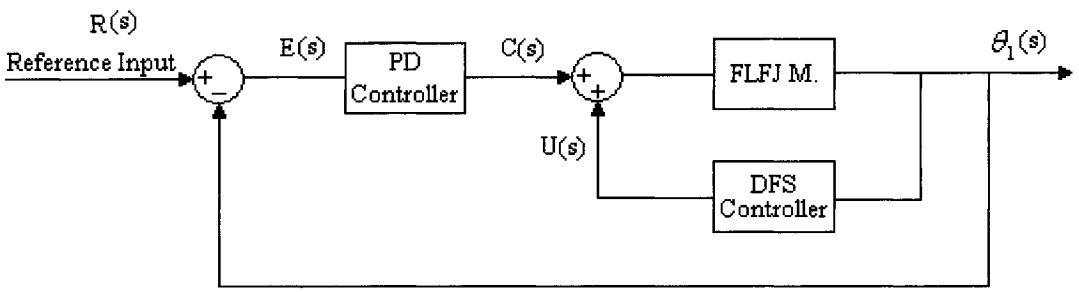

Figure 25: Block diagram of trajectory tracking and vibration damping

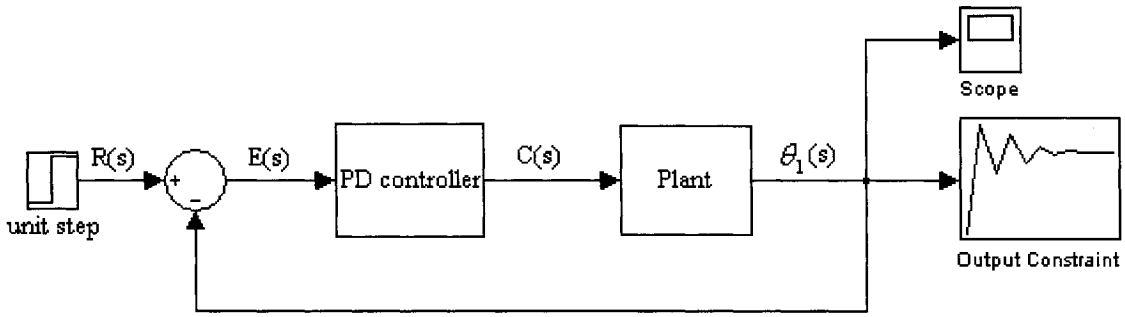

Figure 26: Optimal tuning of gains K_p and K_d for the PD controller

The step response characteristics were specified as:

Rising time: $t_r = 2.5$ sec; Settling time: $t_s = 7.5$ sec

Overshoot=20%; Settling=5%

Before the optimal tuning, the transfer function $\frac{\theta_1(s)}{C(s)}$ of the plant had to be ascertained. Three sets of plants, the open-loop system, the closed-loop system with a position angle DFS controller, and the closed-loop system with a joint deflection DFS controller, were considered in this study.

The open-loop transfer function denoted as G(s) was easily obtained using the Matlab code ss2tf (A, B, C, D) and the known matrices A, B, C and D. Thus,

$$\frac{\theta_1(s)}{C(s)} = G(s) = ss2tf(A,B,C,D) \tag{5.3-1}$$

The transfer function of the closed-loop system with position angle DFS controller was derived as $\frac{G(s)}{1-G(s)H(s)}$, where $H(s)$ was the transfer function of the DFS controller (see Figure 25).

$$U(t) = -K[\theta_1(t) - \theta_1(t-\tau)]$$

Taking the Laplace transformation, we get:

$$U(s) = -K\theta_1(s)[1 - \exp(-s\tau)]$$

$$H(s) = \frac{U(s)}{\theta_1(s)} = -K[1 - \exp(-s\tau)] \tag{5.3-2}$$

$$\frac{\theta_1(s)}{C(s)} = \frac{G(s)}{1 + K[1 - \exp(-s\tau)]G(s)} \tag{5.3-3}$$

For the closed-loop system with a joint deflection DFS controller, the transfer function of the plant was a little more difficult to obtain because the input for the PD controller was $\theta_1(s)$, but that for the DFS controller was $\delta(s)$ ($\delta(s) = \theta_2(s) - \theta_1(s)$). The block diagram of this closed-loop system is shown in Figure 27.

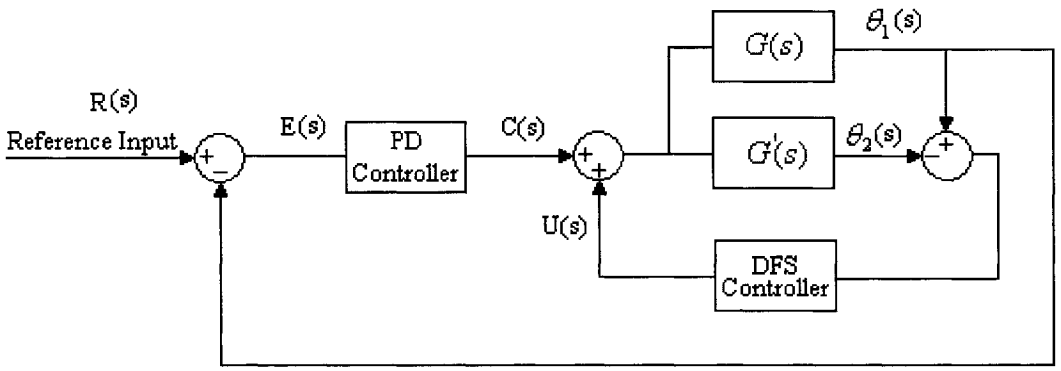

Figure 27: Block diagram of trajectory tracking and vibration damping with a joint deflection DFS controller

The terms G(s) and G'(s) signify the transfer functions to get the signals $\theta_1(t)$ and $\theta_2(t)$, respectively from the input torque $C(s) + U(s)$.

$$\begin{cases} [C(s) + H(s)(\theta_1(s) - \theta_2(s))]G(s) = \theta_1(s) \\ [C(s) + H(s)(\theta_1(s) - \theta_2(s))]G'(s) = \theta_2(s) \end{cases}$$

$$\theta_2(s) = \frac{C(s) + H(s)\theta_1(s)}{1 + H(s)G'(s)}G'(s) \tag{5.3-4}$$

$$\frac{\theta_1(s)}{C(s)} = \frac{G(s)}{1 + H(s)[G'(s) - G(s)]} \tag{5.3-5}$$

Due to the presence of the derivative term in the PD control action, the output of the PD controller $C(s)$ would involve an impulse function when the system was subjected to a step function [37]. Thus the pure derivative term $K_d s$ was substituted by a band-limited term $K_d \frac{s}{0.1s+1}$. The equivalent block diagram of the modified PD controller is shown in Figure 28.

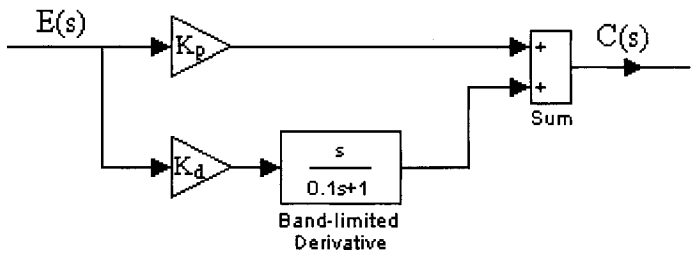

Figure 28: Block diagram of the modified PD controller

Based on the Simulink Response Optimization and the selected step response characteristics, the optimal gain values K_p and K_d for the PD controller of these three sets of plants were obtained as follows:

For the open-loop system:

$$K_p = 0.04, K_d = 0.0551$$

For the closed-loop system with a position angle DFS controller $(K = 300, \tau = 0.001)$:

$$K_p = 0.2621, K_d = -0.0082$$

For the closed-loop system with a joint deflection DFS controller $(K = 40, \tau = 0.001)$:

$$K_p = 0.0784, K_d = 0.1006$$

The tip deflection of the link with respect to the frame $X_l Y_l$, the joint torsional deflection and the angular positions of the motor shaft and the hub/link for all three sets of

systems are shown in Figure 29-31. As seen in the simulation results, the system with a position angle DFS controller had better performance in the unit step tracking. At the same time, the tip deflection of the link and the joint torsional deflection were damped out completely within the desired time. This controller could improve the performance of both the transient and the steady-state response. By comparison, the DFS controller produced by the joint deflection could only improve the transient response. The pictures (b) in Figure 29 and Figure 31 are the zoomed-out pictures with the time range of $t = 31$ sec to $t = 31.5$ sec for the angular position of the FLFJ manipulator (θ_1). There was some oscillation within the steady state responses for the system without a DFS controller and the system with a joint deformation DFS controller. This was not due to the steady-state error inside the system, because through the calculation, the steady-state error was much smaller than the oscillation magnitude. This calculation was derived as follows:

$$R(s) - \theta_1(s) = E(s)$$

$$R(s) - E(s) \cdot G_{contr}(s) \cdot G_{plant}(s) = E(s)$$

$$\frac{E(s)}{R(s)} = \frac{1}{1 + G_{contr} \cdot G_{plant}} \tag{5.3-6}$$

where G_{contr} is the transfer function of the PD controller and G_{plant} denotes the transfer function of those three sets of plants.

$$G_{contr} = K_p + \frac{K_d s}{0.1s + 1} \tag{5.3-7}$$

$$R(s) = \frac{1}{s}$$

$$\lim_{s \to 0} sE(s) = s \cdot \frac{0.1s + 1}{(0.1s + 1) + G_{plant}[(0.1K_p + K_d)s + K_p]} \cdot \frac{1}{s}$$

For the open-loop system, the steady-state error was 1.0559e-10 rad, while it was 1.6113e-11 rad and 5.3846e-11 rad for the closed-loop system with a position angle DFS controller and that with a joint deflection DFS controller, respectively. Obviously, the oscillation within the steady-state response of the angular position for the system without DFS controller and the closed-loop system with a joint deflection DFS controller was much lager than their own steady-state error. This oscillation is thought to be due to the interaction between the rigid body motion of the manipulator and the link bending deformation and the joint torsional deformation. Derived from Equation (3.3-17), the linear model of the system with the state variable vector $X=[\theta_1;\delta;q_1;q_2]$ is given in the following:

$$\begin{bmatrix} J_1+J_2+\rho\int_0^L(r+x)^2dx & J_2+\rho\int_0^L(r+x)^2dx & \rho\int_0^L(r+x)\Phi_1dx & \rho\int_0^L(r+x)\Phi_2dx \\ J_2+\rho\int_0^L(r+x)^2dx & J_2+\rho\int_0^L(r+x)^2dx & \rho\int_0^L(r+x)\Phi_1dx & \rho\int_0^L(r+x)\Phi_2dx \\ \rho\int_0^L(r+x)\Phi_1dx & \rho\int_0^L(r+x)\Phi_1dx & \rho\int_0^L\Phi_1^2dx & 0 \\ \rho\int_0^L(r+x)\Phi_2dx & \rho\int_0^L(r+x)\Phi_2dx & 0 & \rho\int_0^L\Phi_2^2dx \end{bmatrix}\cdot\begin{bmatrix}\ddot{\theta}_1\\ \ddot{\delta}\\ \ddot{q}_1\\ \ddot{q}_2\end{bmatrix}+$$

$$\begin{bmatrix} 0 & 0 & 0 & 0 \\ 0 & 0 & 0 & 0 \\ 0 & 0 & l^2\varsigma\sqrt{AEI}\int_0^L\Phi_1''^2dx & l^2\varsigma\sqrt{AEI}\int_0^L\Phi_1''\Phi_2''dx \\ 0 & 0 & l^2\varsigma\sqrt{AEI}\int_0^L\Phi_1''\Phi_2''dx & l^2\varsigma\sqrt{AEI}\int_0^L\Phi_2''^2dx \end{bmatrix}\begin{bmatrix}\dot{\theta}_1\\ \dot{\delta}\\ \dot{q}_1\\ \dot{q}_2\end{bmatrix}+$$

$$\begin{bmatrix} 0 & 0 & 0 & 0 \\ 0 & Ks & 0 & 0 \\ 0 & 0 & EI\int_0^L\Phi_1''^2dx & EI\int_0^L\Phi_1''\cdot\Phi_2''dx \\ 0 & 0 & EI\int_0^L\Phi_1''\cdot\Phi_2''dx & EI\int_0^L\Phi_2''^2dx \end{bmatrix}\cdot\begin{bmatrix}\theta_1\\ \delta\\ q_1\\ q_2\end{bmatrix}=\begin{bmatrix}1\\0\\0\\0\end{bmatrix}\cdot L(t) \tag{5.3-8}$$

It can be seen from the mass matrix in the above linear system model that there were interactions between the angular position of the FLFJ manipulator θ_1 and the deformation variables δ, q_1 and q_2. In the open-loop system and the closed-loop system with a joint deflection DFS controller, the vibration of the link and the joint was not damped out

completely. Therefore, the oscillation in the steady-state response of the rigid body motion would be caused by residual vibrations. This can be seen as 'an internal disturbance' which causes the oscillation in the steady-state responses. This conclusion is also proven by the response of the system with a position angle DFS controller. In Figure 30, the vibration of the link and the joint in this closed-loop system was almost eliminated, thus the system had good tracking performance for a unit step reference input.

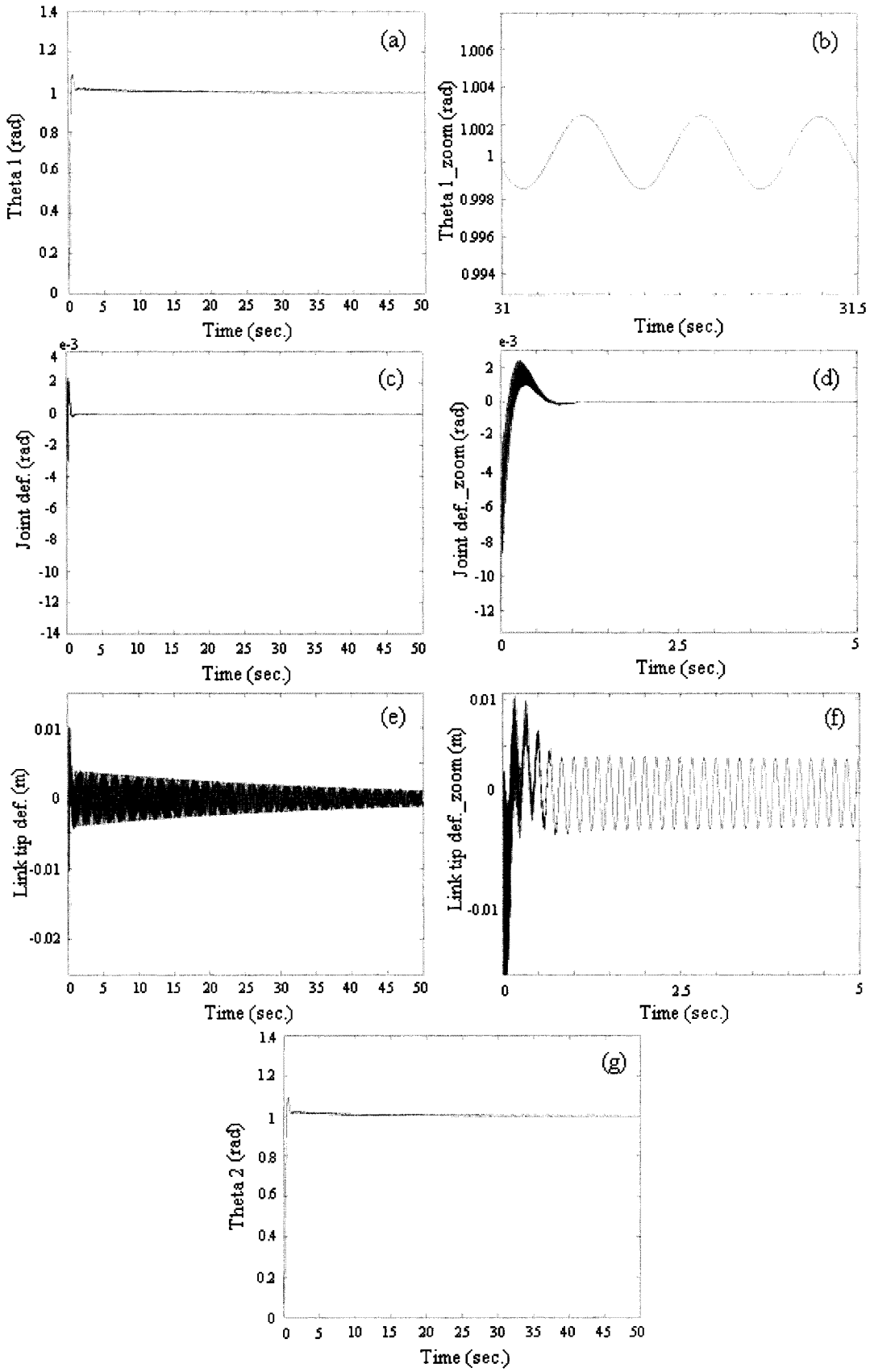

Figure 29: Responses of tracking a unit step for the system without DFS controller

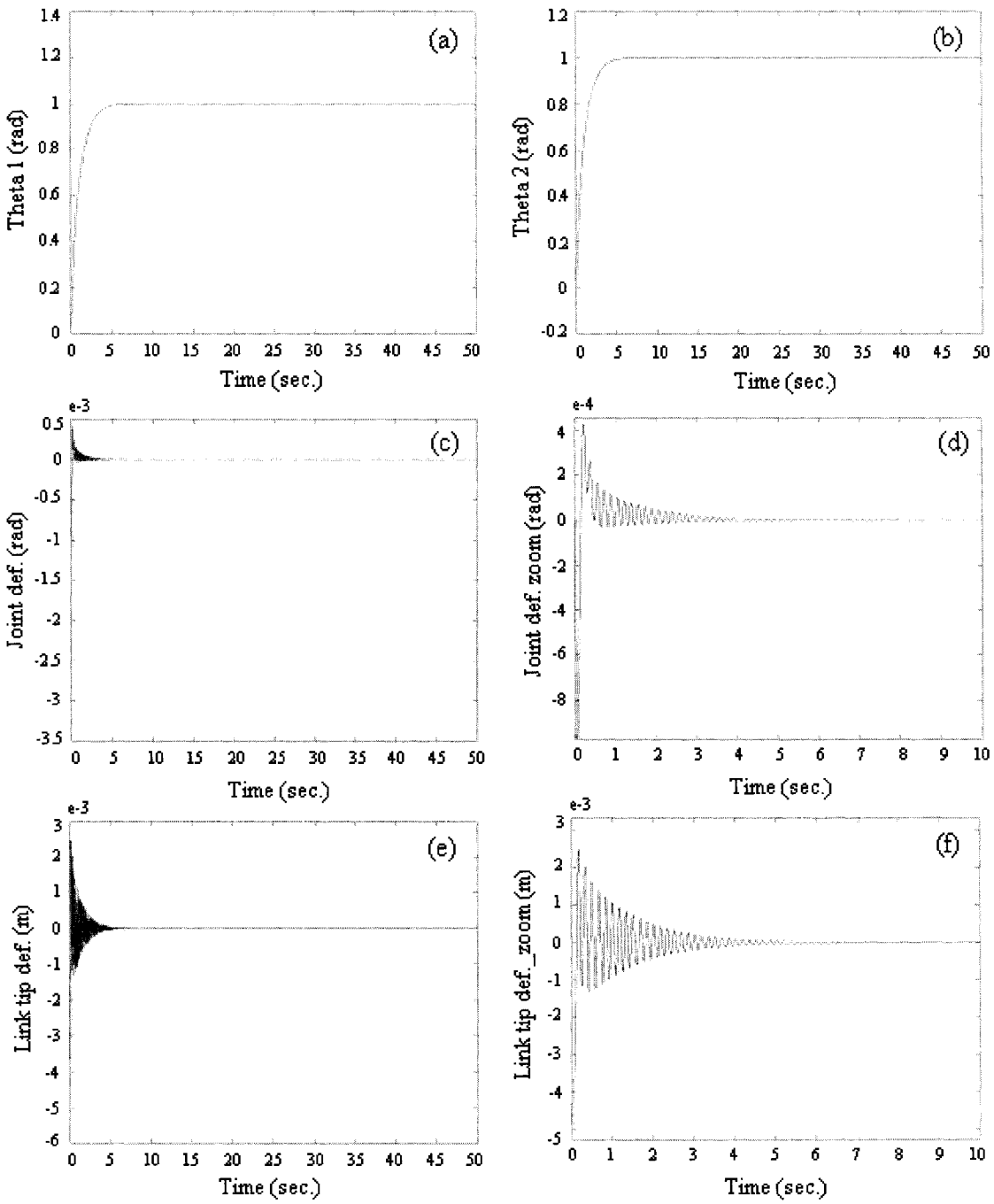

Figure 30: Responses of tracking a unit step for the system with a PD controller and a position angle DFS controller

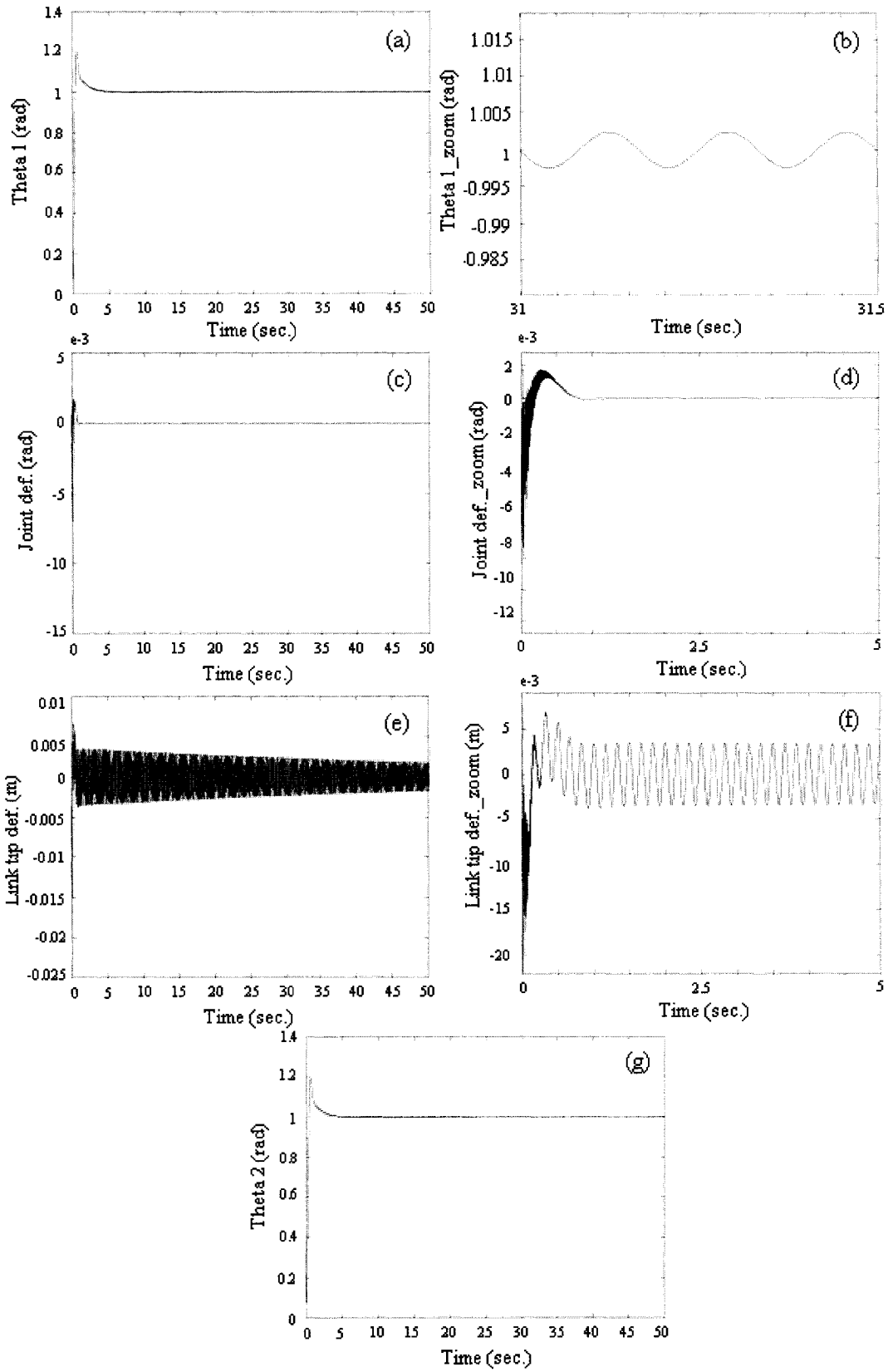

Figure 31: Responses of tracking a unit step for the system with a PD controller and a joint deflection DFS controller

5.4 Discussion and analysis of the position angle DFS controller

Since the position angle DFS controller provides better responses for the FLFJ manipulator, more details about it will be discussed and analyzed in this section. As seen in Table 7, the number of time-delay intervals where the system remained stable decreased and the length of each stable interval also decreased as the control loop gain K increased. The same phenomenon occurred in the system with the joint deflection DFS controller (see Table 13). Investigating the first boundary time point for different gains ranging from 40 to 300, its value located between 0.001845 sec and 0.001347 sec. The time delay $\tau = 0.001$ sec. resulted in stable responses for the system with any gain value between 40 and 300. The control loop gain values $K = 40, 100,$ 150, 200, 250 and 300 were applied to the position angle DFS controller with time delay $\tau = 0.001$ sec. When the manipulator was tracking the desired unit step trajectory, the tip bending deformation of the link and the joint torsional deformation were examined and compared for different gain values to figure out the relationship between the gain value and the system performance.

For both of the link and the joint, zero deflection was desired during the motion of the FLFJ manipulator. However, this was impossible to implement without control. The deformation of the link or the joint must be around the desired zero value and the error between the actual value and the desired value was investigated according to "The Root of Mean Square Error (RMSE)".

The Root of Mean Square Error (RMSE) is equal to the root of the mean of squares of the deviations from the target or desired position. The formula to calculate it takes the following form [41]:

$$RMSE = \sqrt{\frac{1}{m}\sum_{i=1}^{m}(y_i - y_0)^2}$$

In this case, y_i is the tip deflection of the link measured in the moving frame 2 or the joint torsional deflection at one time point, y_0 is the desired zero position (i.e. $y_0 = 0$), and m denotes the number of the total time points involved in the calculation.

As the gain increased, the RMSE of both the tip bending deflection of the link and the joint torsional deflection dropped dramatically (see Figures 32 and 33). However, when the gain reached 200 they began to rise up. The gain $K = 150$ provided the relatively satisfactory responses in comparison with the other five gains, when the time delay τ was kept constant at 0.001 sec.

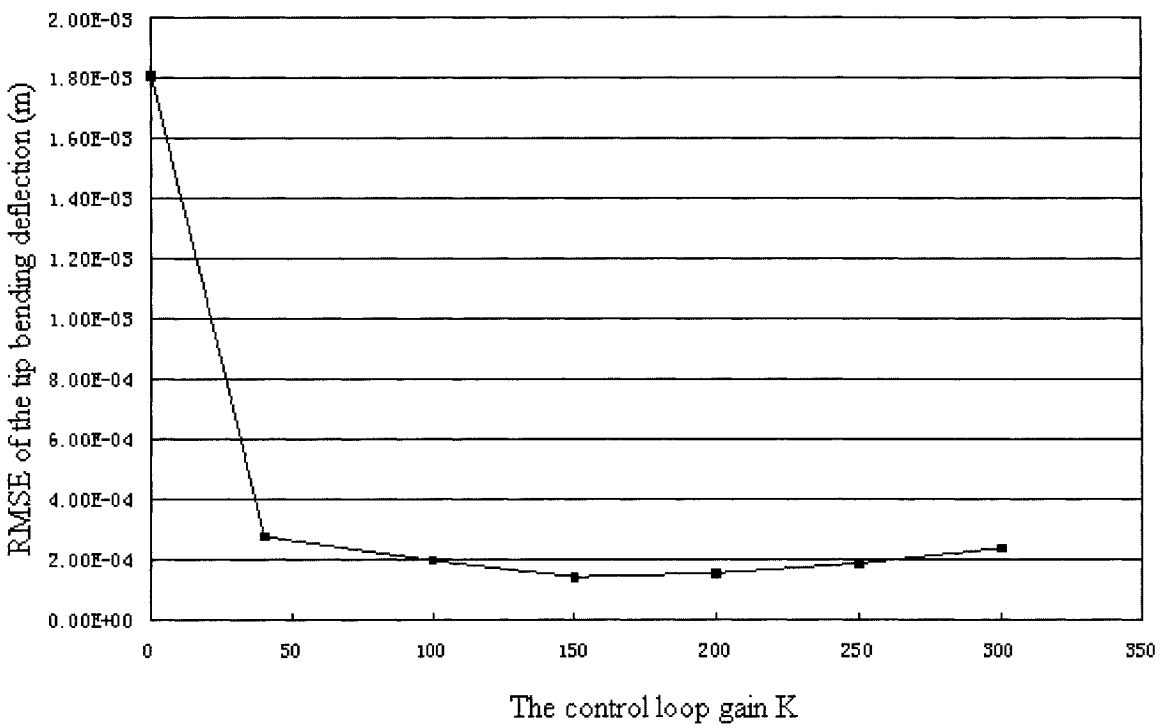

Figure 32: RMSE of the tip bending deflection magnitude for the system with different control loop gain K

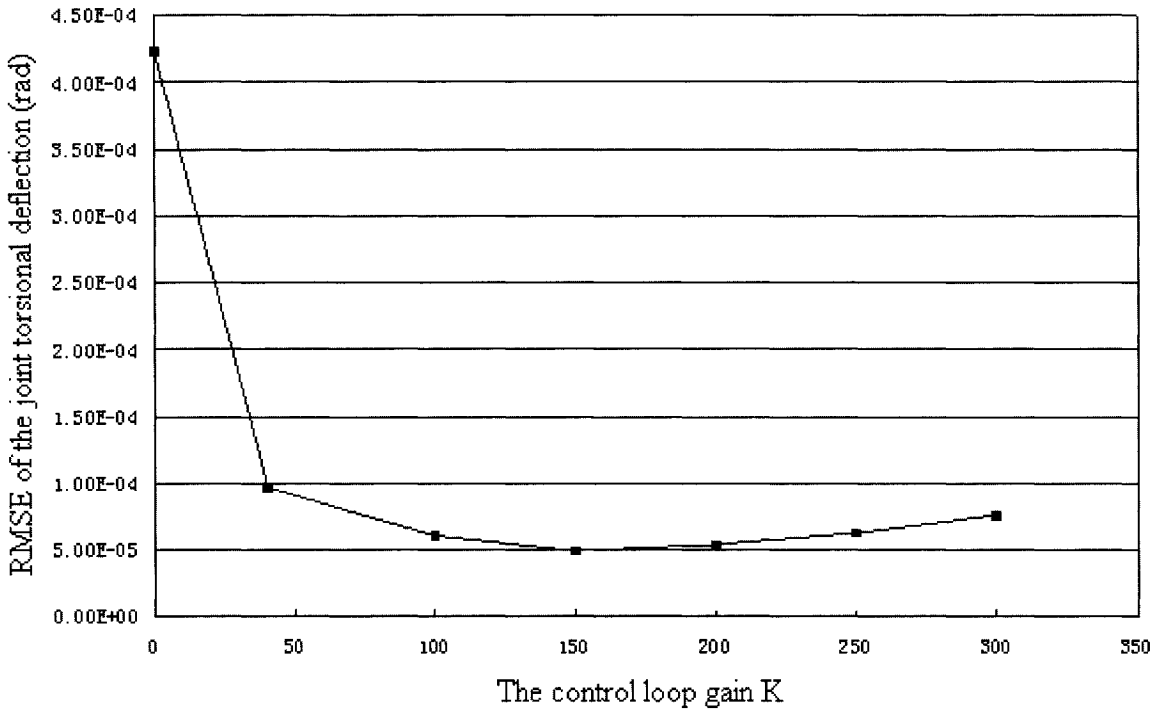

Figure 33: RMSE of the joint torsional deflection magnitude for the system with different control loop gain K

5.5 Comparison between the proposed control system and LQR

Following the analysis in Section 5.4, the position angle DFS controller with gain $K = 150$ and time delay $\tau = 0.001$ sec provided the best dynamic responses in comparison with the other five gains. Hence, the responses of the system under this position angle DFS controller combined with the PD controller were compared with those under the control of a linear quadratic regulator (LQR) to demonstrate the superiority of the DFS controller. The gains in the LQR for each state were obtained using the Matlab code $k = lqr(A, B, Q, R)$ with given matrices Q and R. In the LQR, the control signal is $u = -kx$ (x is an 8-vector) and the matrices Q and R determine the relative important of every mode in the control signal and the expenditure of the energy of the control signal [37]. In this study, it was assumed that Q=eye (8) and R= [1], which means that each mode and the expenditure of the energy have even importance in the control process.

The comparison of the vibrations between the system under the proposed control system and that under an LQR are shown in Figure 34 (a) and (b), while the comparison of the angular position is given in Figure 34(c) and that of the input torque in Figure 34(d).

As seen in these figures, the system controlled by a position angle DFS controller exhibited much smaller deflection magnitude than the system under LQR, while having almost the same settling time. Furthermore, the modified PD controller made the system have good performance of tracking a unit step reference input, but LQR produced an offset for the steady state response. Besides the advantages of the proposed control system mentioned above, the input energy used for it to produce such good responses was even much less than that used for the LQR (see Figure 34(d)). The most significant advantage of the proposed control system was that it only needed to use the position angle of the FLFJ manipulator but not all the state variables. In the proposed control system, only one state variable (θ_1) was fed back to obtain the control signal. In the control signal, two control parameters were included in the DFS path, the feedback gain K and the time delay value τ, and two gains for the PD controller. For LQR, the same number of feedback gains as that of the states had to be decided to obtain the control signal. However, some state variables of the system were difficult or impossible to obtain.

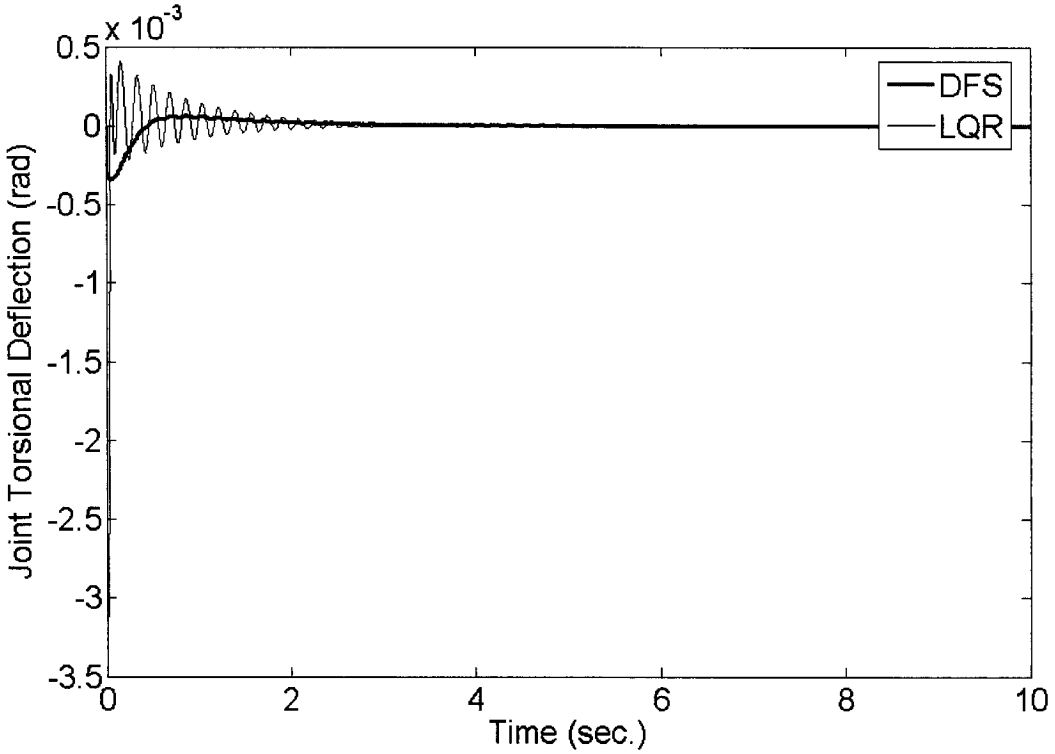

Figure 34(a): Comparison between the joint torsional deflection of the FLFJ manipulator under LQR and that under the proposed control system

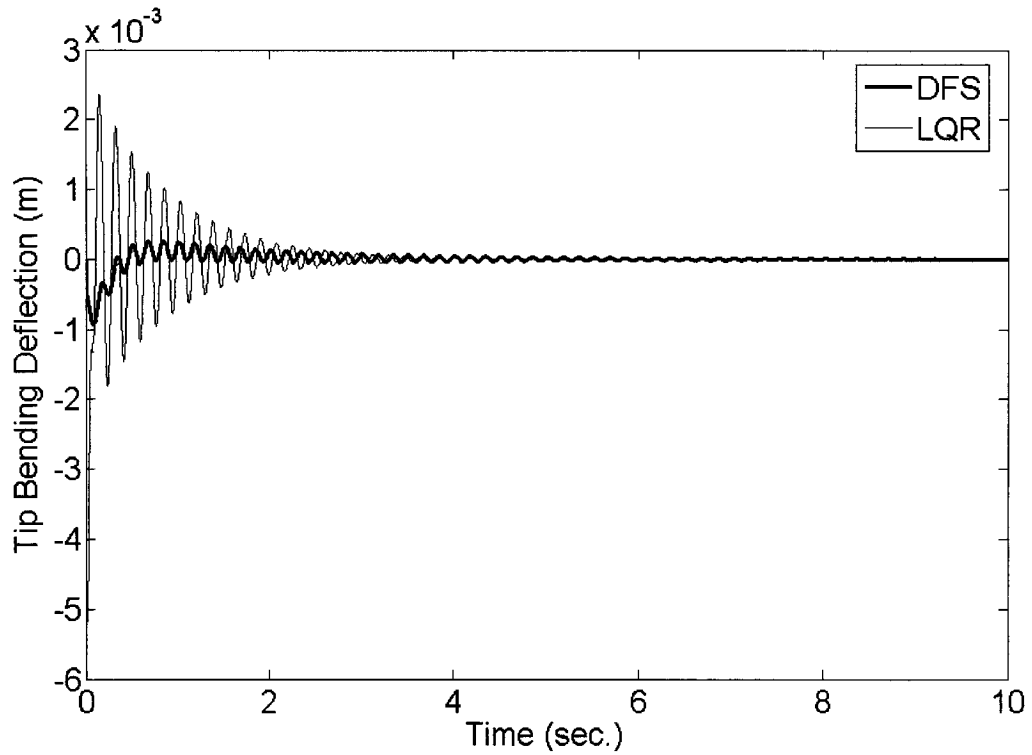

Figure 34(b): Comparison between the tip bending deflection of the FLFJ manipulator under LQR and that under the proposed control system

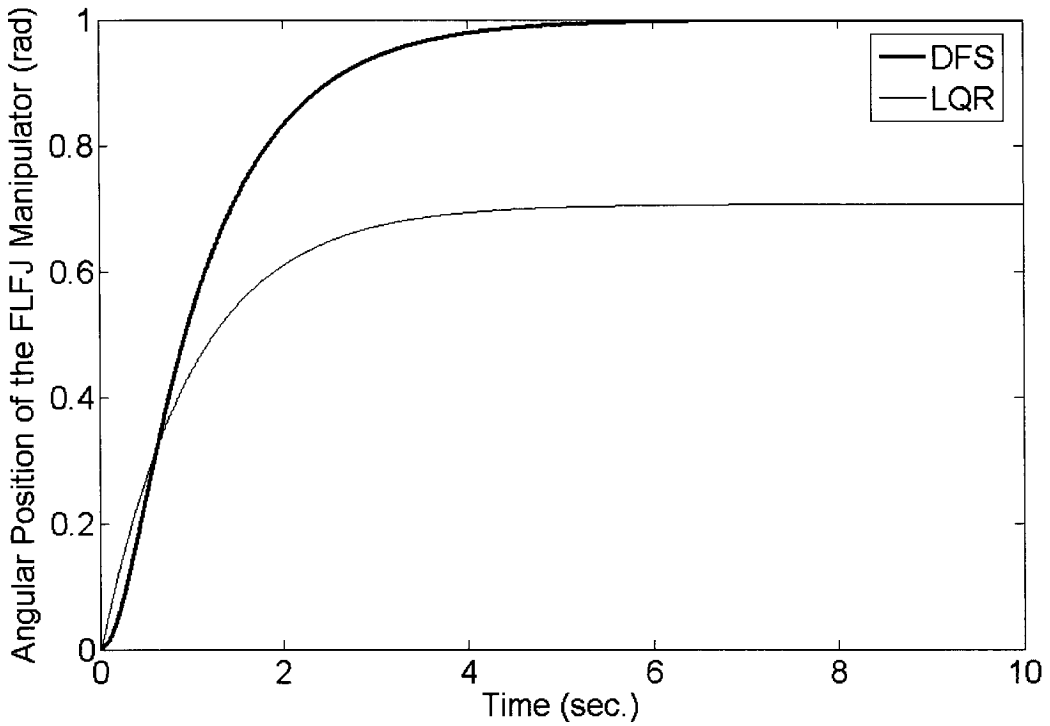

Figure 34(c): Comparison between the angular position of the FLFJ manipulator under LQR and that under the proposed control system

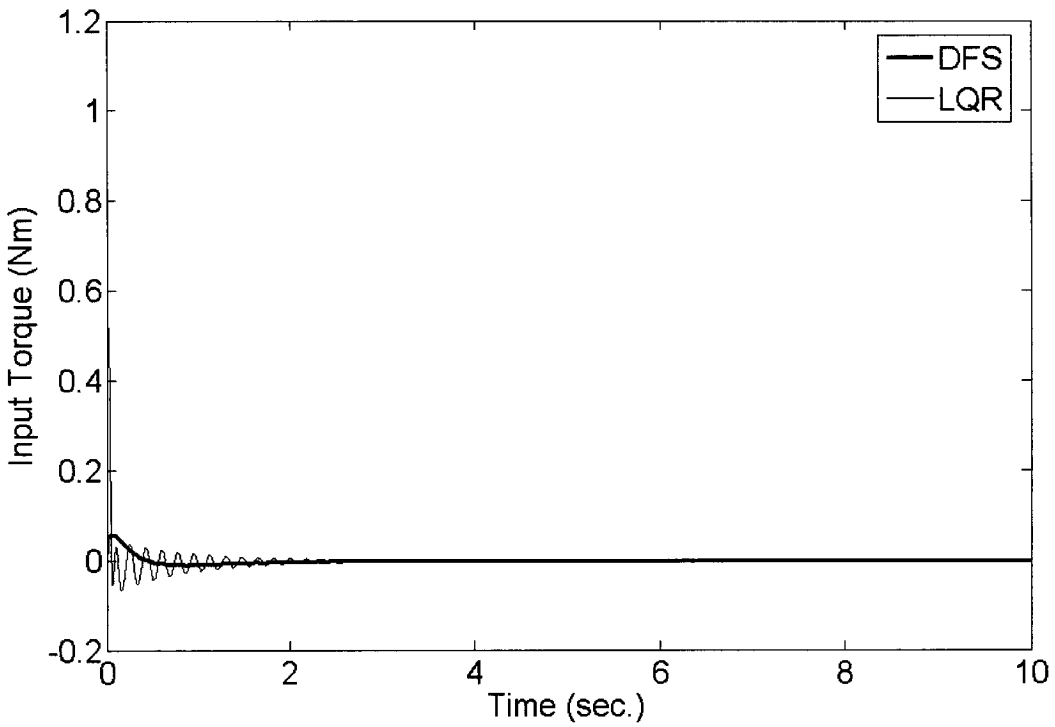

Figure 34(d): Comparison between the input torque of the FLFJ manipulator under LQR and that under the proposed control system

5.6 Robustness of the proposed control system

The robustness of the proposed control system was investigated in two aspects: being subjected to an external disturbance and system parameter uncertainty. The diagram of the controlled system that was subjected to an external disturbance is displayed in Figure 35. The torque disturbance was a single rectangular wave having the form as:

$$D = \begin{cases} 0.15 & 1 \le t \le 1.5 \\ 0 & t \succ 1.5 \cup t \prec 1 \end{cases}$$

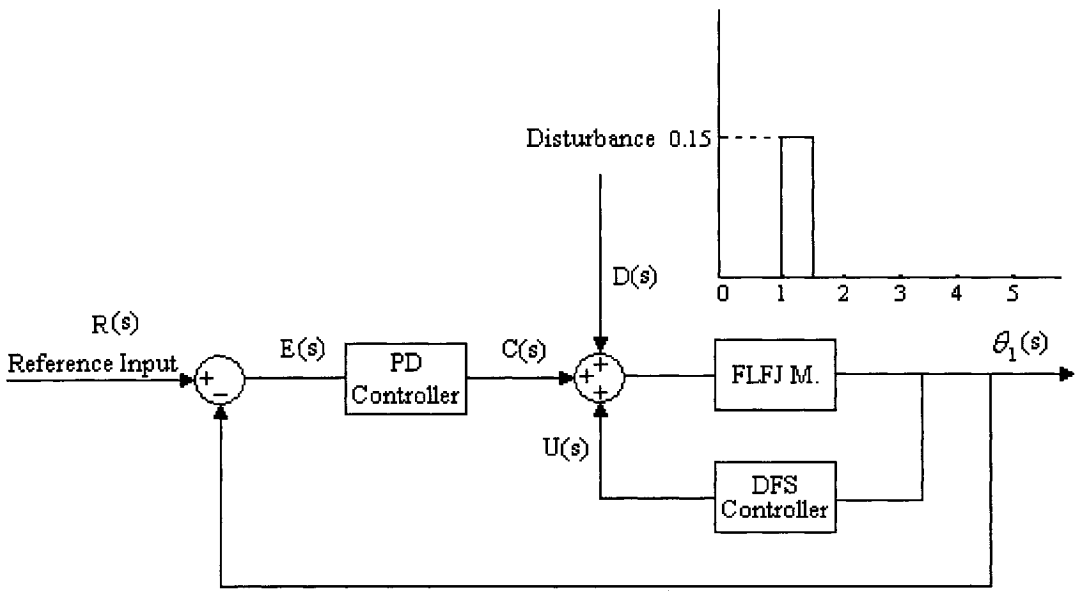

Figure 35: Block diagram of the controlled system with an external disturbance

The responses of the system subjected to such a disturbance are shown in Figure 36. Some overshoot was caused by the disturbance in the angular position θ_1, but it came back to the desired position (1 radian) soon. Both the tip bending deflection of the link and the joint torsional deflection were robust in response to the external disturbance. They were damped out within almost the same settling time as those of a system without disturbance.

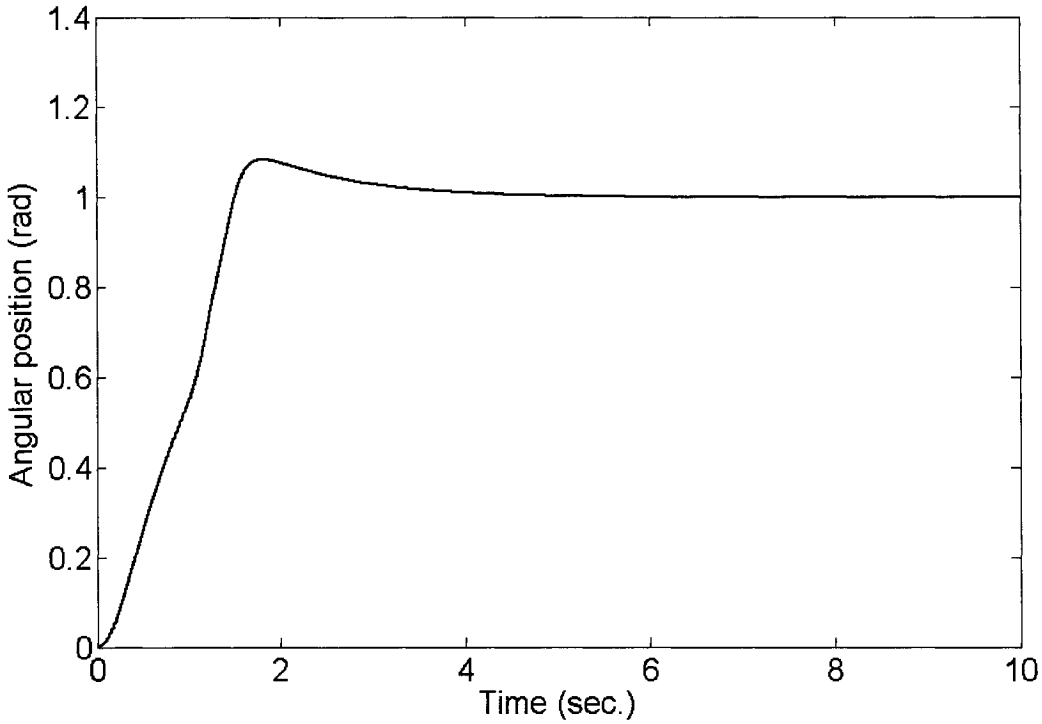

Figure 36(a): Angular position θ_1 of the FLFJ manipulator subjected to an external disturbance

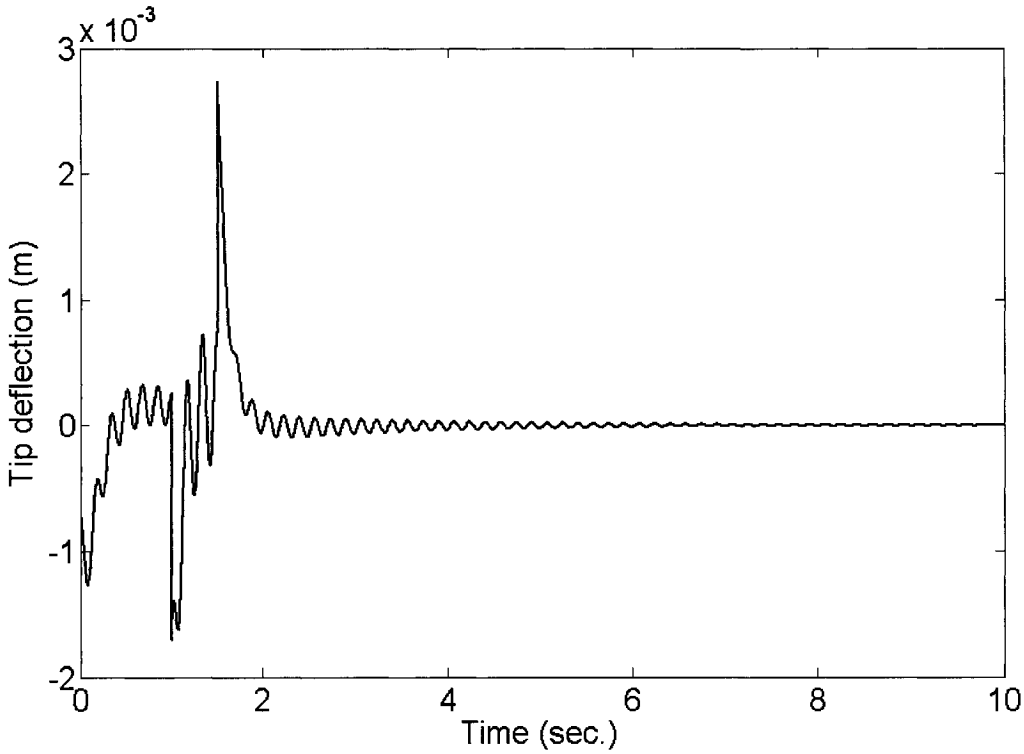

Figure 36(b): Tip bending deflection of the FLFJ manipulator subjected to an external disturbance

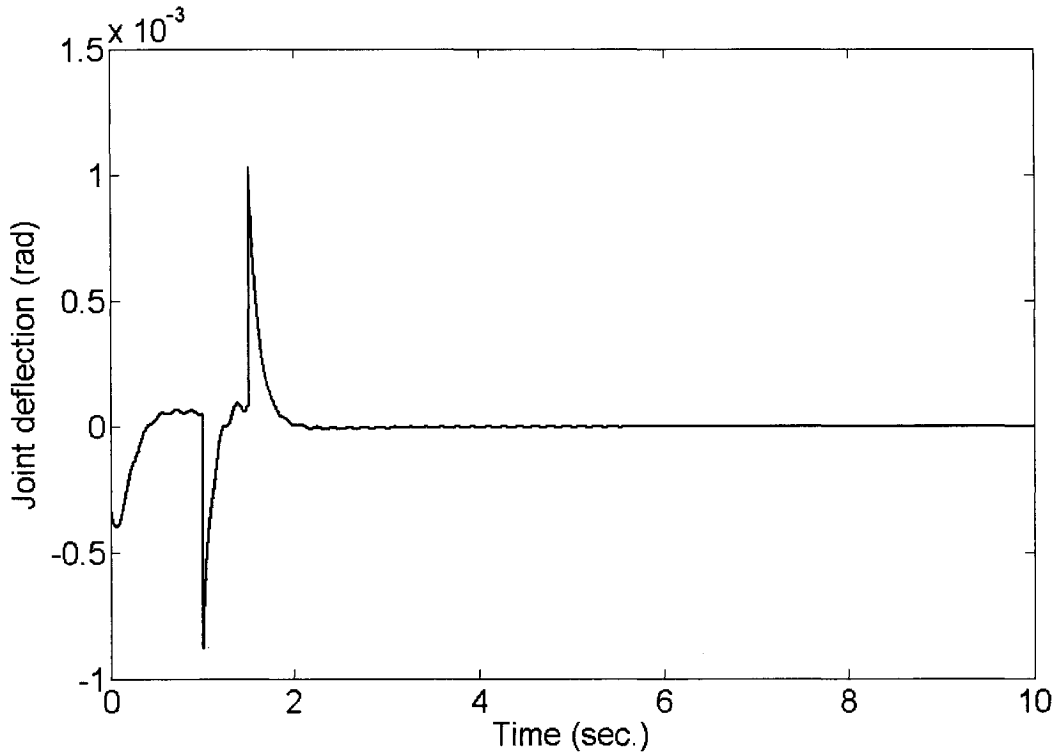

Figure 36(c): Joint torsional deflection of the FLFJ manipulator subjected to an external disturbance

The robustness of the system in response to system parameter uncertainty was tested by increasing the hub inertia by 100% or decreasing the joint stiffness by 50%. The responses were compared with those of the original system and are shown in Figures 37 and 38, respectively. After augmenting the hub inertia, the combination of PD controller and position angle DFS controller still led the manipulator to the desired angular position and meanwhile eliminated the vibration of both the link and the joint. However, the slope of the transient response of the angular position was a little larger than that of the original system and the deflections of the tip and the joint both increased. In decreasing the joint stiffness, the controller also provided satisfactory system performance where the angular position and the tip bending deflection had almost the same motion contrails, but the joint torsional vibration had a larger deformation.

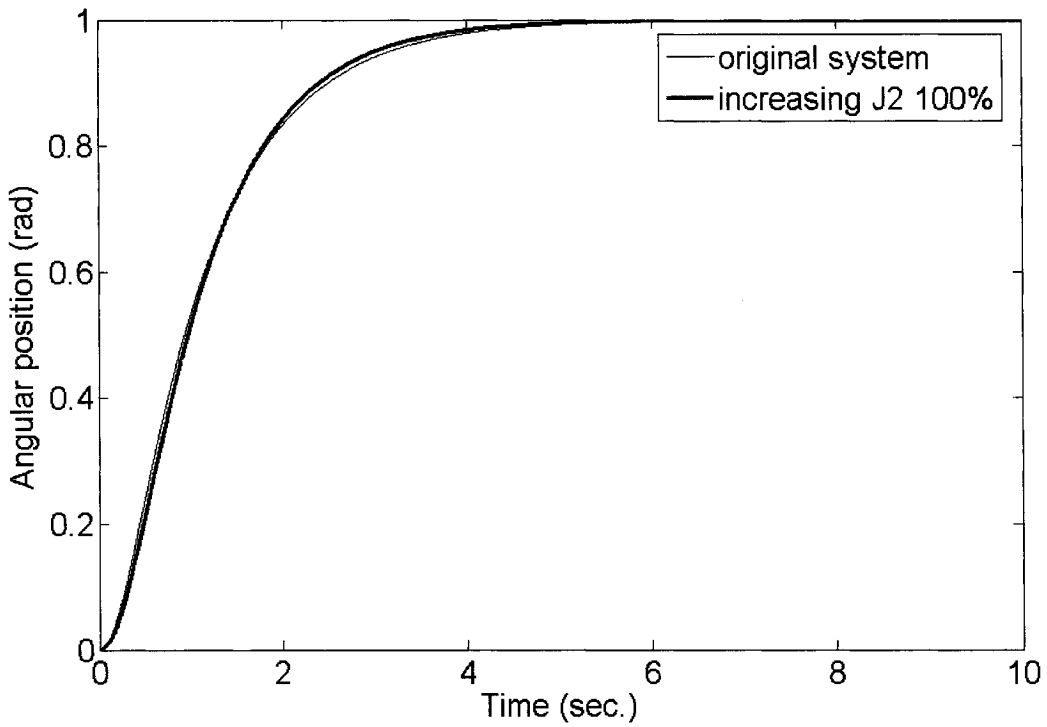

Figure 37(a): Difference between the angular position of the original system and that of the system with a 100% increase in hub inertia

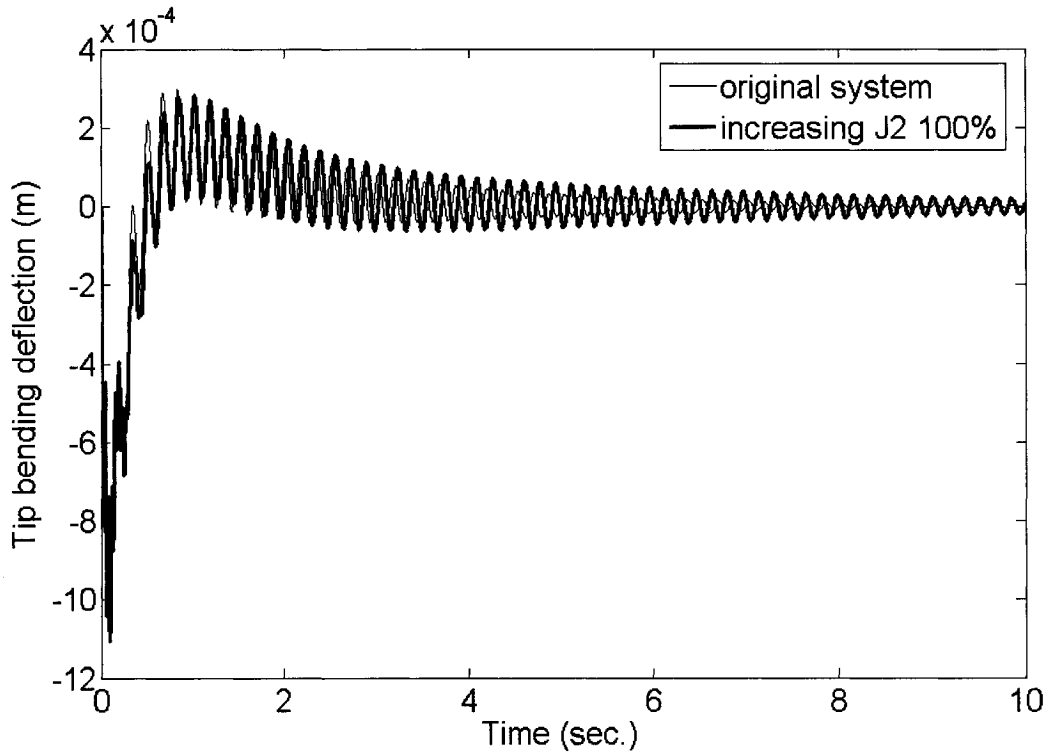

Figure 37(b): Difference between the tip bending deflection of the original system and that of the system with a 100% increase in hub inertia

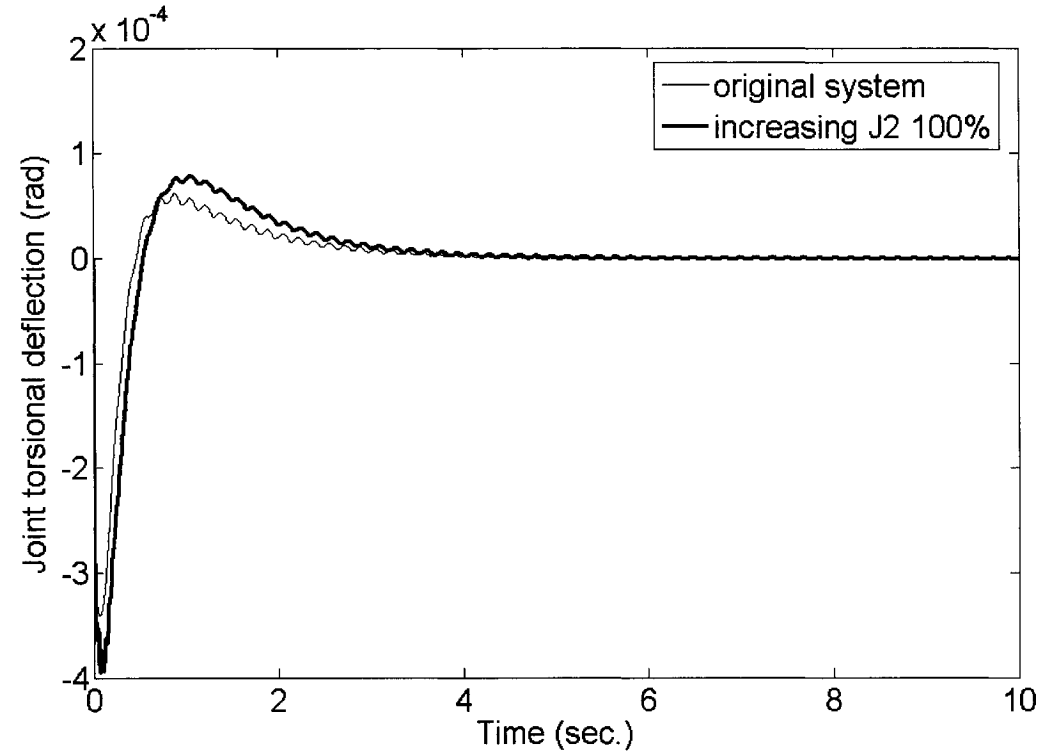

Figure 37(c): Difference between the joint torsional deflection of the original system and that of the system with a 100% increase in hub inertia

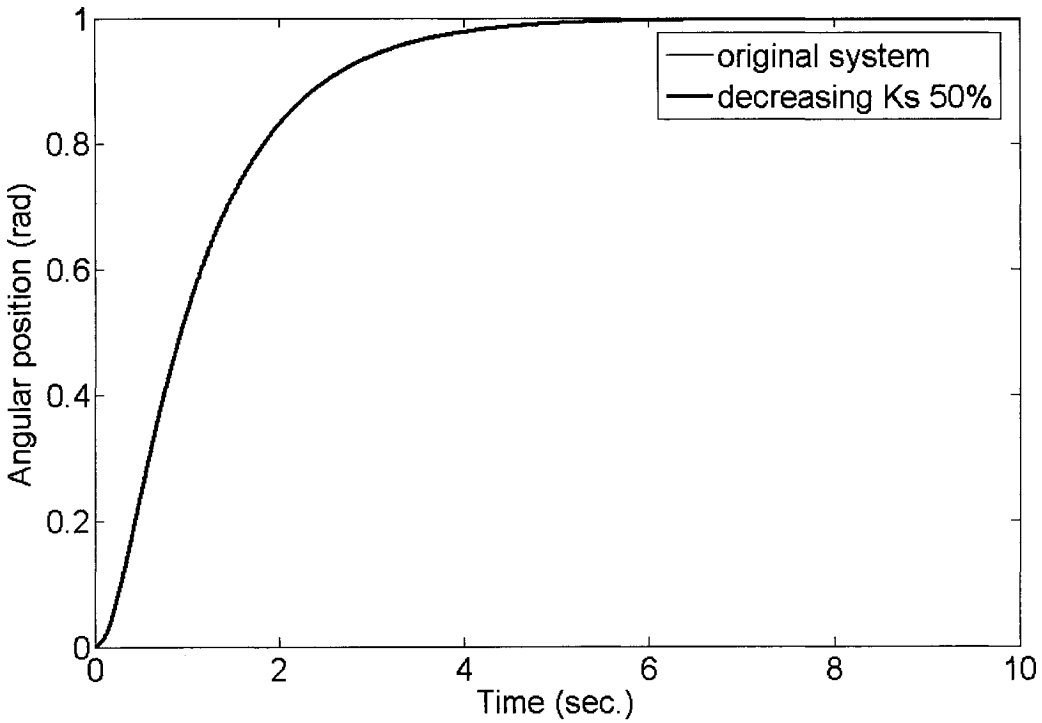

Figure 38(a): Difference between the angular position of the original system and that of the system with a 50% decrease in joint stiffness

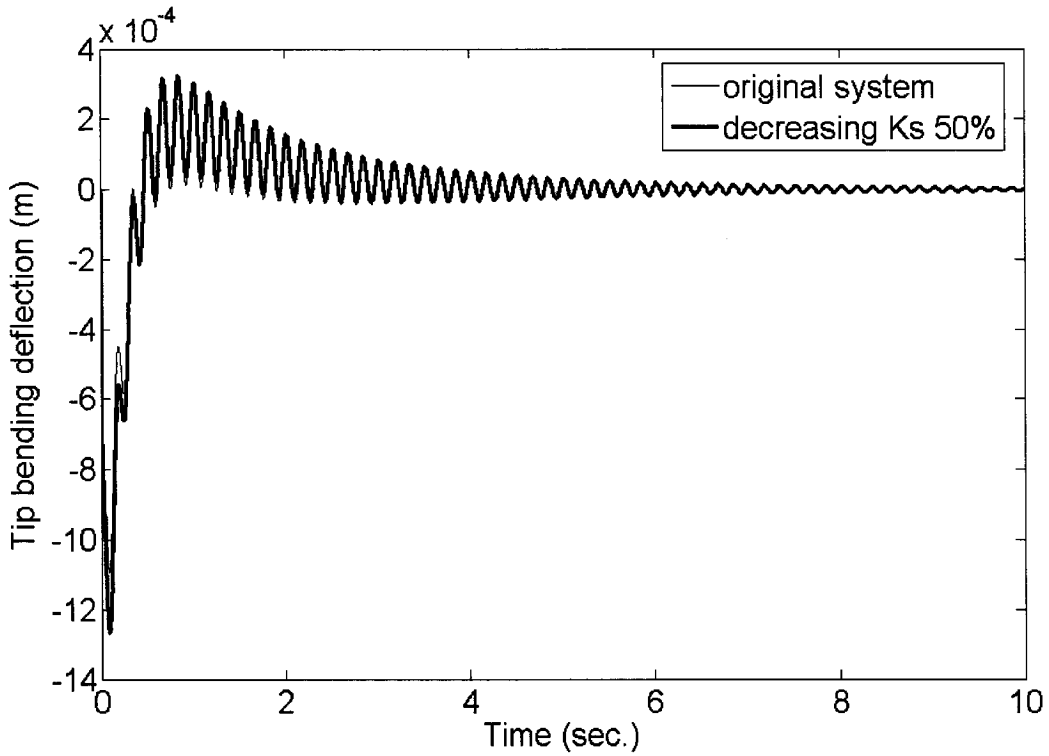

Figure 38(b): Difference between the tip bending deflection of the original system and that of the system with a 50% decrease in joint stiffness

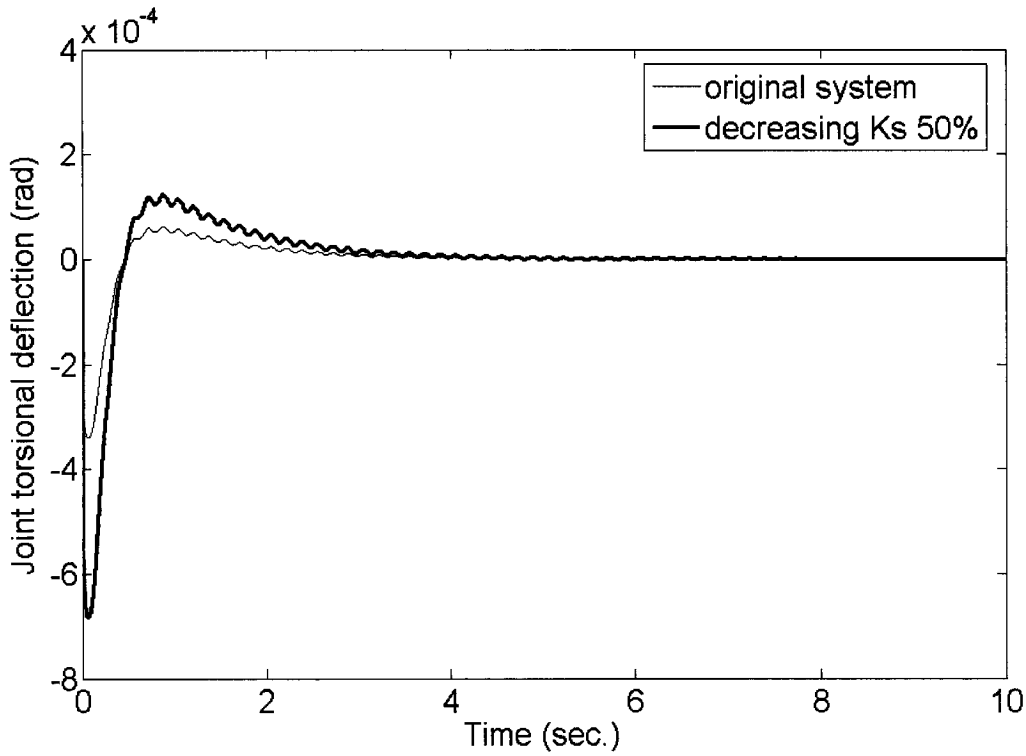

Figure 38(c): Difference between the joint torsional deflection of the original system and that of the system with a 50% decrease in joint stiffness

5.7 Conclusions

The system stability changed as the time delay value in the control loop varied. It was also found that an appropriate combination of control loop gain and time delay could improve the system performance greatly. As the gain value increased, the time-delayed feedback signal controller had better performance. Combined with a modified PD controller, the position angle DFS controller had better performance of tracking reference input and eliminating the unexpected vibration, while the joint deflection DFS controller could only improve the transient responses. In comparison with LQR, under the proposed control system, the flexible manipulator had less deflection and better tracking of the reference input, all of which were produced by rather less input energy. The proposed control system was also robust in response to external disturbances and system parameter uncertainties. The proposed control system was proved to be efficient and easily implemented.

Chapter 6: Experimental Setup and Results

6.1 Introduction

In this chapter, an experimental setup is designed and built to implement the proposed control system in chapter 5 on a prototype of the single FLFJ manipulator. The control system applied on the real model consists of a position angle DFS controller and a modified PD controller, since the position angle DFS controller has better performance than the joint deflection DFS controller with combining with the modified PD controller. The experimental results are compared for the systems with and without the proposed control system to investigate its effectiveness.

6.2 Design steps

The experimental test-bed was designed to be a constrained planar single-link and single-joint flexible manipulator which only operated in the horizontal plane. Therefore, it was required that the height of the link cross section should be much larger than the width. In this design, the height was 25mm and the width was 2.5mm. These dimensions made the link very rigid on the vertical plane and thus the bending deflection in this direction could be ignored. The link was a half meter in length and made of aluminum, and was a flexible arm with small bending motion in the horizontal plane. Because both the small link bending deformation and the small joint torsional deformation were assumed in the previous dynamic model, the joint motion was also constrained. The joint shaft was designed as a little solid shaft and made of aluminum too, since aluminum has a small shear modulus in comparison with other common materials. The shaft had a diameter of 6mm and a length of 20mm and was connected with the motor shaft using two set screws. A hub whose diameter is 184mm

and height is 28mm was added to couple the joint and the link. This experimental setup served mainly to verify if the position angle DFS controller worked in the real model, which had been proven to be better than the joint deflection DFS controller for the vibration damping of the FLFJ manipulator when the rigid body motion was desired to track a unit reference input. The maximum instantaneous shaft speed, the maximum instantaneous torque and continuous torque applied to the armature windings by the magnetic field were considered to select a suitable DC motor. The system parameters of the experimental setup are shown in Table14.

Table 14: Parameter values of the experimental test-bed

Definition	Parameter	Value
Length of the link	l	$0.5\,m$
Height of the link in the cross section	W	$25\,mm$
Width of the link in the cross section	t	$2.5\,mm$
Diameter of the hub	D	$184\,mm$
Height of the hub	H	$28\,mm$
Diameter of the joint shaft	d	$6\,mm$
Height of the joint shaft	h	$20\,mm$

6.3 Instrumentation systems

6.3.1 Driver amplifier and actuator

Based on the maximum shaft speed and the peak and continuous values of the input torque obtained in the simulation, the DC gear motor 9234C212-R3-2C1533 with a gear ratio of 5.9:1 was selected to supply power to the FLFJ manipulator. The most significant advantage of this kind of motor is that it has a Hewlett-Packard optical encoder with 500

CPR at the bottom, which can be used to feedback the position angle of the manipulator θ_1. In addition, the gear head can amplify the torque from motor to load and minimize the motor size with a specific load [42]. A brush type servo amplifier 25A8 was used to power the DC gear motor. This amplifier can be configured in various modes and accept an analog ± 10V command signal. In this experiment, the current mode was selected, which transferred the input voltage to the output current and then gave the motor the required torque.

6.3.2 Hardware-in-the-loop experimentation

A Quanser Q8 Hardware-In-the-Loop (H.I.L.) measurement and control board integrated with XP, Matlab/Simulink and RTW via Quanser WinCon was employed to complete the data acquisition and control. The Q8 board was connected to a terminal board with ribbon cables to simplify the hardware integration. Combined with WinCon and a computer, the Q8 can fulfill real time control for a variety of hardware systems and handle even the most demanding performance requirements. Furthermore, the Q8 board has a maximum count frequency of 8MHz and 15MHz in 4X Quadrature and Non-Quadrature, respectively, which can receive continuous signals from the encoder [43]. The hardware-in-the-loop diagram of the system with a combination of PD controller and DFS controller is shown in Figure 39.

6.3.3 Strain gauges and their amplifiers

The purpose of this experimental test-bed was to test if the tip bending deformation of the link and the joint torsional deformation were reduced after applying the DFS controller in comparison with those before adding the DFS controller. To measure the two deflections, two bending strain gauges and a torque/shear pattern strain gauge were employed. The

bending strain gauge was used to test the largest bending strain at the root-end of the link and then the tip deflection was calculated through a linear formula because the link was assumed to have even geometry and material properties. The torque/shear strain gauge was employed to measure the shear strain and then the joint torsional deflection was obtained. In the literature, a light source at the tip and a camera at the hub were combined to measure the tip deflection, and the mass and inertia of the light source were added to those of the tip payload. However, this kind of non-electrical device is expensive and has high operation requirements. Thus, the widely used electrical strain gauges are smart alternatives due to their practical advantages such as high accuracy, fast response, low cost and high effectiveness, etc. Here, two linear pattern strain gauges EA-06-250BG-120 were applied to the two sides of the link at the root-end in a half bridge configuration to measure the largest bending strain of the link (see Figure 40(a)). One of them was extended and the other was compressed, which increased the signal range. In this way, the strain gauges were more sensitive to stress. Furthermore, this sort of configuration was rather less sensitive to stress in torsion, axial extension and transverse bending, so it was a good choice for the bending strain test. For the joint torsional deformation, a torque/shear pattern strain gauge EA-06-062TW-120 was selected for this design. It had two sections in one pattern, which meant the gauge represented two active elements in a half bridge configuration. This strain gauge is displayed in Figure 40(b) together with its distribution on the shaft. To amplify the output from the bending strain gauge for accurate digital conversion [44], a self-designed open circuit which included a Wheatstone bridge and an operational amplifier LM 741 was employed. Meanwhile, a digital strain indicator VISHAY/ELLIS-20 and an amplifier circuit with LF 412 were used for the torque/shear strain gauge. The diagrams of these two circuits are given in Figures 41 and 42, respectively. Batteries were chosen to supply the DC power

to the circuits instead of a power supply to lessen the noise. For the bending gauge, a voltage regulator and two capacitors were set up with the battery which gave the power to the bridge to supply a stable input voltage (5V), even though the battery might discharge over time. To amplify the output and distinguish the useful signal from noise, a large gain in the operational amplifier loop for the bending strain gauge was selected as $\frac{R_6}{R_5} = 1000$. In addition, a potentiometer was set in the loop to balance the output signal. In the torque/shear strain gauge loop, the maximum amplifier gain was $\frac{R_2}{R_1} = 500$ and this gain value could be adjusted by a potentiometer according to the requirements. The whole experimental setup is displayed in Figure 43.

The values read by the Q8 board were the output voltages of the amplifier circuits. However, there was a certain relation between the out voltage and the strain value and then the strain values which were then converted to actual deflections. For the half bridge, the output of the Wheatstone bridge is equal to:

$$V_o = \frac{G_F \varepsilon}{2} V_i \tag{6.3-1}$$

where V_o is the output of the Wheatstone bridge, which is equal to the input of the amplifier circuit V_{in}, and V_i signify the input voltage over the Wheatstone bridge. In addition, G_F and ε denote the strain gauge factor of the applied strain gauge and the strain value, respectively. Going through an inverting amplifier for signal conditioning, the output of the amplifier circuit has the following form:

$$V_{out} = -\frac{R_o}{R_i} V_{in} \tag{6.3-2}$$

Putting Equation (6.3-1) and $V_{in} = V_o$ into Equation (6.3-2), we get:

$$V_{out} = -\frac{R_o}{R_i} \cdot \frac{G_F \varepsilon}{2} V_i \tag{6.3-3}$$

Therefore, the strain value was derived as:

$$\varepsilon = -\frac{2R_i}{R_o G_F V_i} V_{out} \tag{6.3-4}$$

For the tip bending deflection, the strain ε at the root end of the link can be expressed in terms of the deflection w at the tip of the link if ideal geometry and material properties are assumed for the link. Thus, the largest strain in the link could be written as:

$$\varepsilon = \frac{3wt}{2l^2} \text{ [45]} \tag{6.3-5}$$

where t is the width of the link cross section and l is the length of the link. Therefore, by combining Equation (6.3-4) and (6.3-5), the actual tip deflection of the link w is derived as:

$$w = -\frac{4l^2 R_i}{3tR_o G_F V_i} V_{out} \tag{6.3-6}$$

This procedure could be also applied to obtain the joint torsional deflection and the according strain-displacement relationship is:

$$\gamma = r\frac{\phi}{l} \text{ [45]} \tag{6.3-7}$$

where γ is the shear strain obtained from the torque/shear gauge, ϕ denotes the torsional deflection of the shaft and r_S is the radius of the shaft.

The joint torsional deflection can be thus expressed as:

$$\phi = -\frac{2R_i l}{R_o G_F V_i r} V_{out} \tag{6.3-8}$$

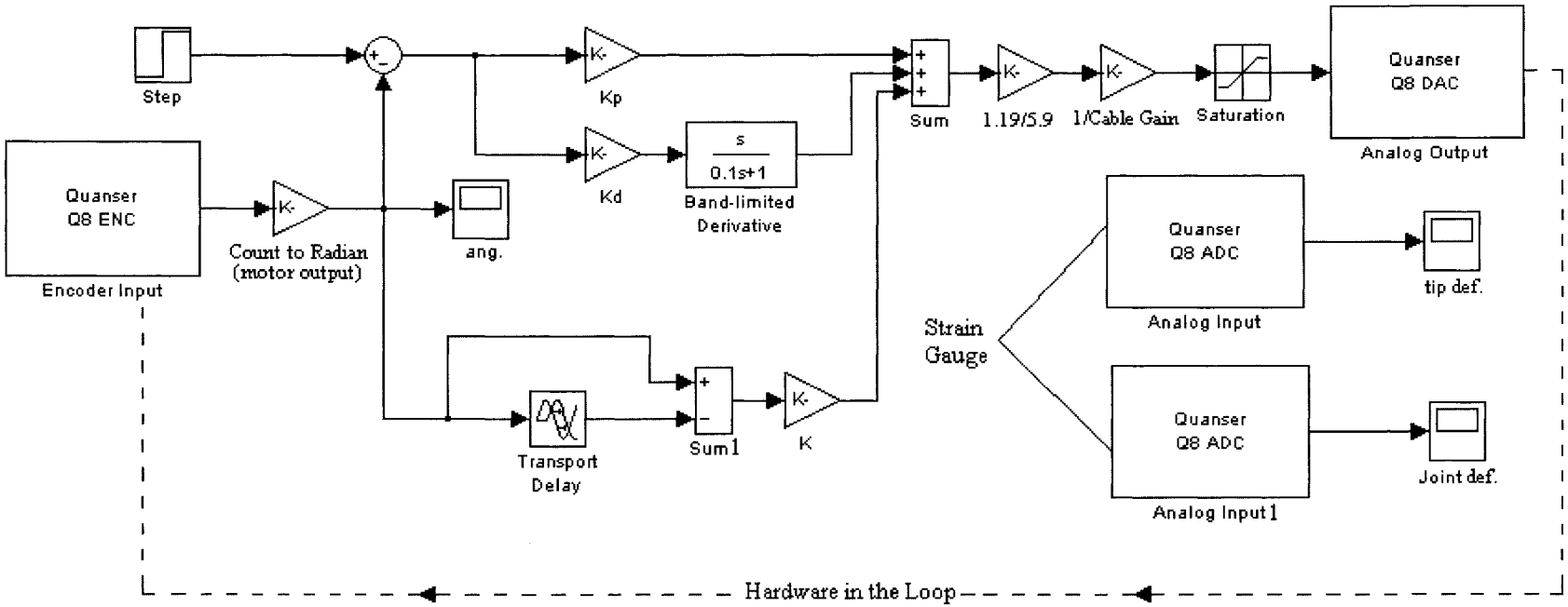

Figure 39: Hardware-in-the-loop diagram of the system with PD controller and DFS controller

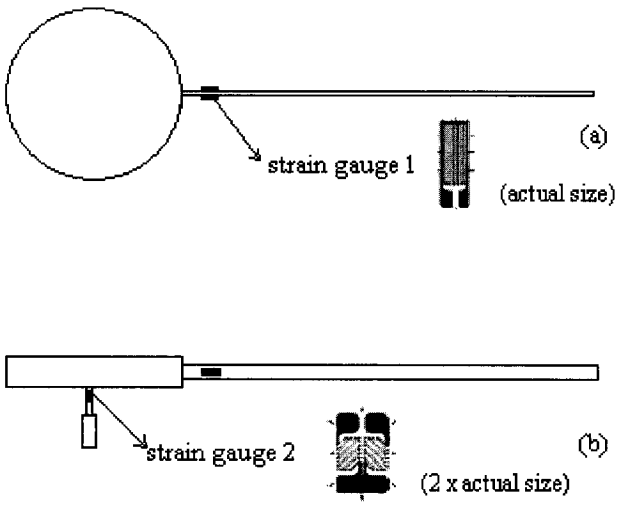

Figure 40: Distribution of the strain gauges

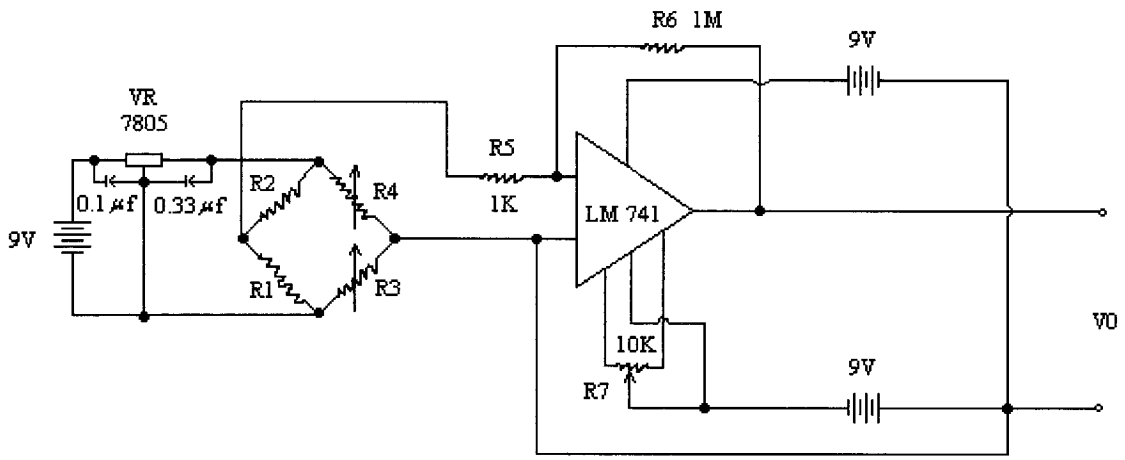

Figure 41: Diagram of the Wheatstone bridge and strain gauge 1's amplifier

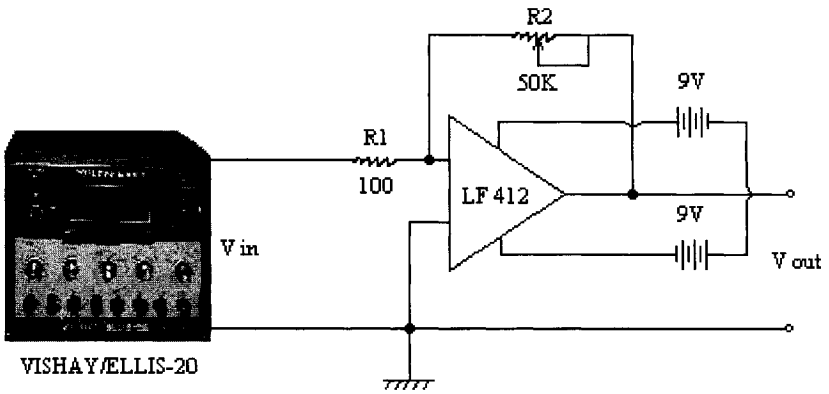

Figure 42: Digital strain indicator and strain gauge 2's amplifier

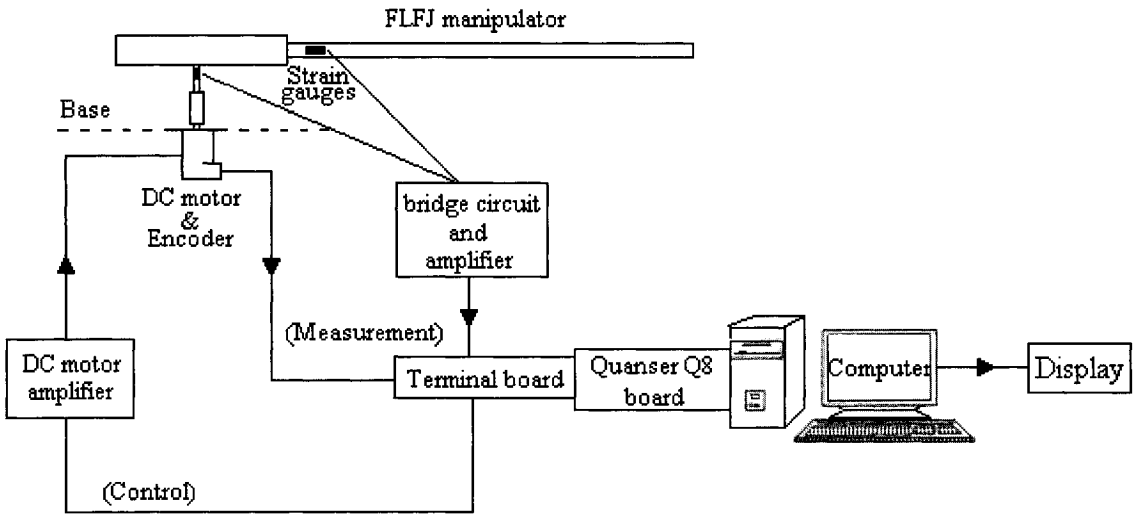

Figure 43: Experiment setup

6.4 Experimental results and discussion

The dynamic responses of the system controlled by the combination of a PD controller and a DFS controller had been predicted in the simulation. The modified PD controller and the position angle DFS controller were proven to have a strong ability to lead the FLFJ manipulator to a desired rigid body position and eliminate the vibration of the link and the joint during the motion. The primary dimensional parameters of the experimental test-bed are listed in Table 14 and the structure drawings are provided in the appendix C as well as its photo are shown in Figure 44.

The position angle DFS controller and the modified PD controller designed in the simulation were used in the experiment. However, the system parameters of the experimental test-bed were not the same as those in the simulation model. Therefore, the controller parameters had to be tuned based on the real model in the experiment. In addition, the gain values in the DFS control loop were constrained in the experiment due to the limit of the motor current. Using the experimental trial method, the maximum gain which could be employed in the experiment setup for the position angle DFS controller with a time delay of 0.001 sec was 40. The values of K_p and K_d in the PD controller obtained in the Matlab & Simulink Response Optimization had to be modified to make the rigid body of the manipulator achieve the desired final position 1 radian (57.3 degrees) from the beginning position. During the experimental trial, the value of K_d was kept unchanged while the value of K_p was raised until the satisfactory tracking response was obtained. The gain values of the PD controller obtained in the simulation $K_p = 0.0998$, $K_d = 0.0011$ were modified to $K_p = 0.25$ and $K_d = 0.0011$ for the system with a position angle DFS controller

($K = 40, \tau = 0.001$). Based on the same procedure, the parameter values of the PD controller for the system without the control of the DFS controller were tuned to $K_p = 0.28$ and $K_d = 0.0551$ from $K_p = 0.04, K_d = 0.0551$. After applying the position angle DFS controller, the excessive vibrations of the flexible link and the flexible joint were both greatly reduced (see Figures 45 and 46), even though the vibrations after 2 seconds were not shown out because the link and the joint in this experimental test-bed were not very flexible. In further work, the link and the joint could be designed to be more flexible to display more vibration in order that the ability of the DFS controller to eliminate excessive vibrations could be further validated. It can be seen from the experimental results that the system responses did not begin at zero due to the circuit balance and some offset was exhibited in the joint deflection since the wires connecting the strain gauge and its indicator gave some unexpected tension to the sensitive strain gauge during testing. However, these factors did not have a significant effect on the experiment results, and it can be still concluded that the excessive vibrations of both the link and the joint were damped out in a large amount by the DFS controller. As well, the manipulator was able to track the desired trajectory under the control of the PD controller at the same time.

Because of the limit placed on the motor current, larger gains in the position angle DFS controller were not verified in the real model, but the performance of the DFS controller with much larger gains was predicted in the simulation (see Figure 30), which indicated that the dynamic responses could be better with a larger gain K.

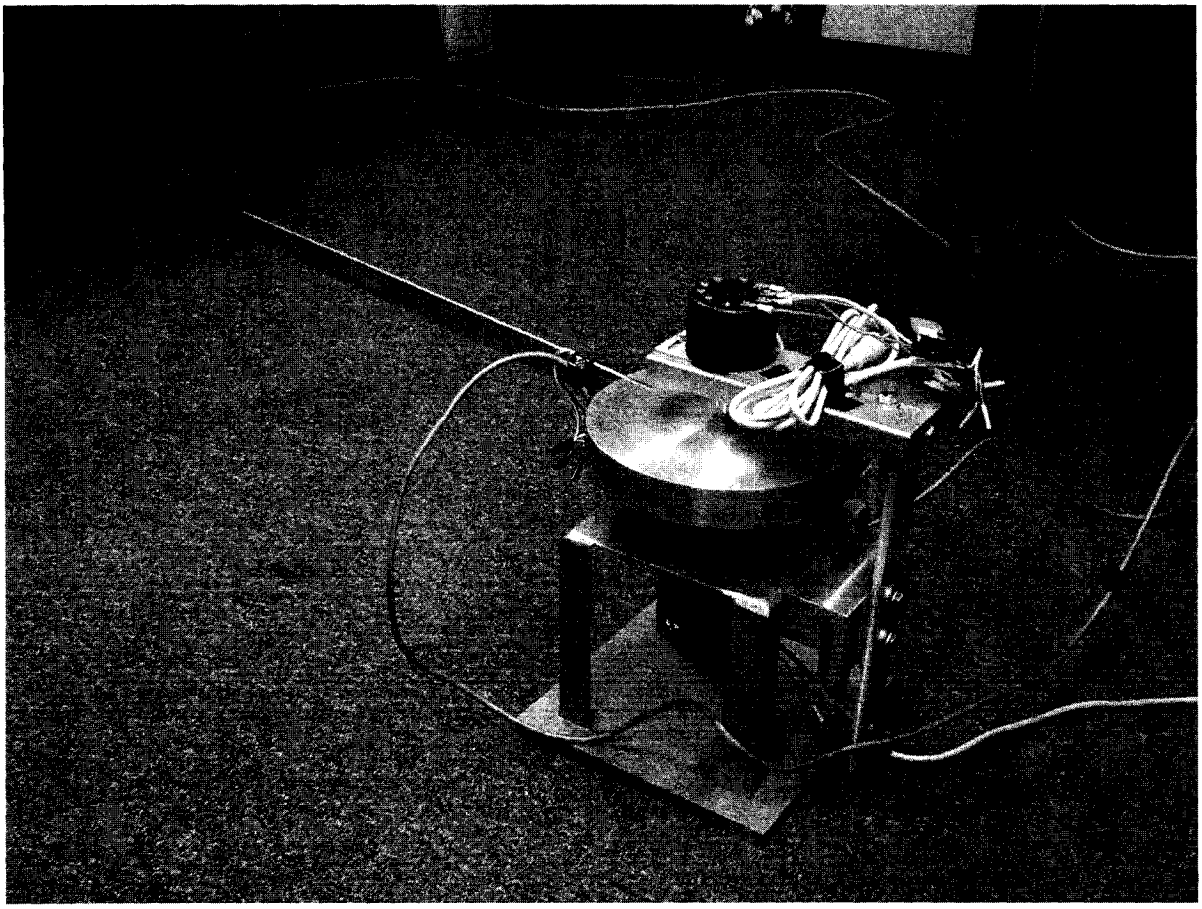

Figure 44: Experimental test-bed

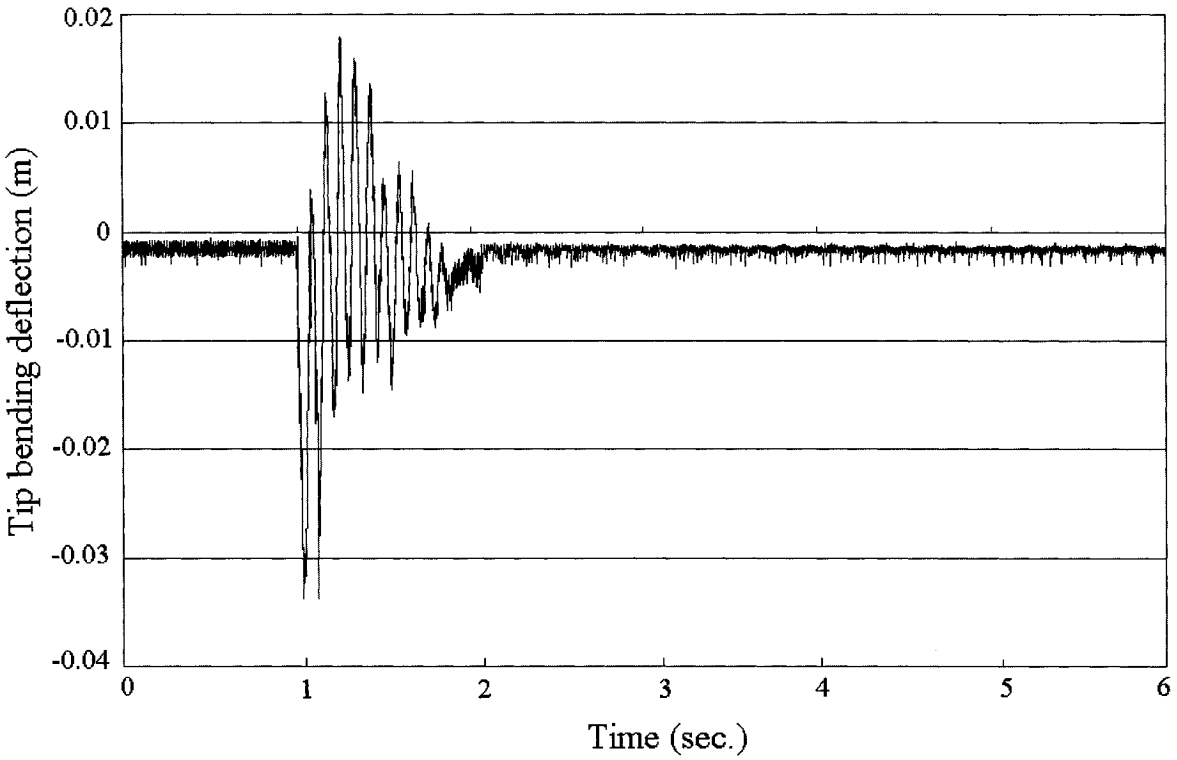

Figure 45(a): Experimental tip deflection of the system without a DFS controller

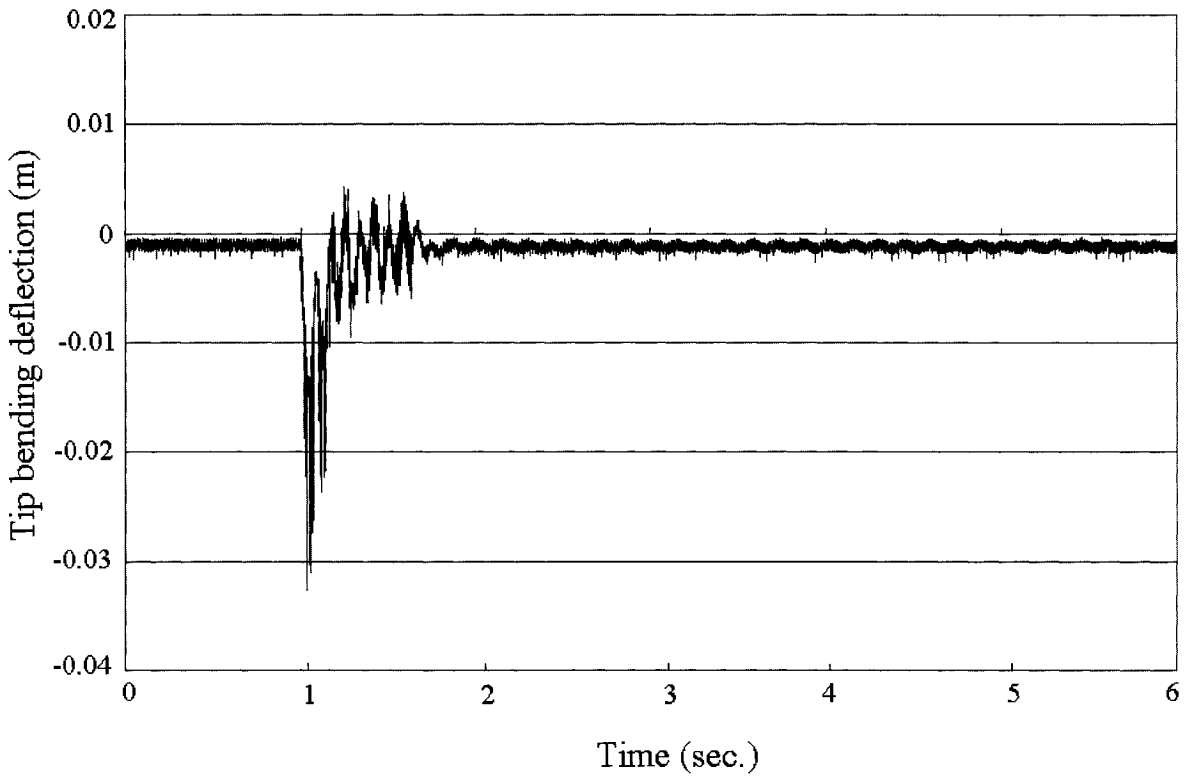

Figure 45(b): Experimental tip deflection of the system with a position angle DFS controller (control loop gain K=40 and time delay τ = 0.001sec.)

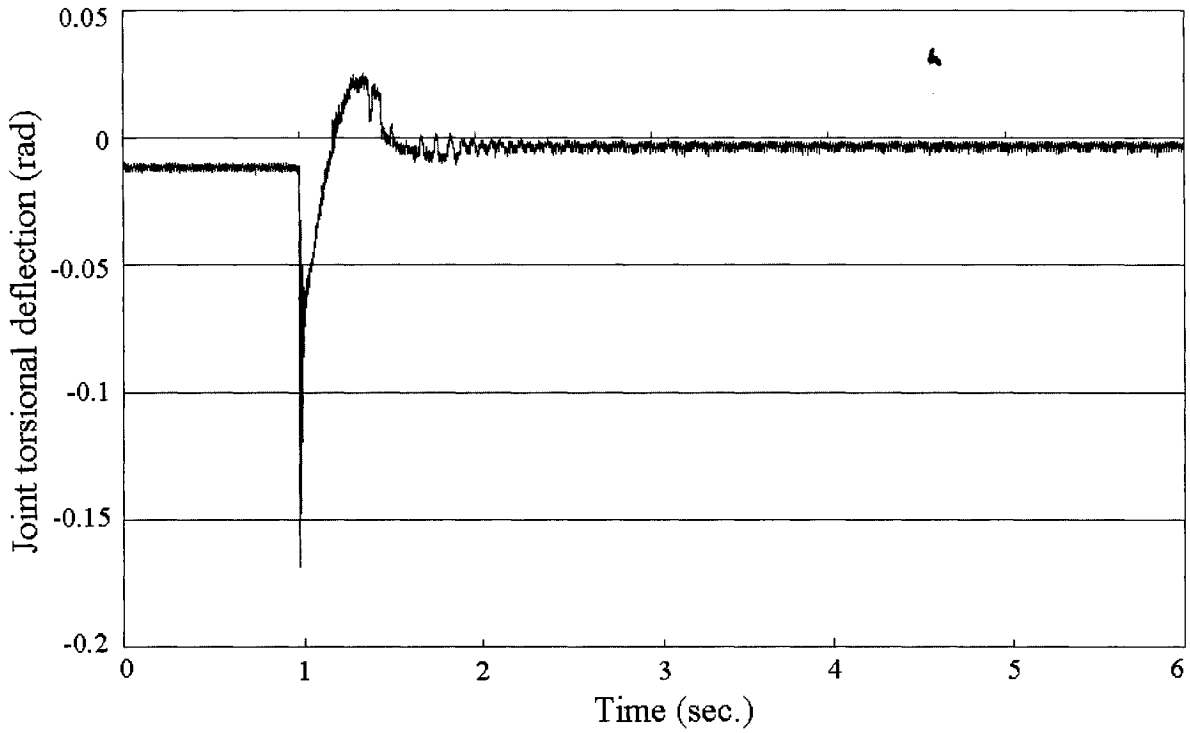

Figure 46(a): Experimental joint deflection of the system without a DFS controller

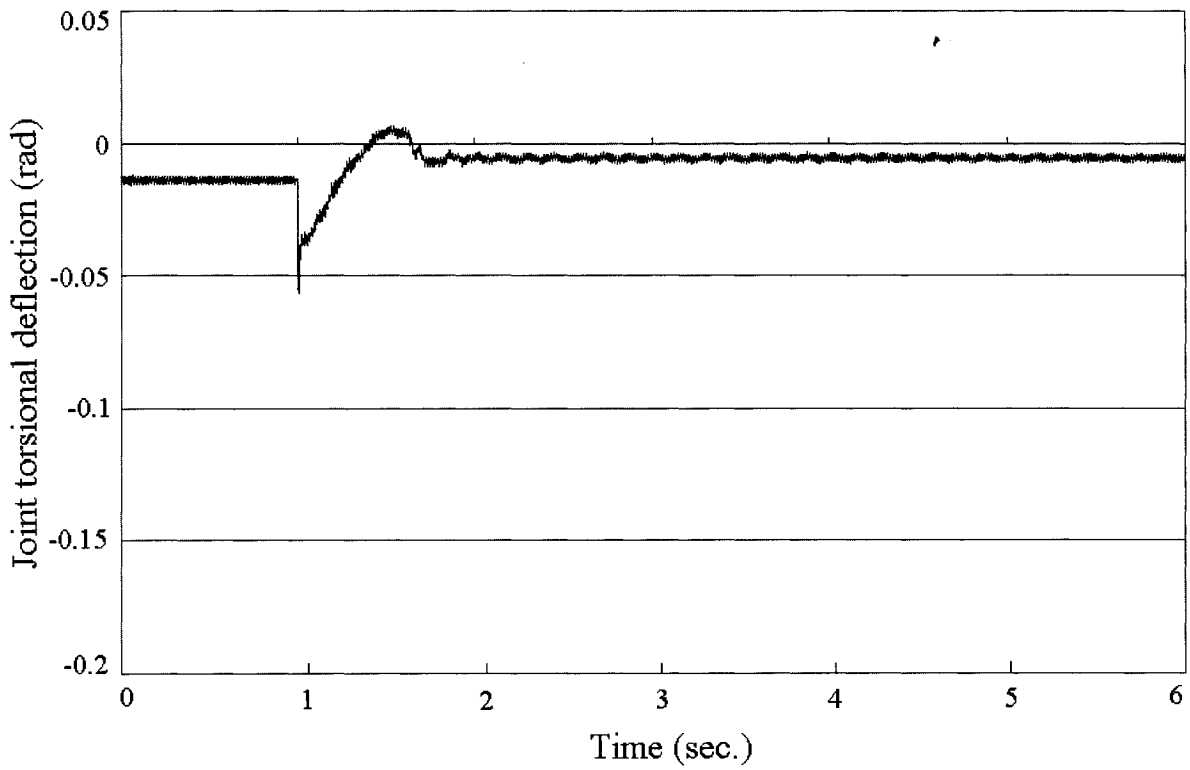

Figure 46(b): Experimental joint deflection of the system with a position angle DFS controller (control loop gain K=40 and time delay τ = 0.001sec.)

6.5 Conclusions

In the experiment, the tip bending deflection of the link and the joint torsional deflection were both greatly reduced under the control of the proposed control system, while having the desired angular position with tuned controller parameters.

Chapter 7: Conclusions and Recommendations for Further Work

7.1 Conclusions

The dynamic model of a single flexible-link flexible-joint manipulator was derived using the assumed modes method and the Lagrange approach with no limitation on the position angle $\theta_1(t)$ of the manipulator. The model was linearized around zero deflection of the link and the joint. In the linear model, it was found that the third and the fourth frequency of the system's characteristic equation increased monotonically with the increment of the relative stiffness of the joint with respect to the link. It was also found that the higher modes of the system are more sensitive to the interaction of the flexible link and the flexible joint. Driven by a sinusoidal torque, the magnitude of the link vibration with respect to the frame $X_m Y_m$ was augmented by the flexible joint. The more flexible it was, the more serious was the effect.

The theory of stability switches of time-delayed systems was developed and applied to the single flexible-link flexible-joint manipulator. After introducing a time delay into the control loop, the critical time delays were ascertained and the stability switching phenomenon was apparent. As the control loop gain increased, both the number of time-delay intervals where the system remained stable and the length of each stable interval decreased. A modified PD controller combined with the DFS controller successfully led the manipulator to track a desired trajectory and damped out the vibration of the flexible link and the flexible joint at the same time. Both the position angle DFS controller and the joint deflection DFS controller improved system performance. In comparison, the former was better since it gave both satisfactory transient responses and steady state responses while the

latter only had an effect on the transient responses. As the control loop gain increased, the position angle DFS controller had a greater ability to eliminate excessive vibrations. However, it was observed to become a bit worse when the gain was set to 200.

It was also found that the residual vibrations which were not eliminated completely by the DFS controller caused the oscillation in the steady-state responses of the angular position. The performance of the combination of PD controller and position angle DFS controller was compared with that provided by the linear quadratic regulator (LQR). It can be concluded that the system under the proposed controller had much less deflection and better tracking of the reference input. Moreover, all of these good responses were produced by rather less input energy in the comparison with the LQR.

Besides all the advantages mentioned above, the designed control system was also robust in response to external disturbances and system parameter uncertainty, which further demonstrated the superiority of this control system.

After applying the proposed control system to the experimental test-bed, the tip bending deflection of the link and the joint torsional deflection were both greatly reduced and the manipulator also achieved the desired angular position with tuned controller parameters.

7.2 Further work recommendations

Even though there was no limitation on the position angle θ_1 of the manipulator, small deflections of the link and the joint were assumed in the dynamic model. In further work, based on the results of this study, the model analysis and control system design can be implemented on a model with large link and joint deflections. Additionally, other items

which were not considered in the dynamic model, such as the friction on the joint and the backlash in the gearbox can be added to provide a more accurate model.

Further work can be conducted on the problem of flexible multi-link and multi-joint manipulators. The analysis of the linear and nonlinear interaction between links and joints would be an interesting topic. The control system including a PD controller and a DFS controller could be extended to control the excessive vibrations of higher order links and joints to see if it is still efficient or needs some modification and changes.

The experiment produced in the present study is just at an initial stage. It was designed mainly to test the effectiveness of the control system on the experimental test-bed. In further work, system identification should be done to obtain the real system parameters before applying the control system. These parameters would then be put into the simulation model to modify the controller and then the modified controller would be employed in the real system to verify the model and controller set up in the simulation. Additionally, the link and the joint can be made more flexible to display more deflection so that the effectiveness of the DFS controller could be further tested and verified.

References

[1] Mehrdad Farid, Stanislaw A. Lukasiewicz, "Dynamic modeling of spatial manipulators with flexible links and joints", *Computers and Structures*, vol. 75, pp. 419-437, 2000.

[2] L.M. Sweet, M.C. Good, "Re-definition of the robot motion control problem: effects of plant dynamics, drive systems, constraints and user requirement", in: *Proceedings of the 23rd IEEE Conference on Decision and Control*, Las Vegas, NV, pp. 724-731,1984.

[3] B.O. Al-Bedoor and A.A. Almusallam, "Dynamics of flexible-link and flexible-joint manipulator carrying a payload with rotary inertia", *Mechanism and Machine Theory*, vol. 35, pp. 785-820, 2000.

[4] S. Yu and M.A. Elbestawi, "Modeling and dynamic analysis of a two-link manipulator with both joint and link flexibilities", *Journal of Sound and Vibration*, vol. 179(5), pp. 839-854, 1995.

[5] B. Subudhi and A.S. Morris, "Dynamic modeling, simulation and control of a manipulator with flexible links and joints", *Robotics and Autonomous Systems*, vol. 41, pp. 257-270, 2002.

[6] Nejat Olgac, Rifat Sipahi, "A new practical stability analysis method for the time delayed LTI systems", *third IFAC Workshop on TIME DELAY SYSTEMS (TDS 2001)*, Santa Fe, NM, December 8-10, 2001.

[7] Z.H. Wang, H.Y. Hu, "Stability switches of time-delayed dynamic systems with unknown parameters", *Journal of Sound and Vibration*, vol. 233(2), pp. 215-233, 2002.

[8] Z.H. Wang, H.Y. Hu, "Delay-independent stability of retarded dynamic systems of multiple degree of freedom", *Journal of Sound and Vibration*, vol. 226, pp. 57-81, 1999.

[9] H.Y. Hu, Z. H. Wang, "Stability analysis of damped SDOF systems with two time delays in state feedback", *Journal of Sound and Vibration*, vol. 214, pp. 213-225, 1998.

[10] Y.X. Qin, Y.Q. Liu, L. Wang and Z.X. Zhen: "Stability of dynamic systems with time delays", *Beijing Science Press*, Beijing, China, 1989.

[11] B. Yang and C.D. Mote, Jr., "Frequency-domain vibration control of distributed gyroscopic systems", *Journal of Dynamic Systems, Measurement, and Control*, vol. 113, pp. 18-25, 1991.

[12] B. Yang and C.D. Mote, Jr., "Active vibration control of the axially moving string in the S domain", *Journal of Applied Mechanics*, vol. 58, pp. 189-196, 1991.

[13] J.M. Krodkiewski, J.S. Faragher, "Stability improvement of the periodic motion of nonlinear systems", in: *Proceedings of the International Conference on Vibration and Noise*, Venice, Italy, pp. 766-774, 1995.

[14] Website of Project "FLEBOT II", *Space Machines Laboratory, Tohoku University*, Sendai, Japan, 2005.

[15] W.J. Book, O. Maizza-Neto, D.E. Whitney, "Feedback control of two beams, two joint systems with distributed flexibility", *ASME J. Dyn. Systems Meas. Control*, vol. 94, pp. 424-431, 1975.

[16] A. Yigit, R.A. Scoot, A.G. Ulsoy, "Flexural motion of a rotating beam attached to a rigid body", *Journal of Sound and Vibration*, vol. 121, pp. 201-210, 1988.

[17] Antonio Ficola, Michele La Cava, Pietro Muraca, "A simplified finite element model of multilink robots with flexible links", *Mathematics and Computers in Simulation*, vol. 37, pp. 491-503, 1994.

[18] Y. Huang, C.S.G. Lee, "Generalization of Newton-Euler formulation of dynamic equations to nonrigid manipulators", *Journal of Dynamic Systems, Measurement and Control*, vol. 110, pp. 308-315, September 1988.

[19] John L. Junkins, Youdan Kim, "Introduction to dynamics and control of flexible structures", *American Institute of Aeronautics and Astronautics, Inc.*, Washington, DC, 1993.

[20] J. N. Reddy, "An introduction to the finite element method", 2nd Edition, *McGraw Hill*, NJ, USA, 1993.

[21] Alessandro De Luca, Bruno Siciliano, "Closes-form dynamic model of planar multilink lightweight robots", *IEEE Transactions on systems, Man and Cybernetics*, vol. 21(4), pp. 826-839, July/August 1991.

[22] A. Jnifene, A. Fahim, "A computed torque/time delay approach to the end-point control of a one-link flexible manipulators", *Dynamics and Control*, vol. 7, pp. 171-189, 1997.

[23] Y.J. Lin, S.D. Gogate, "Modeling and motion simulation of an N-link flexible robot with elastic joints", *Robotics and Manufacturing*, Santa Barbara, California, USA, November 13-15, 1989.

[24] Degao Li, Jean W. Zu, Andrew A. Goldenberg, "Dynamic modeling and mode analysis of flexible-link, flexible-joint robots", *Mech. Mach. Theory*, vol. 33(7), pp. 1031-1044, 1998.

[25] F. Xi, R.G. Fenton, B. Tabarrok, "Coupling effects in a manipulator with both a flexible link and joint", *Journal of Dynamic System, Measurement and Control*, vol. 116, pp. 826-831, December 1994.

[26] B. Siciliano, W.J. Book, "A singular perturbation approach to control of lightweight flexible manipulators", *The International Journal of Robotics Research*, vol. 7(4), pp. 79-90, 1988.

[27] J.M. Skowronski, "Algorithms for adaptive control of two-arm flexible manipulators under uncertainty", *IEEE Trans. on Aerospace and Electronic Systems*, vol. 24(5), pp. 562-570, 1988.

[28] A. Shchuka, A.A. Coldenberg, "Tip control of a single-link flexible arm using a feedforward technique", *Mech. Mach. Theory*, vol. 24(5), pp. 439-455, 1989.

[29] Y.P. Chen, K.S. Yeung, "Sliding mode control of multi-link flexible manipulators", *International Journal of Control*, vol. 54(2), pp. 257-278, 1990.

[30] B. Siciliano, J.V.R. Prasad, A.J. Calise, "Output feedback two-time scale control of multilink flexible arms", *ASME Journal of Dynamic Systems, Measurement and Control*, vol. 114, pp. 70-77, 1992.

[31] A.S. Morris, A. Madani, "Quadratic optimal control of a two-flexible-link robot manipulator", *Robotics*, vol. 16, pp. 97-108, 1998.

[32] J., Knani, "Dynamic modeling and trajectory computer simulation of flexible robotic mechanisms", *Systems Analysis Modelling Simulation*, vol. 43(4), pp.397-409, 2003

[33] Shigang Yue, "Redundant robot manipulators with joint and link flexibility-□. Residual vibration decreasing", *Mech. Mach. Theory*, vol.33 (1/2), pp. 115-122, 1998.

[34] Mansour A. Karkoub, Kumar Tamma, "Modeling and μ-synthesis robust control of two-link flexible manipulators", *5th IEEE Mediterranean Conference on Control and Systems*, Paphos, Cyprus, July, 1997.

[35] J. Pun, S.E. Semercigil, "Joint stiffness control of a one-link flexible arm", *Journal of Sound and Vibration*, vol. 203(2), pp. 341-351, 1997.

[36] A. Warkentin, S.E. Semercigil, "A passive joint controller for the flexible robotic arm", *Journal of Sound and Vibration,* vol. 174(1), pp. 123-134, 1994.

[37] Katsuhiko Ogata, "Modern control engineering", 3rd Edition, *Prentice Hall Inc.*, NJ, USA, 1997.

[38] Singiresu S. Rao, "Mechanical vibration", 3rd Edition, *Addison-Wesley Publishing Company*, 1993.

[39] H.Y. Hu, Z.H. Wang, "Dynamics of controlled mechanical systems with delayed feedback", *Springer-Verlag Berlin Heidelberg*, NY, USA, 2002.

[40] Ahmet S. Yigit, "On the stability of PD control for a two-link rigid-flexible manipulator", *Journal of Dynamic Systems, Measurement, and Control*, vol. 116, pp. 208-215, June 1994.

[41] Glenn J. Battaglia, "Mean square error", *AMP Journal of Technology*, vol. 5, pp. 31-36, June 1996.

[42] M.O. Tokhi, A.K.M. Azad, "Design and development of an experimental flexible manipulator system", *Robotica*, vol. 15, pp. 83-292, 1997.

[43] The user's guide of WinCon 5.0, *Quanser Consulting*, 2004.

[44] Dan Necsulescu, "Mechatronics", 1st Edition, *Prentice Hall*, NJ, USA, 2002.

[45] Roy R. Craig, Jr., "Mechanics of materials", *John Wiley & Sons, Inc.*, 1996.

Appendix A: Formula and Expression Details

$$m_{\theta_1\theta_1} = J_1 + J_2 + (1+\delta^2)\left(\int_0^l \rho(x+r)^2\,dx + \{q\}^T[M]\{q\}\right)$$

$$[M] = \begin{bmatrix} \int_0^l \rho\Phi_1{}^2\,dx & 0 \\ 0 & \int_0^l \rho\Phi_2{}^2\,dx \end{bmatrix}$$

$$m_{\theta_1\delta} = m_{\delta\theta_1} = J_2 + \int_0^l \rho(x+r)^2\,dx + \{q\}^T[M]\{q\}$$

$$m_{\theta_1 q_1} = m_{q_1\theta_1} = (1+\delta^2)\int_0^l \rho(x+r)\Phi_1\,dx$$

$$m_{\theta_1 q_2} = m_{q_2\theta_1} = (1+\delta^2)\int_0^l \rho(x+r)\Phi_2\,dx$$

$$m_{\delta q_1} = m_{q_1\delta} = \int_0^l \rho(x+r)\Phi_1\,dx + \delta\left(q_1\int_0^l \Phi_1{}^2\,dx + q_2\int_0^l \Phi_2{}^2\,dx\right)$$

$$m_{\delta q_2} = m_{q_2\delta} = \int_0^l \rho(x+r)\Phi_2\,dx + \delta\left(q_1\int_0^l \Phi_1{}^2\,dx + q_2\int_0^l \Phi_2{}^2\,dx\right)$$

$$m_{\delta\delta} = J_2 + \int_0^l \rho(x+r)^2\,dx + \{q\}^T[M]\{q\}$$

$$[m_{qq}] = (1+\delta^2)[M]$$

$$[K_{qq}] = [K] - (\dot\theta_1 + \dot\delta)^2[M] + \dot\delta^2[M] - \delta^2\dot\theta_1{}^2[M]$$

$$[K] = \int_0^l EI[\Phi'']^T[\Phi'']dx$$

$$\Phi = [\Phi_1 \quad \Phi_2]$$

$$Q_{\theta_1} = 2(\dot\theta_1 + \dot\delta + \dot\theta_1\delta^2)[M]\{\dot q\} + 2\delta\dot\delta[e]\{\dot q\} + 2\delta\dot\delta\dot\theta_1[\int_0^l \rho(x+r)^2\,dx + \{q\}^T[M]\{q\}]$$

$$Q_\delta = 2(\dot\theta_1 + \dot\delta)[M]\{\dot q\} - 2\delta\dot\theta_1[e]\{\dot q\} - \delta\dot\theta_1{}^2[\int_0^l \rho(x+r)^2\,dx + \{q\}^T[M]\{q\}]$$

$$[e] = \int_0^l \rho(x+r)[\Phi_1 \quad \Phi_2]dx$$

$$[Q_q] = 2\delta\dot{\delta}\dot{\theta}_1[e]^T$$

$$J_2 + \rho\int_0^L (r+x)^2\,dx = J_2 + \frac{\rho(r+l)^3}{3} - \rho\frac{r^3}{3}$$

$$\rho\int_0^L (r+x)\Phi_1 dx = \frac{\rho(l^2+2rl)}{2} + \frac{2\rho l^2}{\pi^2} + \frac{\rho\pi^2 l^2}{8} + \frac{\rho\pi^2 rl}{6}$$

$$\rho\int_0^L (r+x)\Phi_2 dx = \frac{\rho(l^2+2rl)}{2} - \frac{\rho\pi^2 l^2}{2} - \frac{2\rho\pi^2 rl}{3}$$

$$\rho\int_0^L \Phi_1^2 dx = \frac{7\rho L}{2} + \frac{\rho\pi^2 L}{3} + \frac{\rho\pi^4 L}{20}$$

$$\rho\int_0^L \Phi_2^2 dx = \frac{7\rho L}{2} - \frac{4\rho\pi^2 L}{3} + \frac{4\rho\pi^4 L}{5}$$

$$\int_0^l EI\Phi_1''^2 dx = \frac{3EI\pi^4}{2L^3}$$

$$\int_0^l EI\Phi_1''\Phi_2'' dx = -\frac{4EI\pi^4}{L^3}$$

$$\int_0^l EI\Phi_2''^2 dx = \frac{24EI\pi^4}{L^3}$$

$$C_{qq} = l^2\varsigma\sqrt{AEI}\int_0^l [\Phi''(x)]^T[\Phi''(x)]dx$$

$$\Phi''(x) = [\Phi_1''(x) \quad \Phi_2''(x)]$$

The linearization process:

$$\overline{X} = \begin{bmatrix} \theta_1 \\ \theta_2 \\ q_1 \\ q_2 \\ \dot{\theta}_1 \\ \dot{\theta}_2 \\ \dot{q}_1 \\ \dot{q}_2 \end{bmatrix} \qquad \bar{q} = \begin{bmatrix} \theta_1 \\ \theta_2 \\ q_1 \\ q_2 \end{bmatrix} \qquad \overline{X} = \begin{bmatrix} \bar{q} \\ \dot{\bar{q}} \end{bmatrix}$$

The nonlinear equations of motion for the system can be expressed in terms of $\bar{q}$ and $\dot{\bar{q}}$ as:

$$M(\bar{q})\ddot{\bar{q}} + C(\bar{q},\dot{\bar{q}})\dot{\bar{q}} + K(\bar{q},\dot{\bar{q}})\bar{q} + Q(\bar{q},\dot{\bar{q}}) = F$$

$$F = U = \underline{U}L \quad \underline{U} = \begin{bmatrix} 1 \\ 0 \\ 0 \\ 0 \end{bmatrix}$$

The state space model of the system can be written as:

$$\dot{\overline{X}} = f(\overline{X}) + g(\overline{X})L$$

$$f(\overline{X}) = \begin{bmatrix} \dot{\bar{q}} \\ -M^{-1}\left(C\dot{\bar{q}} + K\bar{q} + Q\right) \end{bmatrix} \qquad g(\overline{X}) = \begin{bmatrix} 0_{4\times1} \\ M^{-1}\underline{U} \end{bmatrix}$$

$$M = \begin{bmatrix} m_{\theta_1\theta_1} & m_{\theta_1\delta} & m_{\theta_1 q_1} & m_{\theta_1 q_2} \\ m_{\delta\theta_1} & m_{\delta\delta} & m_{\delta q_1} & m_{\delta q_2} \\ m_{q_1\theta_1} & m_{q_1\delta} & & \\ m_{q_2\theta_1} & m_{q_2\delta} & & [m_{qq}]_{4\times4} \end{bmatrix} \qquad C = 2\delta\dot{\delta}\begin{bmatrix} 0 & 0 & 0 & 0 \\ 0 & 0 & 0 & 0 \\ 0 & 0 & & \\ 0 & 0 & & [M]_{4\times4} \end{bmatrix}$$

$$K = \begin{bmatrix} 0 & 0 & 0 & 0 \\ 0 & K_s & 0 & 0 \\ 0 & 0 & & \\ 0 & 0 & & [K_{qq}]_{4\times4} \end{bmatrix} \qquad Q = \begin{Bmatrix} Q_{\theta_1} \\ Q_{\delta} \\ Q_{q_1} \\ Q_{q_2} \end{Bmatrix}$$

$$A = \frac{\partial}{\partial \overline{X}}\left[f(\overline{X}) + g(\overline{X})L\right]_{X_0,U_0} \quad B = g(\overline{X}_0)$$

$$X_0,U_0: \begin{cases} \delta = 0, & q_1 = 0, & q_2 = 0 \\ \dot{\delta} = 0, & \dot{q}_1 = 0, & \dot{q}_2 = 0 \\ & L = 0 & \end{cases}$$

$$f(\overline{X}) + g(\overline{X})U = \begin{bmatrix} \dot{\overline{q}} \\ M^{-1}\left(\underline{U}L - C\dot{\overline{q}} - K\overline{q} - Q\right) \end{bmatrix}$$

$$A = \frac{\partial M^{-1}}{\partial \overline{X}}\left(\underline{U}L - C\dot{\overline{q}} - K\overline{q} - Q\right) - M^{-1}\left(\frac{\partial C\dot{\overline{q}}}{\partial \overline{X}} + \frac{\partial K\overline{q}}{\partial \overline{X}} + \frac{\partial Q}{\partial \overline{X}}\right)\Bigg/_{X_0,U_0}$$

$$= \begin{bmatrix} 0 & 0 & 0 & 0 & 1 & 0 & 0 & 0 \\ 0 & 0 & 0 & 0 & 0 & 1 & 0 & 0 \\ 0 & 0 & 0 & 0 & 0 & 0 & 1 & 0 \\ 0 & 0 & 0 & 0 & 0 & 0 & 0 & 1 \\ & & & & 0 & 0 & 0 & 0 \\ M^{-1}{}_{X_0} \cdot \left(-K_{linearized}\right) & & & & 0 & 0 & 0 & 0 \\ & & & & 0 & 0 & 0 & 0 \\ & & & & 0 & 0 & 0 & 0 \end{bmatrix}$$

$$B = \begin{bmatrix} 0_{3\times 1} \\ M^{-1}{}_{X_0}\underline{U} \end{bmatrix} \qquad M^{-1}{}_{X_0} = M^{-1}{}_{linearized}$$

$$M_{linearized} = \begin{bmatrix} J_1 + J_2 + \rho\int_0^L (r+x)^2 dx & J_2 + \rho\int_0^L (r+x)^2 dx & \rho\int_0^L (r+x)\Phi_1 dx & \rho\int_0^L (r+x)\Phi_2 dx \\ J_2 + \rho\int_0^L (r+x)^2 dx & J_2 + \rho\int_0^L (r+x)^2 dx & \rho\int_0^L (r+x)\Phi_1 dx & \rho\int_0^L (r+x)\Phi_2 dx \\ \rho\int_0^L (r+x)\Phi_1 dx & \rho\int_0^L (r+x)\Phi_1 dx & \rho\int_0^L \Phi_1^2 dx & 0 \\ \rho\int_0^L (r+x)\Phi_2 dx & \rho\int_0^L (r+x)\Phi_2 dx & 0 & \rho\int_0^L \Phi_2^2 dx \end{bmatrix}$$

$$K_{linearized} = \begin{bmatrix} 0 & 0 & 0 & 0 \\ 0 & Ks & 0 & 0 \\ 0 & 0 & \int_0^l EI\Phi_1''^2 dx & \int_0^l EI\Phi_1''\Phi_2'' dx \\ 0 & 0 & \int_0^l EI\Phi_1''\Phi_2'' dx & \int_0^l EI\Phi_2''^2 dx \end{bmatrix}$$

$$y(x,t) = (\sin\theta_1 + \delta\cos\theta_1)(x+r) + (\cos\theta_1 - \delta\sin\theta_1)w(x,t)$$

$$= (\sin\theta_1\cos\delta + \cos\theta_1\sin\delta)(x+r) + (\cos\theta_1\cos\delta - \sin\theta_1\sin\delta)w(x,t)$$

$$= \sin(\theta_1 + \delta)(x+r) + \cos(\theta_1 + \delta)w(x,t) = \sin\theta_2(x+r) + \cos\theta_2 w(x,t)$$

Appendix B: Matlab M-files for the System Analysis and Control System Design

```
%@@@@@@@@@@@@@@@@@@matlab M-file: FLFJsystem.m@@@@@@@@@@@@@@@@@
%*******************************************************************************
%==============================get the system matrix=============================
%*******************************************************************************

clear;

%===system parameters====

J1=1.45e-4; %the moment of inertia of the motor shaft
r=0.092; %the outer radius of hub
J2=2*pi*2700*28*(((r*1000) ^4-6.35^4)/4)*1e-15; %the density of aluminum=2700(g/m^2);
%the height of hub=28(mm); the inter radius of hub=6.35(mm)
p=0.169; %the density of beam per length
L=0.5; %the length of beam (m)
EI=2.282; %the rigidity of beam
Ks=166; %the equivalent stiffness of joint
a=0.625e-4; %the cross sectional area of beam
l=0.005; %the structural damping radio of beam

%====system matrices=====

M= [J1 0 0 0; 0 J2+p*(r+L)^3/3-p*r^3/3 p*(L^2+2*r*L)/2+2*p*L^2/(pi^2)+p*pi^2*L^2/8+p*r*pi^2*L/6
p*(L^2+2*r*L)/2-p*pi^2*L^2/2-2*p*r*pi^2*L/3;0
p*(L^2+2*r*L)/2+2*p*L^2/(pi^2)+p*pi^2*L^2/8+p*r*pi^2*L/6 7*p*L/2+p*pi^2*L/3+p*pi^4*L/20 0;0
p*(L^2+2*r*L)/2-p*pi^2*L^2/2-2*p*r*pi^2*L/3 0 7*p*L/2-4*p*pi^2*L/3+4*p*pi^4*L/5];`%mass matrix
K= [Ks -Ks 0 0;-Ks Ks 0 0; 0 0 3*EI*pi^4/ (2*L^3) -4*EI*pi^4/L^3; 0 0 -4*EI*pi^4/L^3 24*EI*pi^4/L^3];
%stiffness matrix
F= [1 0 0 0]'; %the weighting matrix
D= [0 0 0 0;0 0 0 0;0 0 3*pi^4/(2*L^3)*l*L^2*(a*EI)^(1/2)
-4*pi^4/(L^3)*l*L^2*(a*EI)^(1/2);0 0 -4*pi^4/(L^3)*l*L^2*(a*EI)^(1/2)
24*pi^4/(L^3)*l*L^2*(a*EI)^(1/2)];%damping matrix
A1=inv (M)*(-K);
A2=inv (M)*(-D);
B0=inv (M)*F;
A= [zeros (4, 4) eye (4); A1 A2]; % A matrix-characteristic matrix
B= [zeros (4, 1); B0]; % B matrix-control the input vector
x=1;
Y1=1-cos (pi*x) + (pi*x) ^2/2;
Y2=1-cos (2*pi*x)-(2*pi*x) ^2/2;
C= eye (8); % C matrix-control the output vector (It can be modified to get any other output.)

%*******************************************************************************
%==============================get the system characteristics=====================
%*******************************************************************************

EE=eig (A); % eigenvalues of the system
m=0;
```

```
For i=1:4
    f(i+m)=sqrt(real(EE(i+m))^2+imag(EE(i+m))^2);
    %natural frequencies of the system (linearly coupled)
    m=m+1;
end

%====get the individual frequency-torsional frequency and bending frequencies====

%@@@@@@@@@@@@@@@@matlab M-file: RLFJsystem.m@@@@@@@@@@@@@@@@
%*********************************************************************************
%======================Rigid-link Flexible-joint Manipulator=======================
%*********************************************************************************

Clear;

%====input the value of parameters====

J1=1.45e-4;
r=0.092;
J2=2*pi*2700*28*(((r*1000) ^4-6.35^4)/4)*1e-15;
p=0.169;
L=0.5;
Ks=10:10:100;
M= [J1 0; 0 J2+ (1/3)*p*L^3];
For i=1: length (Ks)
    K (:,:, i) =[Ks(i) –Ks(i);-Ks(i) Ks(i)];
    A0(:,:,i) =inv(M)*(-K(:,:,i));
    A(:,:,i) =[zeros(2,2) eye(2);A0(:,:,i) zeros(2,2)];
    E_t(:,i)=eig(A(:,:,i));
    m=0;
    for j=1:4
        E_t_re(j+m)=real(E_t(j+m,i));
        E_t_im(j+m)=imag(E_t(j+m,i));
        Fre_t(j+m)=sqrt(E_t_re(j+m,i)^2+E_t_im(j+m,i)^2);
        m=m+1;
     end
end

%@@@@@@@@@@@@@@@@matlab M-file: RJFLsystem.m@@@@@@@@@@@@@@@@
%*********************************************************************************
%======================Flexible-link Rigid-joint Manipulator=======================
%*********************************************************************************

Clear;

%====input the value of parameters====

J1=1.45e-4;
r=0.092;
J2=2*pi*2700*28*(((r*1000)^4-6.35^4)/4)*1e-15;
p=0.169;
L=0.5;
EI=2.282;
a=0.625e-4;
l=0.005;
M=[J1+J2+p*(r+L)^3/3-p*r^3/3 p*(L^2+2*r*L)/2+2*p*L^2/(pi^2)+p*pi^2*L^2/8+p*r*pi^2*L/6
```

```
p*(L^2+2*r*L)/2-p*pi^2*L^2/2-
2*p*r*pi^2*L/3;p*(L^2+2*r*L)/2+2*p*L^2/(pi^2)+p*pi^2*L^2/8+p*r*pi^2*L/6
7*p*L/2+p*pi^2*L/3+p*pi^4*L/20 0;p*(L^2+2*r*L)/2-p*pi^2*L^2/2-2*p*r*pi^2*L/3 0 7*p*L/2-
4*p*pi^2*L/3+4*p*pi^4*L/5];
K=[0 0 0;0 3*EI*pi^4/(2*L^3) -4*EI*pi^4/L^3;0 -4*EI*pi^4/L^3 24*EI*pi^4/L^3];
F=[1 0 0]';
D=[0 0 0;0 3*pi^4/(2*L^3)*l*L^2*(a*EI)^(1/2) -4*pi^4/(L^3)*l*L^2*(a*EI)^(1/2);0 -
4*pi^4/(L^3)*l*L^2*(a*EI)^(1/2) 24*pi^4/(L^3)*l*L^2*(a*EI)^(1/2)];
A1=inv(M)*(-K);
A2=inv(M)*(-D);
A=[zeros(3,3) eye(3);A1 A2];
E_b=eig(A);
for i=1:6
   E_b_re(i)=real(E_b(i));
   E_b_im(i)=imag(E_b(i));
   Fre_b(i)=sqrt(E_b_re(i)^2+E_b_im(i)^2);
end

%@@@@@@@@@@@@@@@@@@matlab M-file:Chara_joint.m@@@@@@@@@@@@@@@@@
%*********************************************************************************
%==============the effect of joint stiffness on eigenvalues and natural frequencies============
%*********************************************************************************

clear;

%====input the value of parameters====

J1=1.45e-4;
r=0.092;
J2=2*pi*2700*28*(((r*1000)^4-6.35^4)/4)*1e-15;
p=0.169;
L=0.5;
EI=2.282;
Ks=10:10:10000;
Kk=(Ks*L)/EI;
a=0.625e-4;
l=0.005;
%define the matrices
freque=zeros(length(Kk),8);
ro=zeros(length(Kk),8);
eigvalu= zeros(length(Kk),8);
eigvalu_re= zeros(length(Kk),8);
eigvalu_im= zeros(length(Kk),8);

M=[J1 0 0 0;0 J2+p*(r+L)^3/3-p*r^3/3 p*(L^2+2*r*L)/2+2*p*L^2/(pi^2)+p*pi^2*L^2/8+p*r*pi^2*L/6
p*(L^2+2*r*L)/2-p*pi^2*L^2/2-2*p*r*pi^2*L/3;0
p*(L^2+2*r*L)/2+2*p*L^2/(pi^2)+p*pi^2*L^2/8+p*r*pi^2*L/6 7*p*L/2+p*pi^2*L/3+p*pi^4*L/20 0;0
p*(L^2+2*r*L)/2-p*pi^2*L^2/2-2*p*r*pi^2*L/3 0 7*p*L/2-4*p*pi^2*L/3+4*p*pi^4*L/5];
D=[0 0 0 0;0 0 0 0;0 0 3*pi^4/(2*L^3)*l*L^2*(a*EI)^(1/2) -4*pi^4/(L^3)*l*L^2*(a*EI)^(1/2);0 0 -
4*pi^4/(L^3)*l*L^2*(a*EI)^(1/2) 24*pi^4/(L^3)*l*L^2*(a*EI)^(1/2)];
F=[1 0 0 0]';
A2=inv(M)*(-D);
B0=inv(M)*F;
B=[zeros(4,1);B0];
For i=1:length(Kk)
        K(:,:,i)=[Ks(i) -Ks(i) 0 0;-Ks(i) Ks(i) 0 0;0 0 3*EI*pi^4/(2*L^3) -4*EI*pi^4/L^3;0 0 -
```

```
        4*EI*pi^4/L^3 24*EI*pi^4/L^3];
        A1(:,:,i)=inv(M)*(-K(:,:,i));
        A(:,:,i)=[zeros(4,4) eye(4);A1(:,:,i) A2];
        eigvalu(:,i)=eig(A(:,:,i));
        eigvalu_re(:,i)=real(eigvalu(:,i));
        eigvalu_im(:,i)=imag(eigvalu(:,i));
        for j=1:8
                freque(i,j)=sqrt(eigvalu_re(j,i)^2+eigvalu_im(j,i)^2);
                ro(i,j)=sqrt(freque(i,j)*L^2*sqrt(p/EI));
        end
end
%%
plot(eigvalu_re(1,:),eigvalu_im(1,:),'pk');
hold on;
plot(eigvalu_re(2,:),eigvalu_im(2,:),'+b');
%%
figure;
plot(eigvalu_re(3,:),eigvalu_im(3,:),'*k');
hold on;
plot(eigvalu_re(4,:),eigvalu_im(4,:),'sb');
%%
figure;
plot(eigvalu_re(5,:),eigvalu_im(5,:),'xk');
hold on;
plot(eigvalu_re(6,:),eigvalu_im(6,:),'db');
%%
figure;
plot(eigvalu_re(7,:),eigvalu_im(7,:),'>k');
hold on;
plot(eigvalu_re(8,:),eigvalu_im(8,:),'ob');
axis([-0.5 0.5 -0.5 0.5]);
%%
figure;
plot(log10(Kk),freque(:,1),'k',log10(Kk),freque(:,3),'k--',log10(Kk),freque(:,5),'k-.',log10(Kk),freque(:,7),'k:');
%%
figure;
plot(log10(Kk),ro(:,1),'k',log10(Kk),ro(:,3),'k--',log10(Kk),ro(:,5),'k-.',log10(Kk),ro(:,7),'k:');

%@@@@@@@@@@@@@@@@@@matlab M-file:respo_joint.m@@@@@@@@@@@@@@@@@
%**************************************************************************************
%====================the effect of joint stiffness on system responses==================
%**************************************************************************************

clear;

%====input the value of parameters====

J1=1.45e-4;
r=0.092;
J2=2*pi*2700*28*(((r*1000)^4-6.35^4)/4)*1e-15;
p=0.169;
L=0.5;
EI=2.282;
Ks=10:1:10000;
Kk=(Ks*L)/EI;
a=0.625e-4;
```

```
l=0.005;
M=[J1 0 0 0;0 J2+p*(r+L)^3/3-p*r^3/3 p*(L^2+2*r*L)/2+2*p*L^2/(pi^2)+p*pi^2*L^2/8+p*r*pi^2*L/6
p*(L^2+2*r*L)/2-p*pi^2*L^2/2-2*p*r*pi^2*L/3;0
p*(L^2+2*r*L)/2+2*p*L^2/(pi^2)+p*pi^2*L^2/8+p*r*pi^2*L/6 7*p*L/2+p*pi^2*L/3+p*pi^4*L/20 0;0
p*(L^2+2*r*L)/2-p*pi^2*L^2/2-2*p*r*pi^2*L/3 0 7*p*L/2-4*p*pi^2*L/3+4*p*pi^4*L/5];
F=[1 0 0 0]';
B0=inv(M)*F;
B=[zeros(4,1);B0];
x=1;
Y1=1-cos(pi*x)+(pi*x)^2/2;
Y2=1-cos(2*pi*x)-(2*pi*x)^2/2;
C=[1 -1 0 0 0 0 0 0;0 0 Y1 Y2 0 0 0 0;0.6 -0.6 Y1 Y2 0 0 0 0];
t=0:0.001:5;
u=sin(2*pi*t);
for i=1:length(Kk)
        K(:,:,i)=[Ks(i) -Ks(i) 0 0;-Ks(i) Ks(i) 0 0;0 0 3*EI*pi^4/(2*L^3) -4*EI*pi^4/L^3;0 0 -
        4*EI*pi^4/L^3 24*EI*pi^4/L^3];
        A1(:,:,i)=inv(M)*(-K(:,:,i));
        A(:,:,i)=[zeros(4,4) eye(4);A1(:,:,i) zeros(4,4)];\
        sys=ss(A(:,:,i),B,C,zeros(3,1));
        y(:,:,i)=lsim(sys,u,t);
        y_max1=max(y(:,1,i);
        y_max2=max(y(:,2,i);
        y_max3=max(y(:,3,i);
end
plot(Kk, y_max1 ,'k--', Kk, y_max2,'k', Kk, y_max3,'k:');

%*****************************************************************************
%==========get the critical time delays for the system with two kinds of controllers==========
%*****************************************************************************

%@@@@@@@@@@@@matlab M-file: finding_criticaltimedelay_angleposi.m@@@@@@@@@@@@

clear;

%====input the value of parameters====

J1=1.45e-4;
r=0.092;
J2=2*pi*2700*28*(((r*1000) ^4-6.35^4)/4)*1e-15;
p=0.169;
L=0.5;
EI=2.282;
Ks=166;
a=0.625e-4;
l=0.005;

%========set up the system=========

M= [J1 0 0 0;0 J2+p*(r+L)^3/3-p*r^3/3 p*(L^2+2*r*L)/2+2*p*L^2/(pi^2)+p*pi^2*L^2/8+p*r*pi^2*L/6
p*(L^2+2*r*L)/2-p*pi^2*L^2/2-2*p*r*pi^2*L/3;0
p*(L^2+2*r*L)/2+2*p*L^2/(pi^2)+p*pi^2*L^2/8+p*r*pi^2*L/6 7*p*L/2+p*pi^2*L/3+p*pi^4*L/20 0;0
p*(L^2+2*r*L)/2-p*pi^2*L^2/2-2*p*r*pi^2*L/3 0 7*p*L/2-4*p*pi^2*L/3+4*p*pi^4*L/5];
K= [Ks -Ks 0 0;-Ks Ks 0 0; 0 0 3*EI*pi^4/ (2*L^3) -4*EI*pi^4/L^3; 0 0 -4*EI*pi^4/L^3 24*EI*pi^4/L^3];
D=[0 0 0 0;0 0 0 0;0 0 3*pi^4/(2*L^3)*l*L^2*(a*EI)^(1/2) -4*pi^4/(L^3)*l*L^2*(a*EI)^(1/2);0 0 -
4*pi^4/(L^3)*l*L^2*(a*EI)^(1/2) 24*pi^4/(L^3)*l*L^2*(a*EI)^(1/2)];
```

```
F= [1 0 0 0]';
A1=inv (M)*(-K);
A2=inv (M)*(-D);
B0=inv (M)*F;
A= [zeros (4, 4) eye (4); A1 A2];
B= [zeros (4, 1); B0];

%============for the system controller by the angle position DFS controller==================

C= [1 0 0 0 0 0 0 0];
syms s k t e;
MM=s*eye (8)-A+k*B*C*(1-e^ (-s*t));
dd =det (MM);
k=20:40:300;
for i=1: length (k)
        u1= [1 0 -2.2872e6 0 6.466e11 0 -9.0855e14 0 0];
        u2=-k (i)*[0 0 6.8966e3 0 -7.8782e9 0 4.6089e13 0 -4.4765e16];
        u3= [0 -3.657 0 4.2355e6 0 -1.1887e10 0 0 0];
        u4=-k (i)*[0 0 0 -2.522e4 0 3.3705e8 0 -5.8568e11 0];
        w1=conv(u1,u1);
        w2=2*conv(u1,u2);
        w3=conv(u3,u3);
        w4=2*conv(u3,u4);
        w=w1+w2+w3+w4;
        ww(i,:)=roots(w);
        ii=1;
        for z=1: length (ww (i, :))
                if (imag (ww (i,z))==0 & real(ww(i,z))>0)==1
                        W (ii,i)=ww(i,z);
                        ii=ii+1;
                end
        end
        for j=1: length (W (:, i))
                if W (j,i)>0
                        PR(j)=W(j,i)^8-2.2872e6*W(j,i)^6+6.466e11*W(j,i)^4-9.0855e14*W(j,i)^2+(-
                        6.8966e3*W(j,i)^6+7.8782e9*W(j,i)^4-4.6089e13*W(j,i)^2+4.4765e16)*k(i);
                        PI(j)=-3.657*W(j,i)^7+4.2355e6*W(j,i)^5-1.1887e10*W(j,i)^3+(2.522e4*W(j,i)^5-
                        3.3705e8*W(j,i)^3+5.8568e11*W(j,i))*k(i);
                        QR(j)=-(-6.8966e3*W(j,i)^6+7.8782e9*W(j,i)^4-
                        4.6089e13*W(j,i)^2+4.4765e16)*k(i);
                        QI(j)=-(2.522e4*W(j,i)^5-3.3705e8*W(j,i)^3+5.8568e11*W(j,i))*k(i);
                        sin(i,j)=(QR(j)*PI(j)-PR(j)*QI(j))/(QR(j)^2+QI(j)^2);
                        cos(i,j)=-(PR(j)*QR(j)+QI(j)*PI(j))/(QR(j)^2+QI(j)^2);
                        sig1=sign (sin (i,j));
                        sig2=sign (cos (i,j));
                        theta1 (j)=asin(sin(i,j));
                        if theta1(j)>0
                                if sig2>0
                                        theta(i,j)=theta1(j);
                                else    theta(i,j)=pi-theta1(j);
                                end
                        end
                        if theta1(j)<0;
                                if sig2<0
                                        theta(i,j)=pi-theta1(j);
                                else    theta(i,j)=2*pi+theta1(j);
```

```
                    end
                end
            end
        end
        for j=1:length(W(:,i))
            if W(j,i)>0
                for jj=1:20
                    timde(i,j,jj)=(theta(i,j)+2*(jj-1)*pi)/W(j,i);
                end
            end
        end
end

%================finding the final time point which could make the system stable==============

timde_row=zeros (length (k), 140);
row_sign=zeros (length (k), 140);
for i=1: length (k)
        m=0;
        for jj=1:20
            for j=1:7
                timde_row (i,j+m)=timde(i,j,jj);
                if (fix(j/2))*2==j
                    row_sign(i,j+m)=-1;
                else    row_sign(i,j+m)=1;
                end

            end
            m=m+7;
        end
end
for i=1: length (k)
        for j=1:(140-1)
            for ii=(j+1):140
                if timde_row(i,j)>timde_row(i,ii)
                    temp=timde_row(i,ii);
                    timde_row(i,ii)=timde_row(i,j);
                    timde_row(i,j)=temp;
                    temp_sign=row_sign(i,ii);
                    row_sign(i,ii)=row_sign(i,j);
                    row_sign(i,j)=temp_sign;
                end
            end
        end
end
row_signsum=zeros(length(k),140);
for i=1:length(k)
        sum=0;
        for j=1:140
            sum=sum+row_sign(i,j);
            row_signsum(i,j)=sum;
        end
end

%@@@@@@@@@@@@matlab M-file: finding_criticaltimedelay_jointdef.m@@@@@@@@@@@@
```

```
clear;

%====input the value of parameters====

J1=1.45e-4;
r=0.092;
J2=2*pi*2700*28*(((r*1000) ^4-6.35^4)/4)*1e-15;
p=0.169;
L=0.5;
EI=2.282;
Ks=166;
a=0.625e-4;
l=0.005;

%========set up the system=========

M= [J1 0 0 0;0 J2+p*(r+L)^3/3-p*r^3/3 p*(L^2+2*r*L)/2+2*p*L^2/(pi^2)+p*pi^2*L^2/8+p*r*pi^2*L/6
p*(L^2+2*r*L)/2-p*pi^2*L^2/2-2*p*r*pi^2*L/3;0
p*(L^2+2*r*L)/2+2*p*L^2/(pi^2)+p*pi^2*L^2/8+p*r*pi^2*L/6 7*p*L/2+p*pi^2*L/3+p*pi^4*L/20 0;0
p*(L^2+2*r*L)/2-p*pi^2*L^2/2-2*p*r*pi^2*L/3 0 7*p*L/2-4*p*pi^2*L/3+4*p*pi^4*L/5];
K= [Ks -Ks 0 0;-Ks Ks 0 0; 0 0 3*EI*pi^4/ (2*L^3) -4*EI*pi^4/L^3; 0 0 -4*EI*pi^4/L^3 24*EI*pi^4/L^3];
D=[0 0 0 0;0 0 0 0;0 0 3*pi^4/(2*L^3)*l*L^2*(a*EI)^(1/2) -4*pi^4/(L^3)*l*L^2*(a*EI)^(1/2);0 0 -
4*pi^4/(L^3)*l*L^2*(a*EI)^(1/2) 24*pi^4/(L^3)*l*L^2*(a*EI)^(1/2)];
F= [1 0 0 0]';
A1=inv (M)*(-K);
A2=inv (M)*(-D);
B0=inv (M)*F;
A= [zeros (4, 4) eye (4); A1 A2];
B= [zeros (4, 1); B0];

%============for the system controller by the joint deflection DFS controller================

C= [1 -1 0 0 0 0 0 0];
syms s k t e;
MM=s*eye (8)-A+k*B*C*(1-e^ (-s*t));
dd =det (MM);
k=5:5:45;
for i=1:length(k)
        u1=[1 0 -2.2864e6 0 6.4626e11 0 -9.0798e14 0 0];
        u2=-k1(i)*[0 0 6.8966e3 0 -3.8529e9 0 5.4307e12 0 0];
        u3=[0 -3.6547 0 4.2328e6 0 -11.88 0 0 0];
        u4=-k1(i)*[0 0 0 -2.5205e4 0 7.1052e7 0 0 0];
        w1=conv(u1,u1);
        w2=2*conv(u1,u2);
        w3=conv(u3,u3);
        w4=2*conv(u3,u4);
        w=w1+w2+w3+w4;
        ww(i,:)=roots(w);
        Ii=1;
        for z=1:length(ww(i,:))
                if (imag(ww(i,z))==0 & real(ww(i,z))>0)==1
                        W(ii,i)=ww(i,z);
                        ii=ii+1;
                end
        end
        for j=1:length(W(:,i))
```

```
                if W(j,i)>0
                        PR(j)=W(j,i)^8-2.2864e6*W(j,i)^6+6.4626e11*W(j,i)^4-9.0798e14*W(j,i)^2+(-
                        6.8966e3*W(j,i)^6+3.8529e9*W(j,i)^4-5.4307e12*W(j,i)^2)*k1(i);
                        PI(j)=-3.6547*W(j,i)^7+4.2328e6*W(j,i)^5-11.88*W(j,i)^3+(2.5205e4*W(j,i)^5-
                        7.1052e7*W(j,i)^3)*k1(i);
                        QR(j)=-(-6.8964e3*W(j,i)^6+3.8529e9*W(j,i)^4-5.4307e12*W(j,i)^2)*k1(i);
                        QI(j)=-(2.5205e4*W(j,i)^5-7.1052e7*W(j,i)^3)*k1(i);
                        sin(i,j)=(QR(j)*PI(j)-PR(j)*QI(j))/(QR(j)^2+QI(j)^2);
                        cos(i,j)=-(PR(j)*QR(j)+QI(j)*PI(j))/(QR(j)^2+QI(j)^2);
                        sig1=sign(sin(i,j));
                        sig2=sign(cos(i,j));
                        theta1(j)=asin(sin(i,j));
                        if theta1(j)>0
                                if sig2>0
                                        theta(i,j)=theta1(j);
                                else    theta(i,j)=pi-theta1(j);
                                end
                        end
                        if theta1(j)<0;
                                if sig2<0
                                        theta(i,j)=pi-theta1(j);
                                else    theta(i,j)=2*pi+theta1(j);
                                end
                        end
                end
        end
        for j=1:length(W(:,i))
                if W(j,i)>0
                        for jj=1:50
                                timde(i,j,jj)=(theta(i,j)+2*(jj-1)*pi)/W(j,i);
                        end
                end
        end
end

%==============finding the final time point which could make the system stable==============

timde_row=zeros (length (k), 200);
row_sign=zeros (length (k), 200);
for i=1: length (k)
        m=0;
        for jj=1:50
                for j=1:4
                        timde_row(i,j+m)=timde(i,j,jj);
                end
                m=m+4;
        end
end
for i=1: length (k)
        for j=1:200
                if (fix(j/2))*2==j
                        row_sign(i,j)=-1;
                else    row_sign(i,j)=1;
                end
        end
end
```

```
for i=1: length (k)
        for j=1:(200-1)
                for ii=(j+1):200
                        if timde_row(i,j)>timde_row(i,ii)
                                temp=timde_row(i,ii);
                                timde_row (i,ii)=timde_row(i,j);
                                timde_row (i,j)=temp;
                                temp_sign=row_sign (i,ii);
                                row_sign (i,ii)=row_sign(i,j);
                                row_sign (i,j)=temp_sign;
                        end
                end
        end
end
row_signsum=zeros(length (k),200);
for i=1: length (k)
        sum=0;
        for j=1:200
                sum=sum+row_sign(i,j);
                row_signsum(i,j)=sum;
        end
end

%*****************************************************************************
%==========get the transfer function of three plants for the PD controller tuning==========
%*****************************************************************************

%@@@@@@@@@@@@@@@@matlab M-file: transfer_functions.m@@@@@@@@@@@@@@@@

clear;

%====input the value of parameters====

J1=1.45e-4;
r=0.092;
J2=2*pi*2700*28*(((r*1000)^4-6.35^4)/4)*1e-15;
p=0.169;
L=0.5;
EI=2.282;
Ks=166;
a=0.625e-4;
l=0.005;

%========set up the system=========

M= [J1 0 0 0;0 J2+p*(r+L)^3/3-p*r^3/3 p*(L^2+2*r*L)/2+2*p*L^2/(pi^2)+p*pi^2*L^2/8+p*r*pi^2*L/6
p*(L^2+2*r*L)/2-p*pi^2*L^2/2-2*p*r*pi^2*L/3;0
p*(L^2+2*r*L)/2+2*p*L^2/(pi^2)+p*pi^2*L^2/8+p*r*pi^2*L/6 7*p*L/2+p*pi^2*L/3+p*pi^4*L/20 0;0
p*(L^2+2*r*L)/2-p*pi^2*L^2/2-2*p*r*pi^2*L/3 0 7*p*L/2-4*p*pi^2*L/3+4*p*pi^4*L/5];
K= [Ks -Ks 0 0;-Ks Ks 0 0; 0 0 3*EI*pi^4/ (2*L^3) -4*EI*pi^4/L^3; 0 0 -4*EI*pi^4/L^3 24*EI*pi^4/L^3];
D=[0 0 0 0;0 0 0 0;0 0 3*pi^4/(2*L^3)*l*L^2*(a*EI)^(1/2) -4*pi^4/(L^3)*l*L^2*(a*EI)^(1/2);0 0 -
4*pi^4/(L^3)*l*L^2*(a*EI)^(1/2) 24*pi^4/(L^3)*l*L^2*(a*EI)^(1/2)];
F= [1 0 0 0]';
A1=inv (M)*(-K);
A2=inv (M)*(-D);
B0=inv (M)*F;
```

```
A= [zeros (4, 4) eye (4); A1 A2];
B= [zeros (4, 1); B0];

%==============================the open system================================

C1=[1 0 0 0 0 0 0 0];
sys1=ss(A,B,C1,0);
sys1_tf=tf(sys1);

%=========================feedback is theta1+DFS_theta1=========================

num1=[0 0 6897 2.522e4 7.878e9 3.37e8 4.609e13 5.857e11 4.477e16];
den1=[zeros(1,8) 1 3.657 2.287e6 4.235e6 6.467e11 1.189e10 9.086e14 467.8 1.89e5];
H1=[0 0 0 0 0 0 0 -0.2 0];%k=-200, td=0.001
num_new=num1;
den_all=den-conv(H1,num1);
for i=9:17
        den_new(i-8)=den_all(i);
end

%=========================feedback is theta1+DFS_delta=========================

C2=[-1 1 0 0 0 0 0 0];
num2=[0 0 6897 2.522e4 7.878e9 3.37e8 4.609e13 5.857e11 4.477e16];
num3=[0 0 0 0 4.023e9 2.659e8 4.065e13 5.857e11 4.477e16];
den2=[zeros(1,8) 1 3.657 2.287e6 4.235e6 6.467e11 1.189e10 9.086e14 467.8 1.89e5]; %den3
H2=[0 0 0 0 0 0 0 -0.04 0];%%k=-40, td=0.001
num_all1=[zeros(1,8) 0 0 6897 2.522e4 7.878e9 3.37e8 4.609e13 5.857e11 4.477e16];;
den_all1=den2+conv(H2,(num3-num2));
for i=9:17
  num_new1(i-8)=num_all1(i);
  den_new1(i-8)=den_all1(i);
end

%*****************************************************************************
%====================get the system with parameter uncertainty=================
%*****************************************************************************

%@@@@@@@@@@@@@@@matlab M-file: perturbed_system.m@@@@@@@@@@@@@@@

%=====================increasing the inertia of hub by 100%=====================
clear;

%====input the value of parameters====

J1=1.45e-4;
r=0.092;
J2=2*pi*2700*28*(((r*1000)^4-6.35^4)/4)*1e-15*2;
p=0.169;
L=0.5;
EI=2.282;
Ks=166;
a=0.625e-4;
l=0.005;
%========set up the system=========
```

```
M= [J1 0 0 0;0 J2+p*(r+L)^3/3-p*r^3/3 p*(L^2+2*r*L)/2+2*p*L^2/(pi^2)+p*pi^2*L^2/8+p*r*pi^2*L/6
p*(L^2+2*r*L)/2-p*pi^2*L^2/2-2*p*r*pi^2*L/3;0
p*(L^2+2*r*L)/2+2*p*L^2/(pi^2)+p*pi^2*L^2/8+p*r*pi^2*L/6 7*p*L/2+p*pi^2*L/3+p*pi^4*L/20 0;0
p*(L^2+2*r*L)/2-p*pi^2*L^2/2-2*p*r*pi^2*L/3 0 7*p*L/2-4*p*pi^2*L/3+4*p*pi^4*L/5];
K= [Ks -Ks 0 0;-Ks Ks 0 0; 0 0 3*EI*pi^4/ (2*L^3) -4*EI*pi^4/L^3; 0 0 -4*EI*pi^4/L^3 24*EI*pi^4/L^3];
D=[0 0 0 0;0 0 0 0;0 0 3*pi^4/(2*L^3)*l*L^2*(a*EI)^(1/2) -4*pi^4/(L^3)*l*L^2*(a*EI)^(1/2);0 0 -
4*pi^4/(L^3)*l*L^2*(a*EI)^(1/2) 24*pi^4/(L^3)*l*L^2*(a*EI)^(1/2)];
F= [1 0 0 0]';
A1=inv (M)*(-K);
A2=inv (M)*(-D);
B0=inv (M)*F;
A= [zeros (4, 4) eye (4); A1 A2];
B= [zeros (4, 1); B0];

%=====================decreasing the joint stiffness by 50%=========================

clear;

%====input the value of parameters====

J1=1.45e-4;
r=0.092;
J2=2*pi*2700*28*(((r*1000)^4-6.35^4)/4)*1e-15;
p=0.169;
L=0.5;
EI=2.282;
Ks=166*0.5;
a=0.625e-4;
l=0.005;

%========set up the system=========

M= [J1 0 0 0;0 J2+p*(r+L)^3/3-p*r^3/3 p*(L^2+2*r*L)/2+2*p*L^2/(pi^2)+p*pi^2*L^2/8+p*r*pi^2*L/6
p*(L^2+2*r*L)/2-p*pi^2*L^2/2-2*p*r*pi^2*L/3;0
p*(L^2+2*r*L)/2+2*p*L^2/(pi^2)+p*pi^2*L^2/8+p*r*pi^2*L/6 7*p*L/2+p*pi^2*L/3+p*pi^4*L/20 0;0
p*(L^2+2*r*L)/2-p*pi^2*L^2/2-2*p*r*pi^2*L/3 0 7*p*L/2-4*p*pi^2*L/3+4*p*pi^4*L/5];
K= [Ks -Ks 0 0;-Ks Ks 0 0; 0 0 3*EI*pi^4/ (2*L^3) -4*EI*pi^4/L^3; 0 0 -4*EI*pi^4/L^3 24*EI*pi^4/L^3];
D=[0 0 0 0;0 0 0 0;0 0 3*pi^4/(2*L^3)*l*L^2*(a*EI)^(1/2) -4*pi^4/(L^3)*l*L^2*(a*EI)^(1/2);0 0 -
4*pi^4/(L^3)*l*L^2*(a*EI)^(1/2) 24*pi^4/(L^3)*l*L^2*(a*EI)^(1/2)];
F= [1 0 0 0]';
A1=inv (M)*(-K);
A2=inv (M)*(-D);
B0=inv (M)*F;
A= [zeros (4, 4) eye (4); A1 A2];
B= [zeros (4, 1); B0];
```

Appendix C: Structural Drawings of the Experiment Test-bed

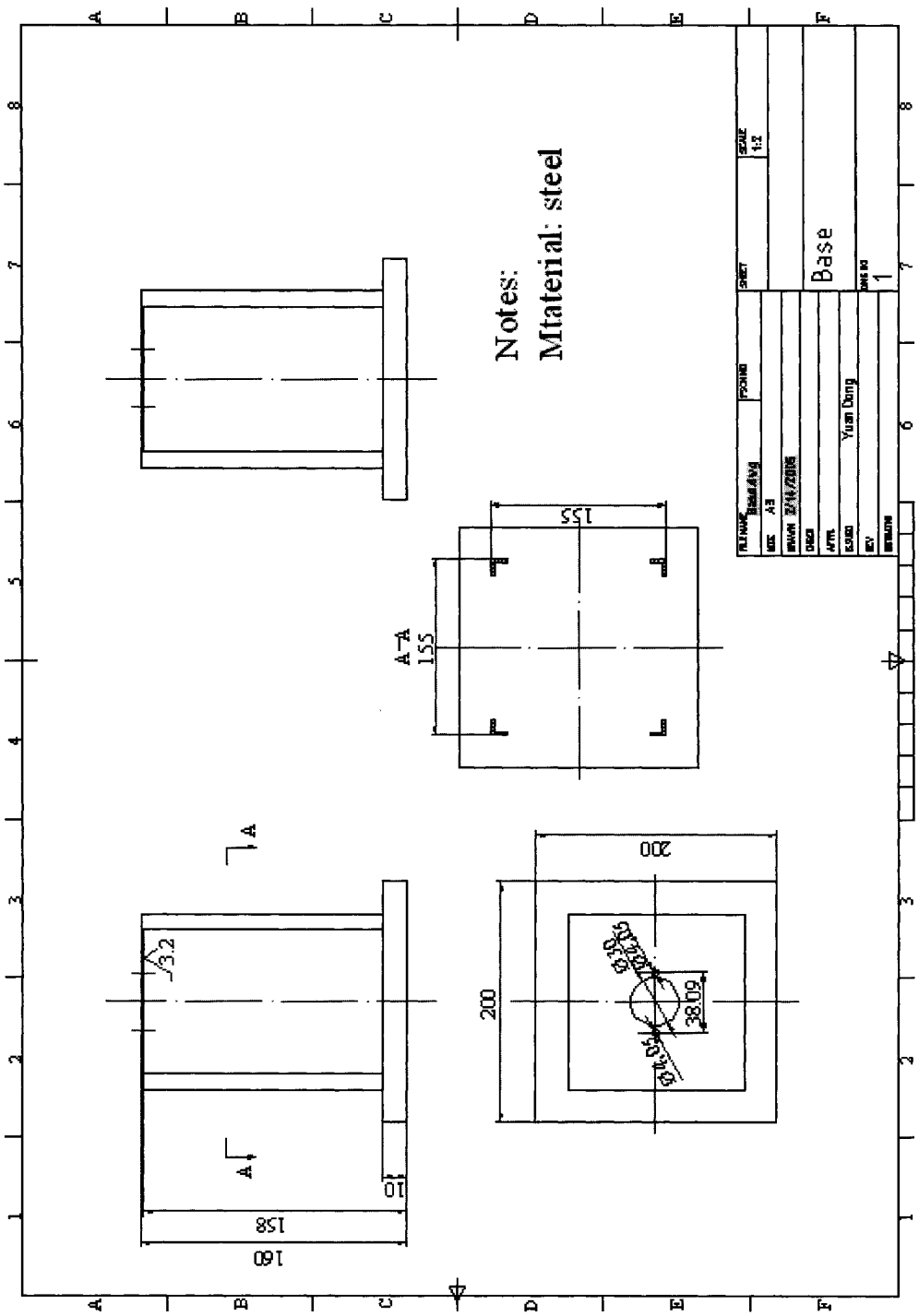

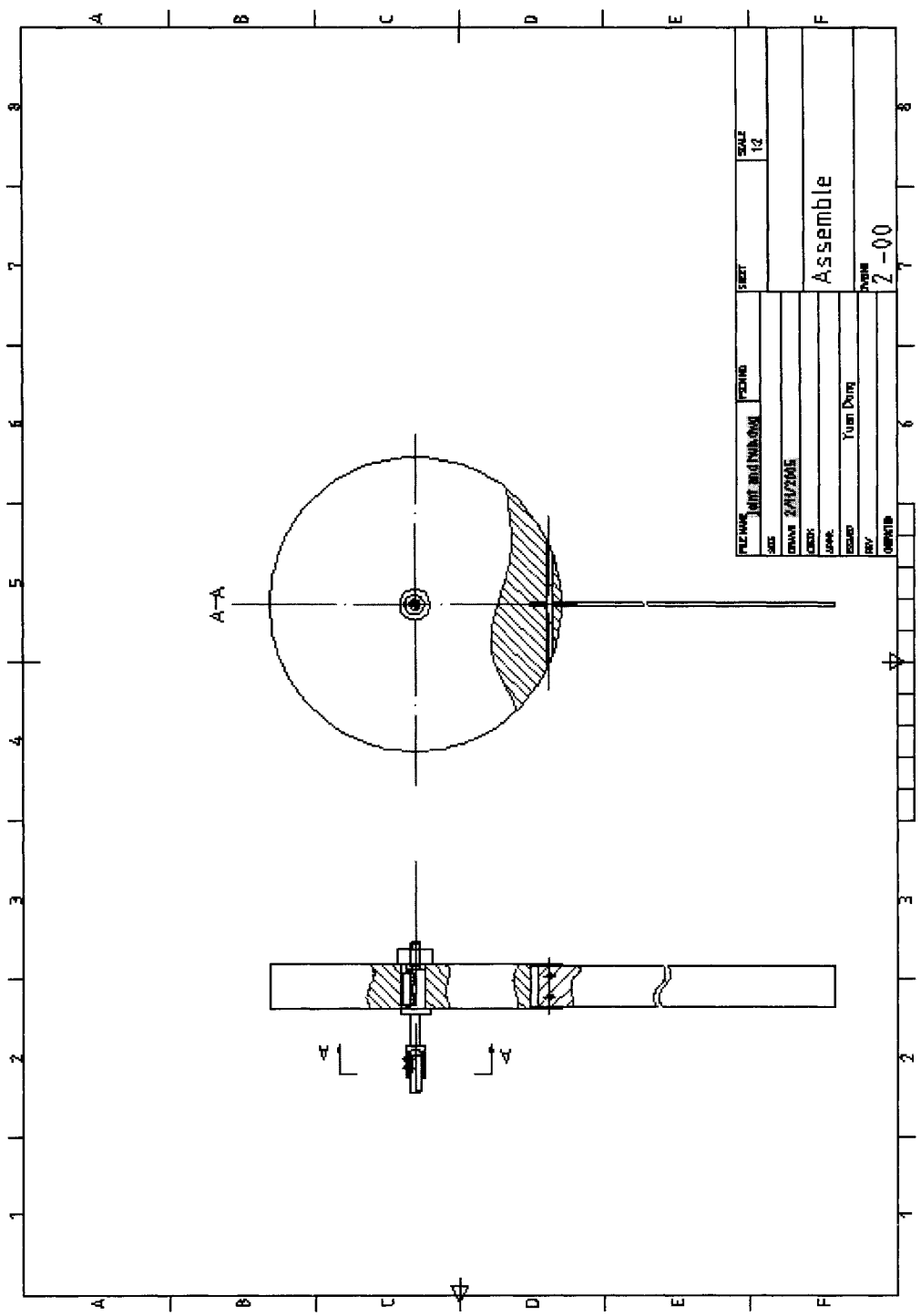
A
B
C
D
E
F
1
2
3
4
5
6
7
8
A–A
SCALE 1:2
Assemble
2-00
Yuan Dong

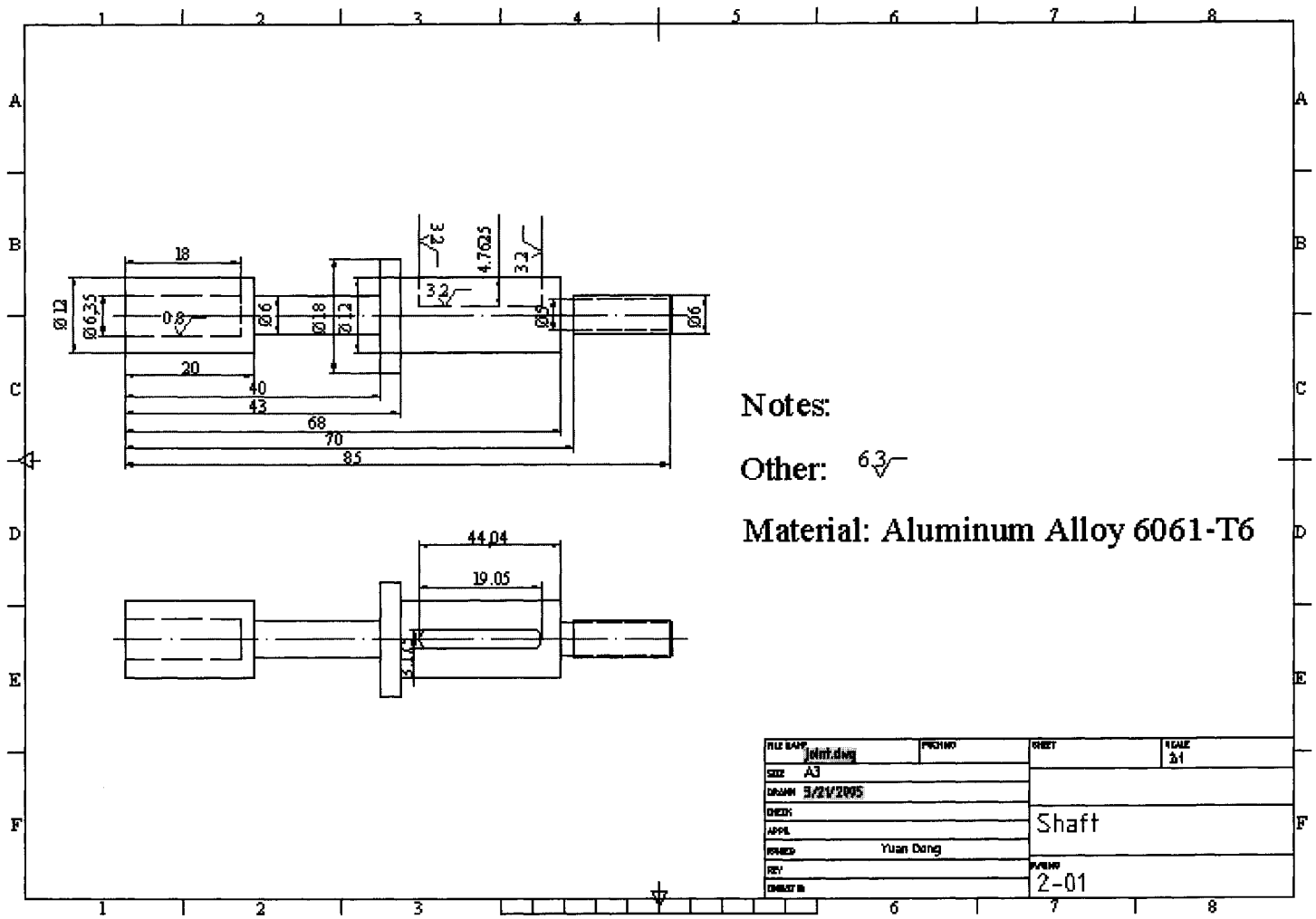
18
Ø12
Ø6.35
0.8
Ø6
Ø18
Ø12
3.2
4.76±0.5
3.2
3.2
Ø5
Ø6
20
40
43
68
70
85
44.04
19.05
Notes:
Other: 6.3
Material: Aluminum Alloy 6061-T6
Shaft
Yuan Dong
3/21/2005
A3
2-01

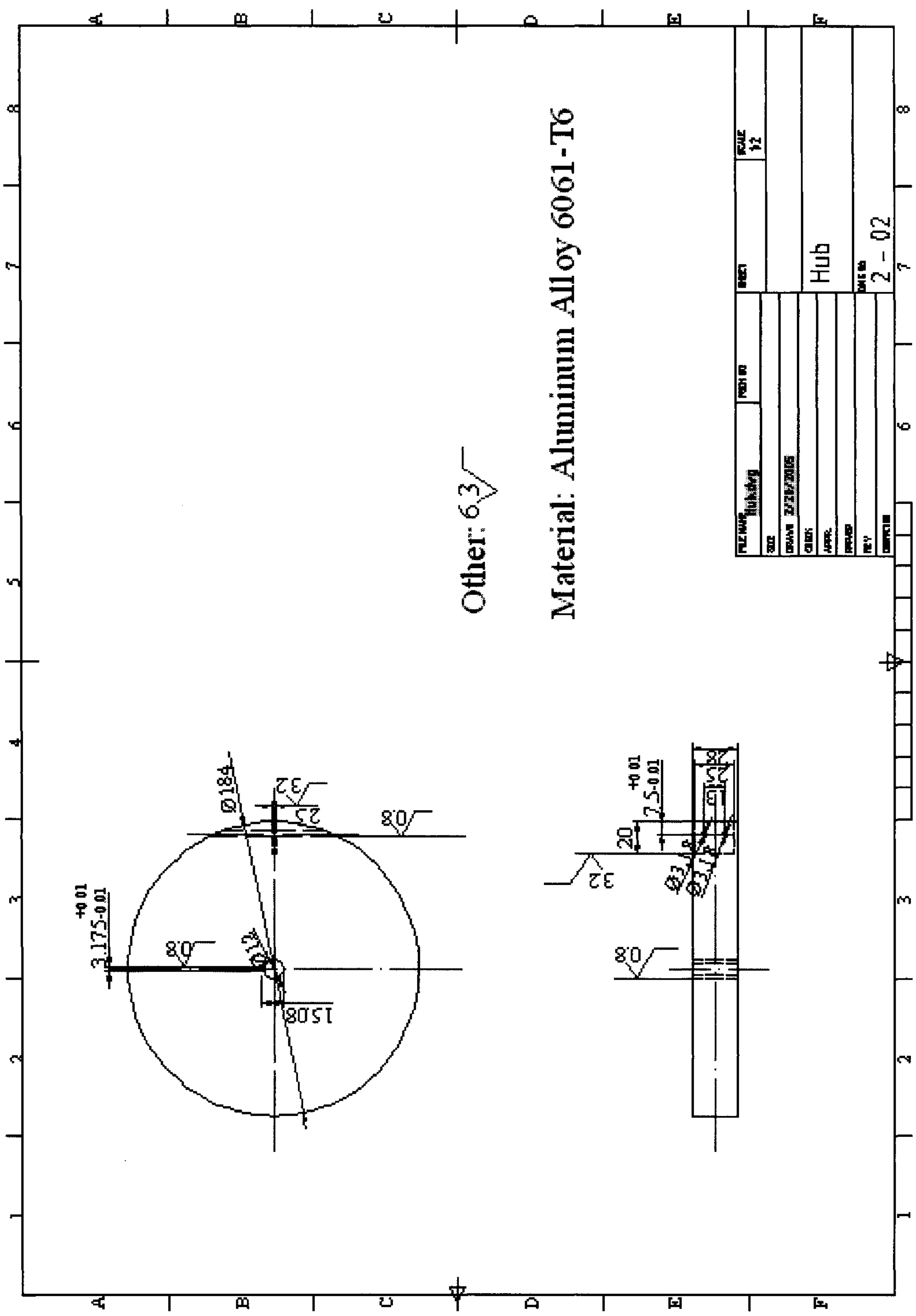
Other: 6.3
Material: Aluminum Alloy 6061-T6
Hub
2 - 02

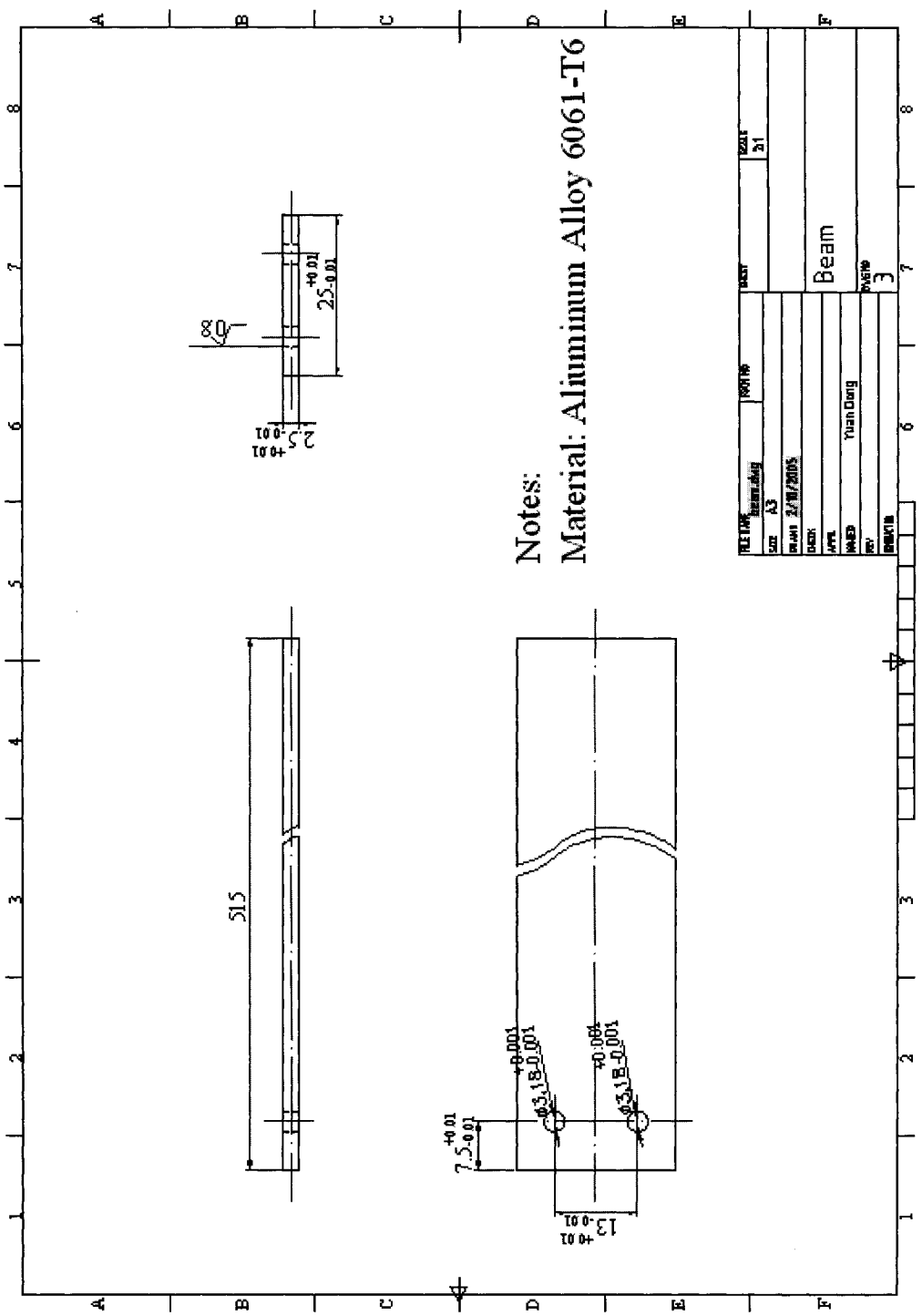
Notes:
Material: Aluminum Alloy 6061-T6
Beam
Yuan Dong
515
25-0.01
12-0.01
7.5-0.01
13-0.01